Reactor Safety Research Programs

Quarterly Report
October-December 1979

8009100403

ABSTRACT

This document summarizes the work performed by Pacific Northwest Laboratory from October 1 through December 31, 1979, for the Division of Reactor Safety Research within the Nuclear Regulatory Commission. Evaluation of nondestructive examination (NDE) techniques and instrumentation are reported; areas of investigation include demonstrating the feasibilty of determining structural graphite strength, evaluating the feasibilty of detecting and analyzing flaw growth in reactor pressure boundary systems, examining NDE reliability and probabilistic fracture mechanics, and assessing the remaining integrity of pressurized water reactor steam generator tubes where service-induced degradation has been indicated. Test assemblies and analytical support are being provided for experimental programs at other facilities. These programs include the loss-of-coolant accident simulation tests at the NRU reactor, Chalk River, Canada; the fuel rod deforma ion and post-accident coolability tests for the ESSOR Test Reactor Program, Ispra, Italy; the blowdown and reflood tests in the test facility at Cadarache, France; the instrumented fuel assembly irradiation program at Halden, Norway; and the experimental programs at the Power Burst Facility, Idaho National Engineering Laboratory. These programs will provide data for computer modeling of reactor system and fuel performance during various abnormal operating conditions.

CONTENTS

FIGURES

INTEGRATION OF NONDESTRUCTIVE EXAMINATION RELIABILITY
AND FRACTURE MECHANICS

GRAPHITE NONDESTRUCTIVE TESTING

STEAM GENERATOR TUBE INTEGRITY

TABLES

CORE THERMAL MODEL DEVELOPMENT[a]

D. S. Trent, Program Manager
M. J. Thurgood, Project Manager
K. L. Bas hore
K. R. Crowell
J. M. Cuta
T. L. George
T. E. Guidotti
J. M. Kelly
A. S. Koontz
G. A. Sly

SUMMARY

Several separate-effects experiments have been simulated with COBRA/TRAC to assess the physical models used in the code. Models that were assessed include the interfacial shear, entrainment rate, wall heat transfer, and, to a lesser extent, the interfacial heat transfer. Assessment was accomplished by comparing the code calculations with data from these experiments: counter-current flow in several different geometries; EG&G jet pump; rod position indicator (RPI) two-dimensional, flat-plate phase separation; and FLECHT reflood. Comparison of these data has indicated the need to improve some models used in the code. The overall agreement with data is reasonable.

INTRODUCTION

The COBRA-TF computer code is part of the analysis techniques being developed by the Nuclear Regulatory Commission Water Reactor Safety Research Program. The purpose of this work is to provide better digital computer codes to be used in computing the behavior of full-scale reactor systems under postu-lated accident conditions. The resulting codes are presently being used to perform pre- and post-test analysis of the effects of such accident conditions on light water reactor components and systems. This project has two main objectives:

- to develop a hot bundle/hot channel analysis capability that will be used to evaluate the thermal-hydraulic performance of light water reactor fuel bundles during postulated accidents

- to develop the capability to simulate a water reactor primary system for modeling complex internal vessel geometries such as those encountered in pressurized water reactors (PWRs) with upper head injection.

COBRA-TF is formulated to model fully three-dimensional, two-phase flow using a three-field representation. The fields are the vapor field, the continuous liquid field, and the droplet field. The model allows thermal nonequilibrium between the liquid and vapor phases and allows each of the three fields to move with different velocities. Thus, one can mechanistically treat a continuous liquid core or film moving at a low, or possibly negative velocity, from which liquid droplets are stripped off and carried away with the vapor phase. This is an essential feature in the treatment of the hydrodynamics encountered during the reflooding phase of a loss-of-coolant accident (LOCA). Because of this model, it has been possible to predict liquid carryover in the FLECHT low reflood series of experiments. The treatment of the droplet field is also essential for prediction of other phenomena such as counter-current flow limiting and upper plenum de-entrainment and fall back.

The code also features flexible noding which permits the modeling of complex geometries encountered in reactor vessel internals, such as slotted control rod guide tubes, jet pumps, core bypass regions, etc. These geometries are not easily modeled in regular cartesian or cylindrical mesh coordinates; but because of their significant impact on the thermal-hydraulic response of the system, reasonably accurate modeling is essential.

The fuel rod heat transfer model utilizes a rezoning mesh that automatically reduces the rod heat transfer mesh size in regions of high heat flux or steep temperature gradients and increases the mesh size in regions of low heat flux. This model has proven very effective for resolving the boiling curve in the region of the quench front.

COBRA-TF has been implemented into TRAC-P1A as the vessel module, providing a capability for simulating the above vessel systems. The resulting code is referred to as COBRA/TRAC and is being used to simulate several experiments, including FLECHT, SEMISCALE, and JAERI.

During the past quarter, COBRA/TRAC has been applied to several separate-effects experiments in two-phase flow. As a part of the developmental assessment task, this was done to evaluate the adequacy of various physical models in the code. Areas requiring further development are discussed in this report, along with the results of the simulations.

UNIVERSITY OF HOUSTON COUNTER-CURRENT FLOW EXPERIMENT

A two-phase counter-current flow experiment[1] performed at the University of Houston by A. E. Dukler and his associates was simulated with COBRA/TRAC to assess the interfacial shear and entrainment rate models used for film flow in the vessel component.

DESCRIPTION OF EXPERIMENT

The experimental apparatus consisted of an approximately 12-ft long vertical test section made of 2-in. ID thermoplastic pipe. Air flow was introduced at the bottom of the test section through an inlet nozzle, and liquid was injected through a porous metal section located halfway up the test section. The facility was operated at atmospheric conditions. During the experiment, liquid was injected through the porous area coating the test section with film below the injection point. The air flow rate was then set to the desired value and equilibrium flow reestablished. The amount of liquid flowing down in the film was then measured by weighing the water that reached the air entrance section. Similarly, the water flowing as a film out the top of the test section was separated from the air flow and measured as was the water carried by the air flow in droplet form. Thus, both film flow and liquid entrainment rate were measured for the various air flow rates. Pressure drops accross the test section above and below the liquid injection point were measured. Film thicknesses were also measured, although none were shown in the report.[1] A

3

drawing of the test section is shown in Figure 1. The inlet and outlet of the test section were flared to allow separation of the film from the air stream without inducing entrainment. Data was taken for liquid injection rates of 100, 250, 500, and 1000 lbm/hr and air flow rates from 136 to 301 lbm/hr. Superficial gas velocities corresponding to these flows varied from 21.4 to 50.0 ft/sec.
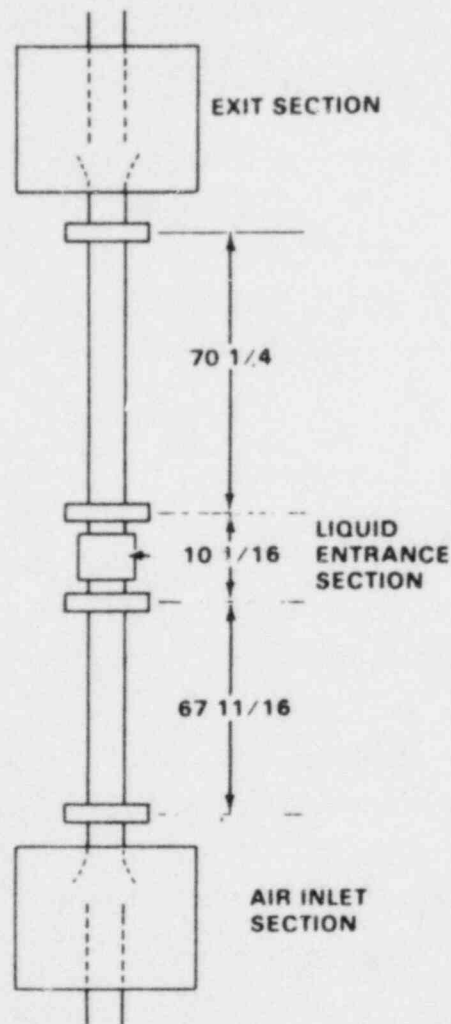
FIGURE 1. Experimental Test Section

4

COBRA/TRAC MODEL

The 500 lbm/hr liquid injection case was chosen for this simulation. A single subchannel separated into 1-ft long nodes was used in the simulation, shown in Figure 2. A pipe and fill were connected to the bottom of the fourth node for air injection. Liquid was introduced at the center of the test section by specifying a liquid source term. Air was modeled in the code by using saturated steam at a pressure that provided the correct gas density. The simulation was initiated in the same way the experiment was run: first a downward flowing film was established, then the air was injected.
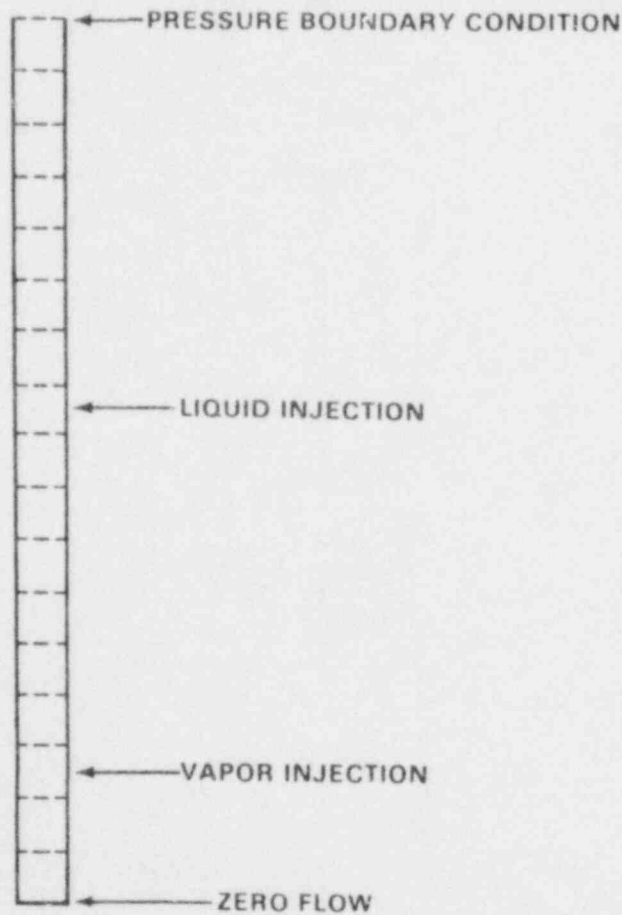
FIGURE 2. COBRA-TF Model

5

DATA COMPARISON

The computed flow pattern for air flow rates that allowed partial liquid downflow is shown in Figure 3. Air entering the bottom of the test section entrained liquid from the downward flowing liquid film. The amount of liquid entrained in the liquid core increased up to the liquid injection point, where the entrainment rate was at its peak. Above the injection point, drops were deposited on the wall forming a liquid film. The top portion of the film above the injection point flowed upward out of the test section; the lower part flowed down into the injected liquid. Thus, a recirculation pattern was formed with liquid being entrained at the injection point, deposited above it and flowing back down into it. A similar pattern was observed experimentally

FLOW PATTERN
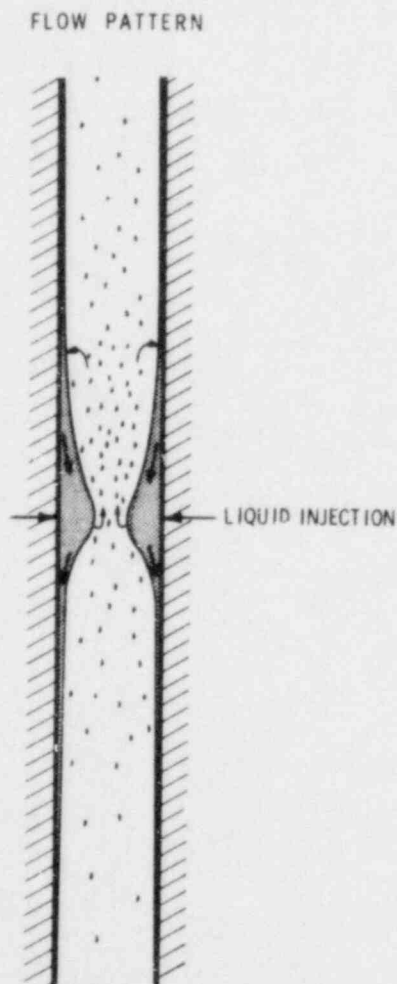
LIQUID INJECTION

FIGURE 3. Computed Flow Pattern

6

for the higher liquid injection rate tests.[1] Drops not deposited on the film above the injection point were carred out of the test section by the air flow.

The liquid film downflow as a function of air flow is shown in Figure 4. The open symbols are the experimental values and the solid symbols are from the COBRA/TRAC calculations. All of the liquid injected (500 lbm/hr) flowed down at air flow rates of less than 194 lbm/hr in both the experiment and the calculations. The decrease in liquid downflow with increasing air flow observed experimentally was calculated with the code. At the lower air flow rates, the decrease in downflow is apparently completely accounted for by entrainment of drops from the liquid film. At higher air flow rates, flow reversal within the film itself contributes to the reduction of the downward liquid flow rate.

The code predicted larger downward liquid flow rates than were measured experimentally at the higher air flow rates. This indicates that the expression in the code used for interfacial drag underpredicts the interfacial
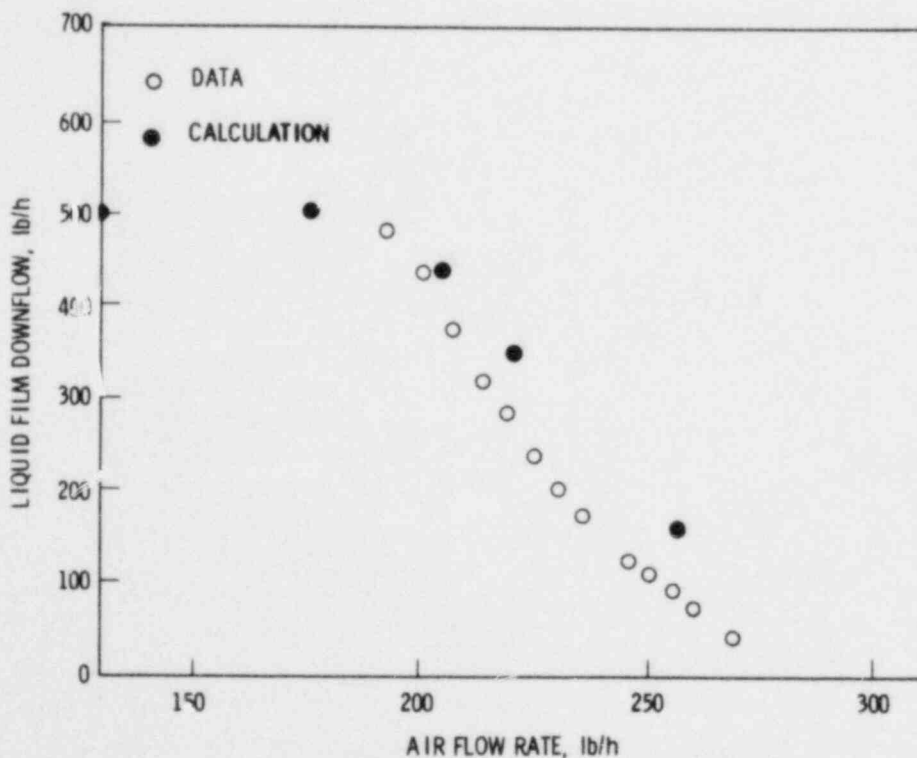
FIGURE 4. Downflow in the Liquid Film

shear force. At the onset of entrainment, more pronounced wave action takes place, resulting in a sudden increase in interfacial shear stress. This increase is not taken into account in the present interfacial shear model for film flow; however, there is a modified Wallis correlation available that does account for this effect. This correlation will be implemented into the code and should improve the code prediction significantly.

The rate at which drops are carried out of the test section is shown in Figure 5. Again, the code predictions (solid symbols) are in reasonable agreement with the data (open symbols). At lower air flow rates the entrainment was underpredicted, indicating that the droplet disposition model may cause too much de-entrainment above the injection point. The overprediction of entrainment at higher air flow rates is a result of the overprediction of the downward film flow rate over the same range of air flow rates. The code did not adequately predict pressure drops above the liquid feed, Figure 6, and below the liquid feed, Figure 7. This also can be attributed to the underprediction of the interfacial shear after the inception of entrainment.
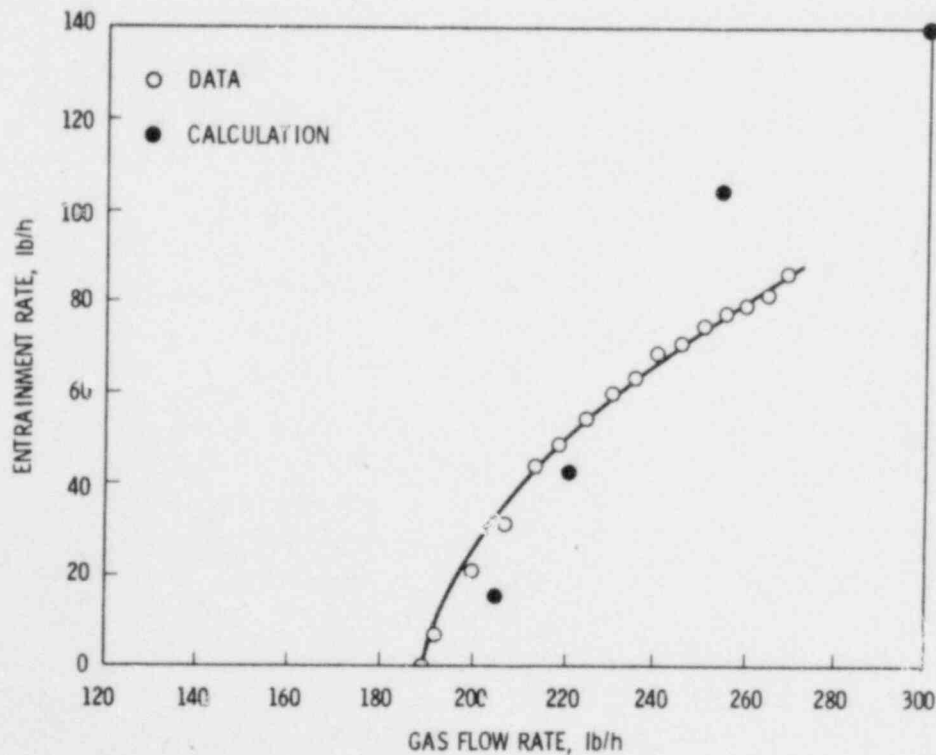
FIGURE 5. Net Rate of Entrainment

8
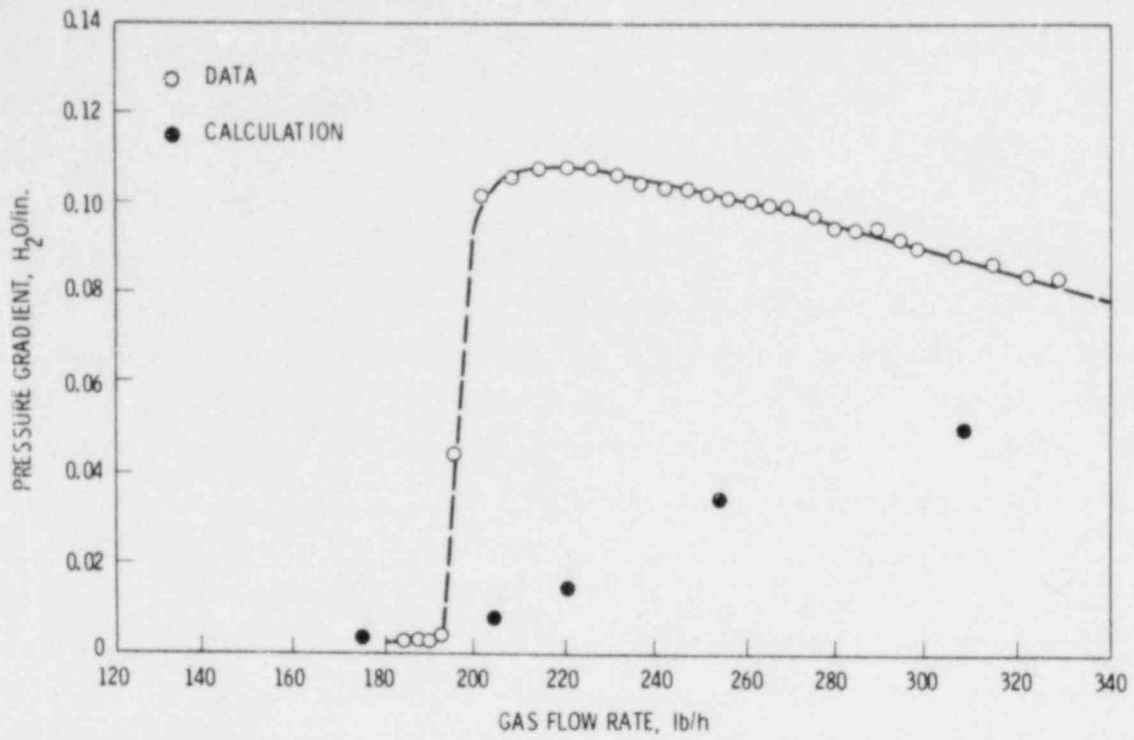
FIGURE 6. Mean Pressure Gradient Above Liquid Entrance
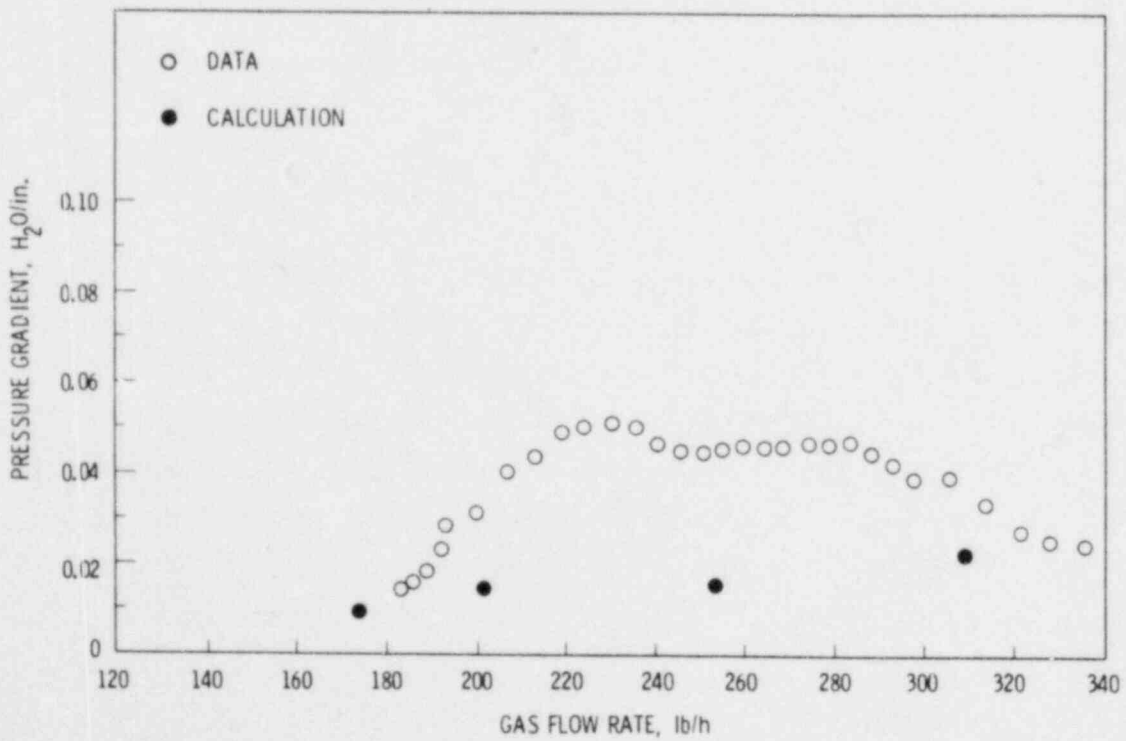
FIGURE 7. Mean Pressure Gradient Below Liquid Entrance

9

DISCUSSION OF RESULTS

The results of the simulation are considered good and indicate that the method used to determine the entrainment rate for film flow is adequate. A physically based model is needed to determine the onset of entrainment in counter-current flow before the model can be considered generally applicable. The present model is empirical, based on nondimensional parameters developed for co-current flow. Results with the improved model for interfacial shear are expected to be closer to the data. This problem took 0.0032 CPU sec per time step/mesh cell to execute on the CDC 7600 computer. The time step was limited by the Courant criterion and ranged from 0.0146 to 0.1 sec. The average ratio of CPU time to real transient time was 5.0 to 1.0.

DARTMOUTH COUNTER-CURRENT FLOW EXPERIMENT

Counter-current flow experiments have been conducted at Dartmouth College by T. Lovell.[2] COBRA/TRAC has been used to simulate one of these experiments to assess the treatment of counter-current flow in a tube, the upper end of which is submerged in a liquid pool. A similar situation is expected to occur during a LOCA at the upper core plate of a PWR as a result of liquid de-entrainment in the upper plenum, upper plenum injection of emergency core coolant, or upper head injection.

DESCRIPTION OF EXPERIMENT

The experimental apparatus consisted of an approximately 4-ft vertical test section made of 2-in. ID Plexiglas pipe. Each end of this test section was connected to a fifty-five gallon drum (upper and lower plenums for the test section). Air was injected into the lower plenum through a 10-in. pipe. The air flowed up through the test section to the upper plenum where it exited through an outlet pipe. Liquid was injected into the upper plenum at a fixed rate. The initial air flow was set high enough to prevent any liquid flow down the test section. When the level of the pool was stabilized with liquid flowing out of the outlet pipe, the air flow was decreased until liquid penetration was observed at the top of the test section. The air flow was then

10

held constant while the liquid penetration through the test section (the rate of liquid accumulation in the lower plenum) was measured. The air flow was then lowered to a new value and the penetration rate again measured. This process was repeated until the complete flooding curve was developed for this test configuration. A more in-depth description of the experimental procedure and apparatus can be found in Lovell's report.

COBRA/TRAC MODEL

COBRA/TRAC was used to simulate the experiment. As shown in Figure 8, the simulation included a lower plenum, an upper plenum, and a connecting test section of pipe. The test section was modeled using a single subchannel with five

NODALIZATION SCHEME
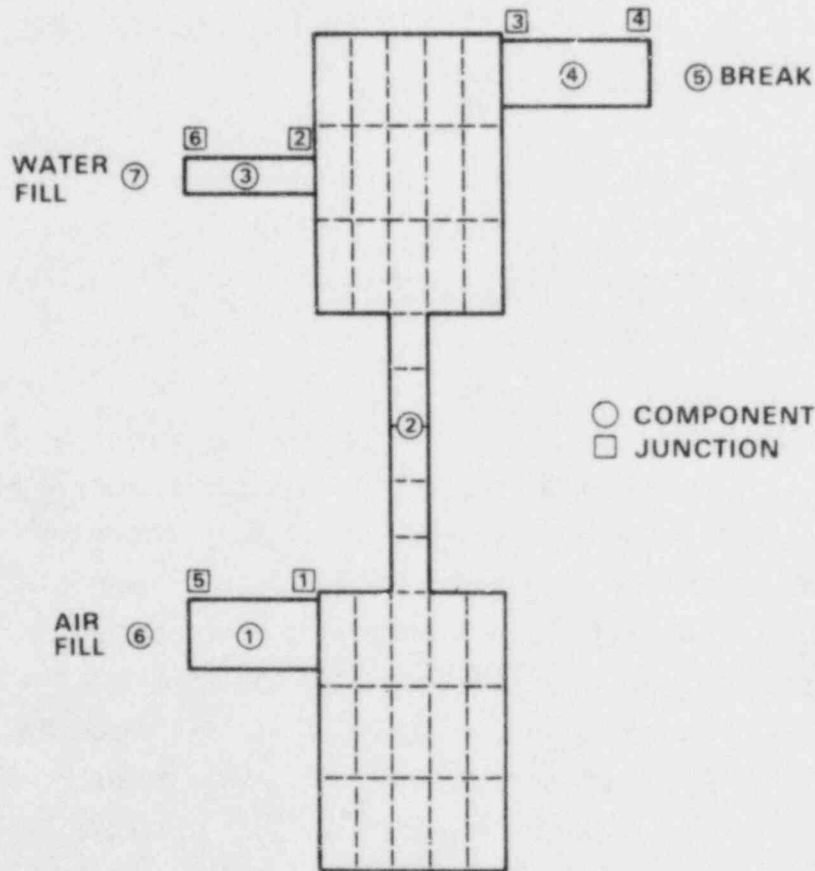
FIGURE 8. Nodalization for Dartmouth Counter-Current Flow Experiment

axial nodes. It was connected to the center of three concentric subchannels in the upper and lower plenums. The upper and lower plenums also contained three axial levels. An air source was connected to the third node from the bottom of the lower plenum through a 10-in. pipe and a fill component. A 10-in. pipe and break component was attached to the top node of the upper plenum to assure a water level of 22 in.[a] Steam pressures and densities equivalent to the air properties used in the experiment were specified at the air fill. A flow and temperature boundary condition was applied at the water fill. Atmospheric pressure was specified at the break.

The COBRA/TRAC simulation was made following the same procedures as those used during the actual experiment. First, an air flow was introduced and allowed to stabilize within the test section. After the air flow was established, the water flow was initated and the upper plenum was filled to the 22-in. level. After the flow was fully established, the amount of water downflow was calculated. The injected air flow was reduced, and the simulation process started over again.

DATA COMPARISON

Several air flow rates were simulated. The COBRA/TRAC predicted and experimental downward liquid flow rates as a function of air flow rate were compared and are presented in Figure 9. Both the water and air flow rates have been made dimensionless[3] with $j^{*1/2}$ equal to the dimensionless air flow rates and $j^{*1/2}$ equal to the dimensionless water flow rates. As can be seen from Figure 9, the experimental data exhibits a constant increase in the nondimensional water flow rate with constant decrease in the air flow rate. The flooding curve can be approximated by the Wallis correlation. The extrapolated intercept with the zero water penetration axis has a value of $j^{*1/2}$ equal to 0.7, which corresponds to an air velocity (within this particular test section) of 9.5 m/s. The COBRA/TRAC simulation, on the other hand, shows that an air velocity of 15.8 m/s will produce the zero water downflow condition. Liquid

---

(a) It was later learned that the actual pool dep . .as 8 in.
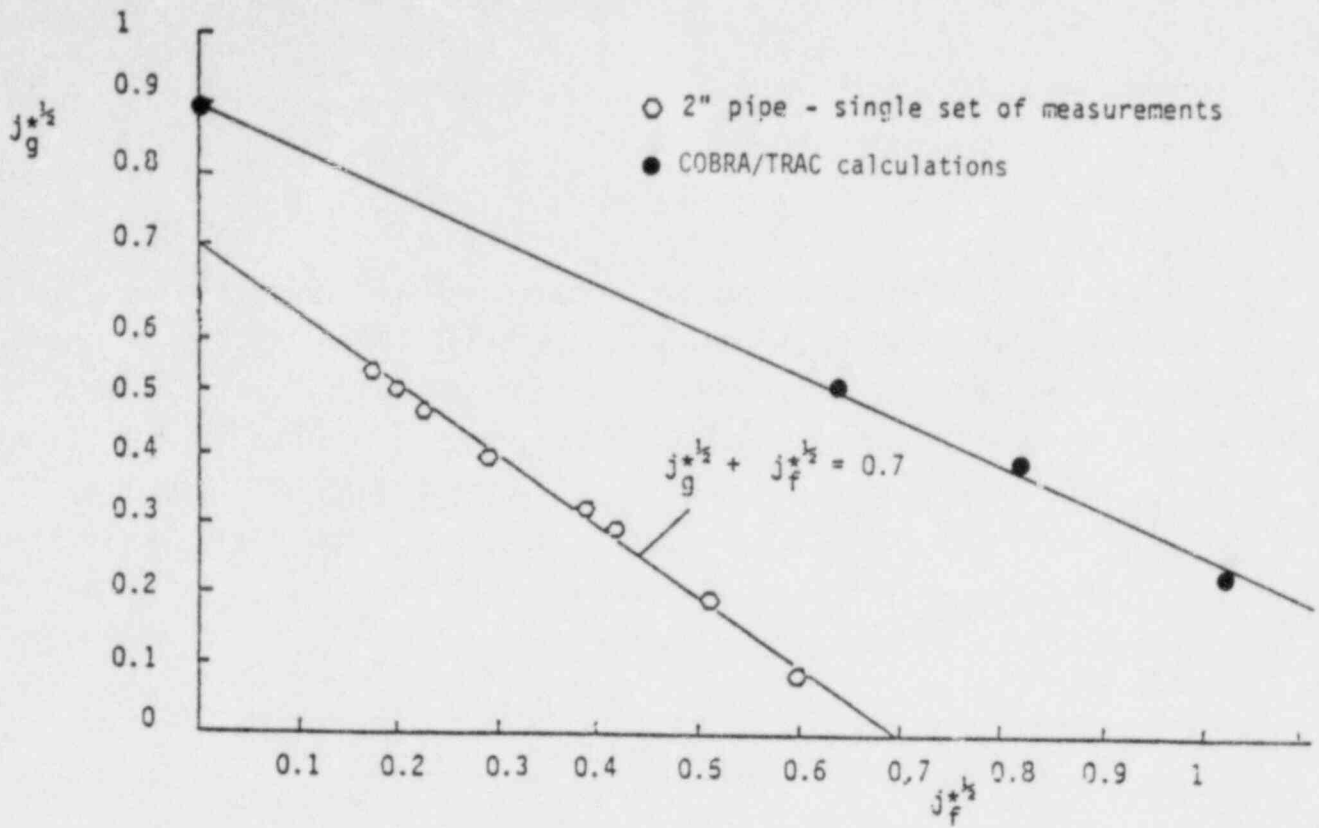
FIGURE 9. COBRA/TRAC Data Comparison with Dartmouth
Counter-Current Flow Experiment - 2-in. Tube

penetration rates computed at all air flow rates are larger than those measured experimentally. The calculations do exhibit the same trend as the data in regard to decreasing air flow rates.

The poor comparison with the data may be attributed in part to the flow selection logic in the code. The calculation oscillated from a bubbly to an annular flow regime in the upper plenum cells directly above the test section. The large magnitude of change in the interfacial drag between these two flow regimes caused an oscillatory flow with intermittent dumping of liquid through the test section into the lower plenum. The code's treatment of flow through liquid pools is currently being reviewed in order to improve the method used to select the flow regime in such situations. Resolution of liquid flow into

13

the tube may require finer mesh sizes than are practical in full vessel calculations. It may be necessary to treat flow at the upper core plate with a correlation.

CREARE DOWNCOMER EXPERIMENTS

Counter-current flow experiments have been conducted at CREARE, Inc. to evaluate the downward penetration of emergency core cooling water against the up-flow of steam in a PWR downcomer. The effects of counter-current flow, lower plenum voiding, superheated downcomer walls, and condensation were investigated separately and in combination under test conditions that included elevated pressures, transient steam flows, and a range of geometric parameters.[4] A test was simulated to use steady steam flow, unheated wall, injection of emergency coolant at $212^{\circ}F$, a deep plenum, and uncontrolled pressure. The COBRA/TRAC simulation assessed the applicability of the code's vessel flow pattern selection logic and physical models for interfacial drag, wall shear, and entrainment to the geometry of the downcomer in a PWR.

DESCRIPTION OF EXPERIMENT

The test apparatus consisted of a cylindrical vessel containing a 1/15-scale PWR downcomer and an extended lower plenum, Figure 10. The downcomer gap and circumference were 0.5 in. and 34.6 in., respectively. Three intact cold legs and one broken cold leg were connected to the top of the downcomer. Emergency core cooling water was injected into each of the three intact cold legs; the broken cold leg was connected to a separator. Steam was injected in the top of the vessel on the inside of the core barrel to simulate reverse core steam flow. Tests were run by first injecting a constant steam flow rate through the vessel, purging the vessel of air, and then injecting water at a constant rate through the intact cold legs. The flow was then allowed to achieve dynamic equilibrium, and the liquid penetration rate into the lower plenum was measured. This procedure was repeated at different steam flow rates for each liquid injection rate, covering the range from complete bypass of the injected liquid out the broken cold leg to complete penetration of the liquid

14
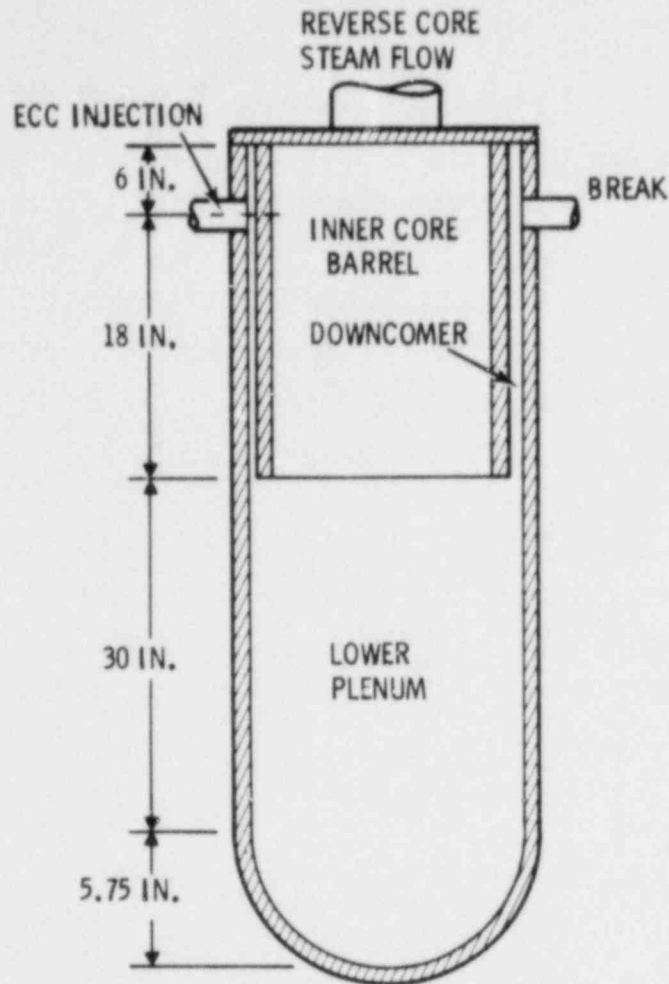
FIGURE 10. CREARE 1/15-Scale Cylindrical Vessel

into the lower plenum. A more detailed description of the experimental appa-
ratus and procedure is given in the test report.[4]

COBRA/TRAC MODEL

The test vessel was simulated using a 2-section, 6-subchannel model with
24 hydrodynamic mesh cells. A pressure boundary condition was used on the
broken cold leg, and liquid flow boundary conditions of 1.34 lbm/sec (10 GPM)
at 212°F were specified at each of the th. intact cold legs. Reverse core
steam flows were specified over the range of values used in the experiment. A
sketch of the nodalizaion used is shown in Figure 11. The downcomer is modeled

15

using four azimuthal subchannels having four axial nodes each. The lower plenum and core region were modeled with single subchannels having four axial nodes each. Steam was injected at the top of the core region of the vessel.

The calculation was initiated by specifying a reverse core steam flow rate that was sufficiently high to cause complete emergency cooling bypass. Once the initial steam flow reached a steady state, cooling liquid was initiated and allowed to establish a steady state. The rate of liquid accumulation in the lower plenum was then calculated and compared with the experimentally measured value. This procedure was repeated for several steam flow rates.
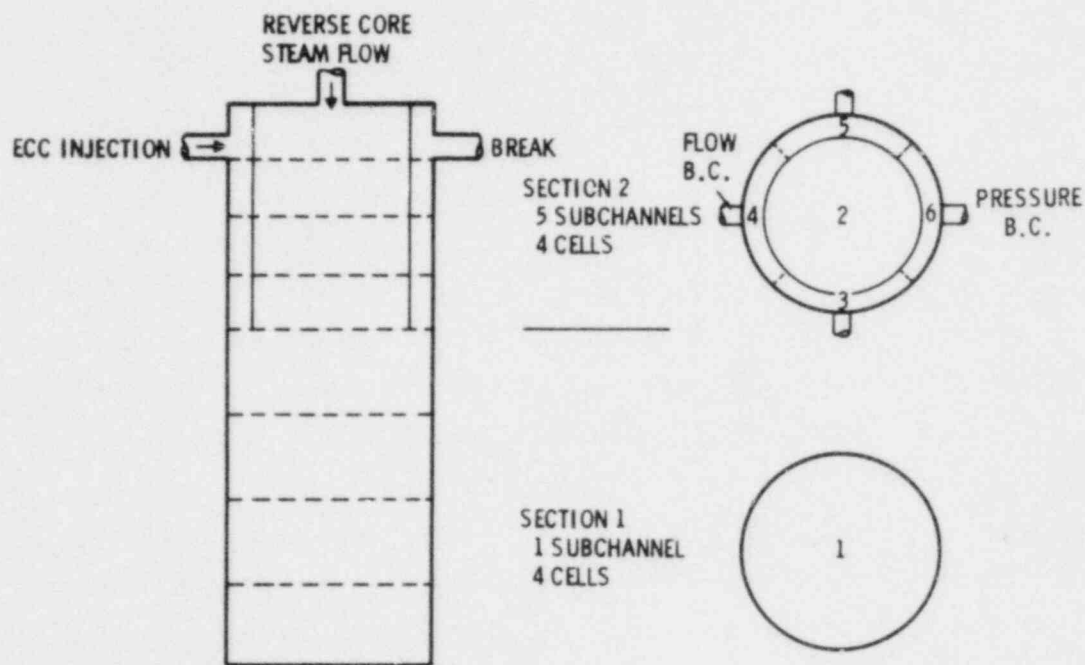
FIGURE 11. COBRA/TRAC Nodalization of CREARE Vessel

16

DATA COMPARISON

The results of the calculations are compared with the data in Figure 12, which is a plot of the dimensionless counter-current steam flow, J_{gc}, versus dimensionless water flow delivered to the lower plenum, J_{fd}. The dimensionless flows are defined as

$$J_{gc}^* = j_g \rho_g^{1/2} [gw\Delta\rho]^{-1/2}$$

and

$$J_{fd}^* = j_f \rho_f^{1/2} [gw\Delta\rho]^{1/2}$$

where j_g and j_f is the vapor and liquid volumetric fluxes, and w is the downcomer circumference. The experimental data indicates that complete bypass occurs for dimensionless steam flows greater than 0.18, partial penetration for steam flows between 0.18 and 0.04, and the complete penetration below 0.04. The COBRA/TRAC simulation compares very favorably with the data for this liquid injection rate. However, at a higher liquid injection rate of J_{fd} (0.23), liquid penetration rates were larger in the calculation than those observed experimentally. This was a result of complete liquid penetration in the sub-channel opposite the broken cold leg. The model for interfacial shear used in the code for downcomer geometries and vapor flows near the flooding point appears insufficient. This model will be modified before proceeding with further downcomer simulations. This calculation required from 19 to 57 sec computer time for each second of real time, depending on the steam flow rate.

17
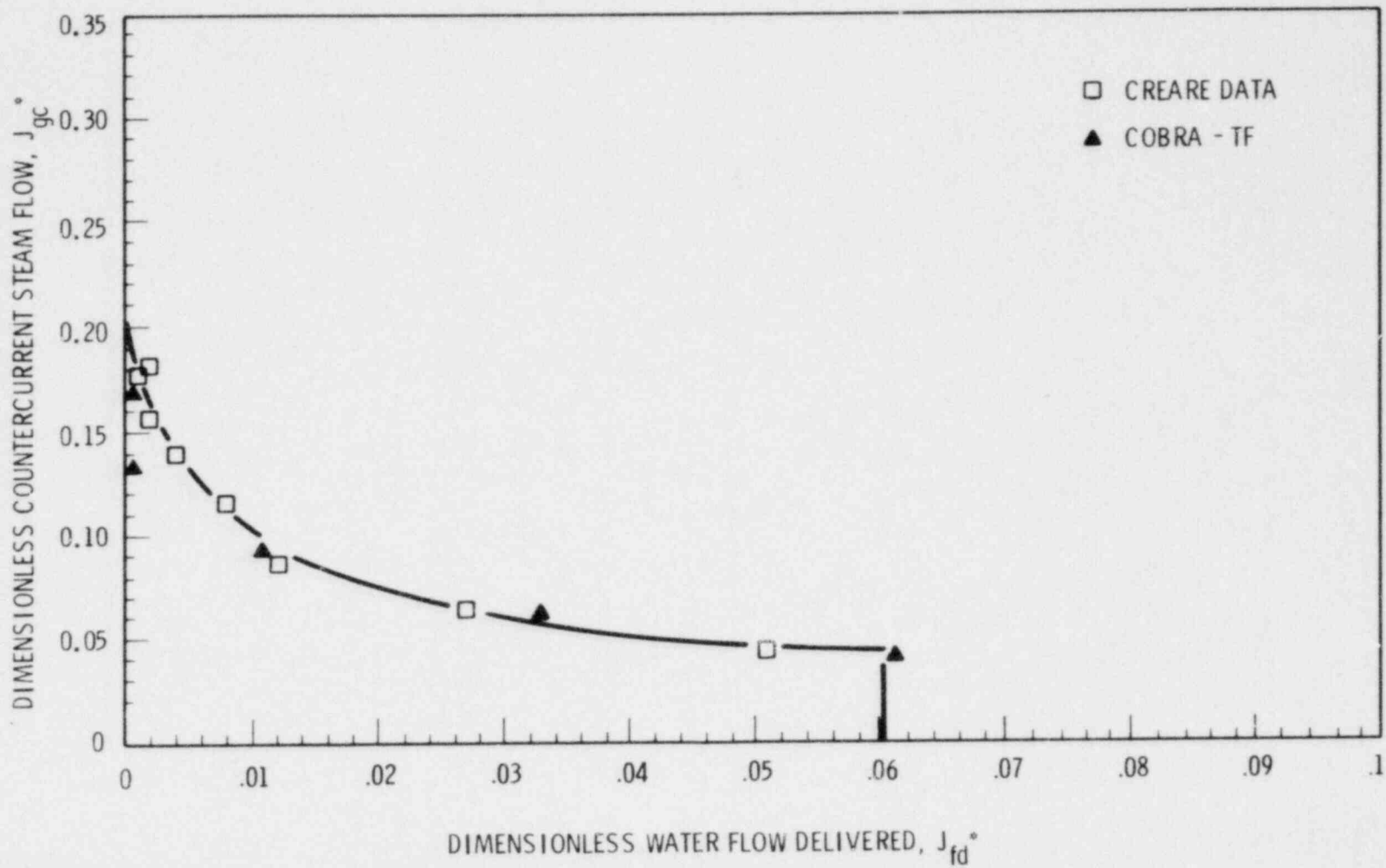
FIGURE 12. COBRA/TRAC Comparison with CREARE Data

18

EG&G JET PUMP SIMULATION

A simulation of the EG&G jet pump experiments was performed to assess the logic of the momentum transfer between channel splitting sections.

DESCRIPTION OF EXPERIMENT

The test apparatus, shown in Figure 13, housed the 1/6-scale boiling water reactor jet pump. The assembly was filled with subcooled water at 533K and 7.6 MPa. During an experiment, the mass flow rates into the vessel penetrations were set at a desired value. The EG&G test assembly was capable of providing positive or negative flow to the suction, drive, or discharge. After
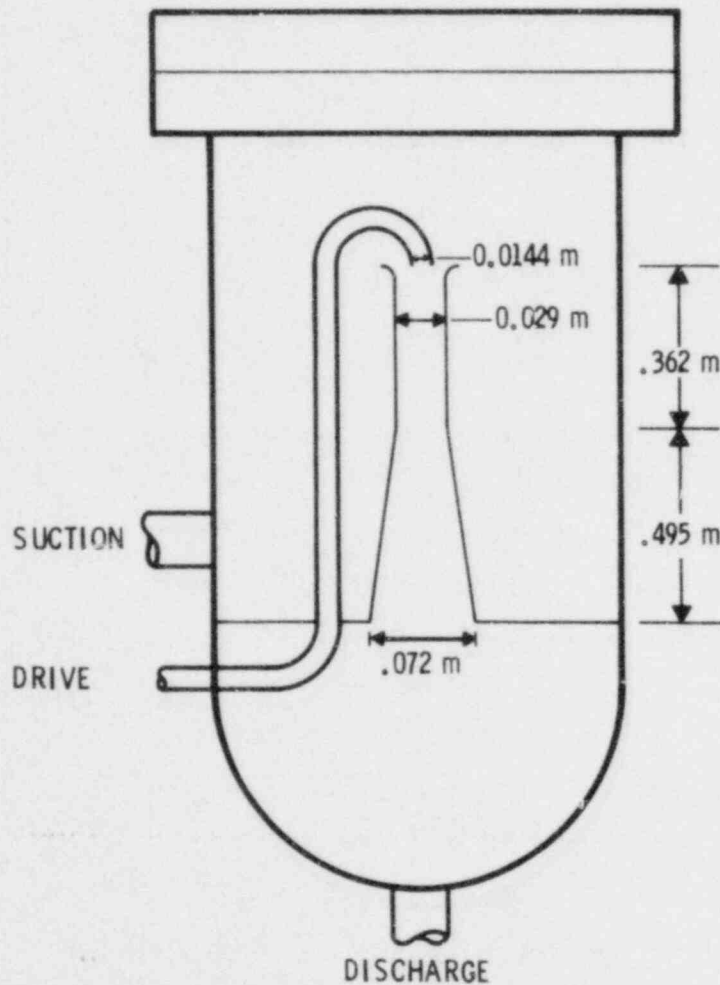
FIGURE 13. EG&G Jet Pump Test Assembly

19

steady mass flows were reached, pressure measurements were taken at suction, drive, and discharge locations. This was repeated 240 times for various flow combinations. Further details regarding the experimental apparatus and procedure may be obtained from the experimenter's report.[5]

COBRA/TRAC MODEL

This experiment was simulated using the 3-section, 6-subchannel COBRA/TRAC model shown in Figure 14. The jet pump was simulated using a single channel with variation in axial area that modeled the expansion of the diffuser. Flow boundary conditions were specified at the suction and drive inlets with the discharge being treated as a pressure boundary condition. After steady flow conditions were reached, the kinetic pressures were plotted as a function of flow. Figure 15 shows the data comparison in terms of the N-M curve, a non-dimensional pressure-versus-flow curve. Considering the large noding and lack of a momentum mixing model in the jet pump throat, COBRA/TRAC did reasonably well in predicting the general behavior of the jet pump. A turbulent shear stress model is currently being added to COBRA/TRAC, which should improve the data comparison.

RPI PHASE SEPARATION EXPERIMENTS

COBRA/TRAC simulations have been run for two experiments in the RPI phase separation series.[6] The purpose of these simulations was to test the ability of the code to predict the void fraction distribution in a two-phase recirculating flow and thus help determine the necessity of including viscous and turbulent stress modeling in the code.

EXPERIMENT DESCRIPTION

The experimental apparatus, shown in Figure 16, consisted of a two-dimensional thermoplastic test section, measuring 1/2 in. x 12 in. x 36 in. An air-water mixture was injected at the bottom and withdrawn from outlets near the top. Tests were conducted with various flowrates and inlet qualities.
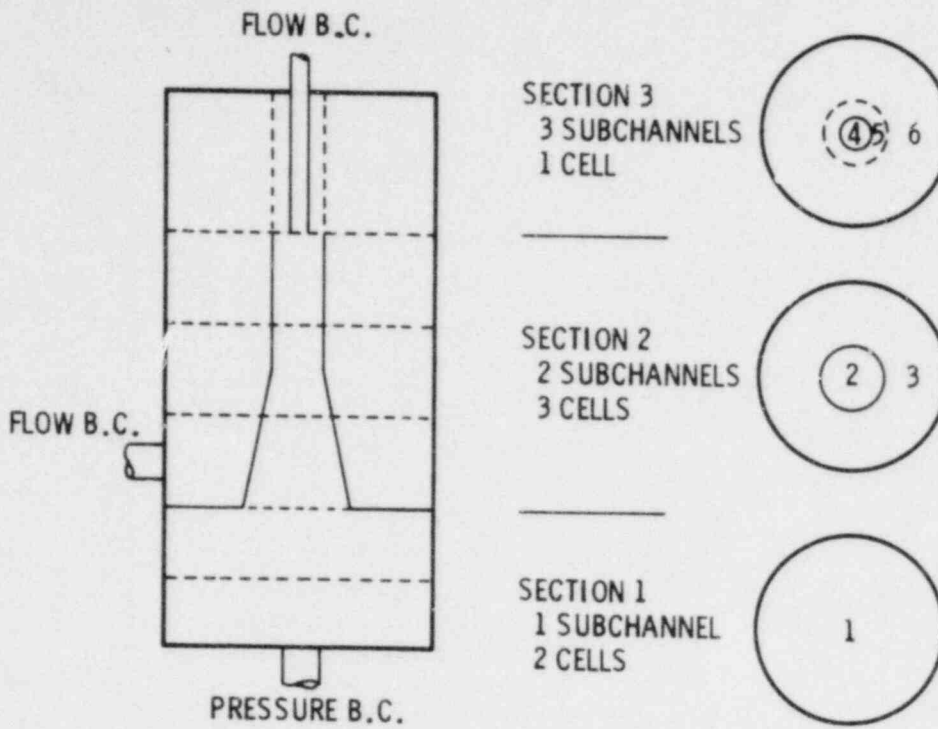
FIGURE 14. COBRA/TRAC Nodalization of EG&G Jet Pump Test

$$M = \frac{\text{SUCTION FLOW}}{\text{DRIVE FLOW}}$$

$$N = \frac{P_{disch} - P_{suct}}{P_{drive} - P_{disch}}$$

—— EG & G DATA
▲ COBRA - TF
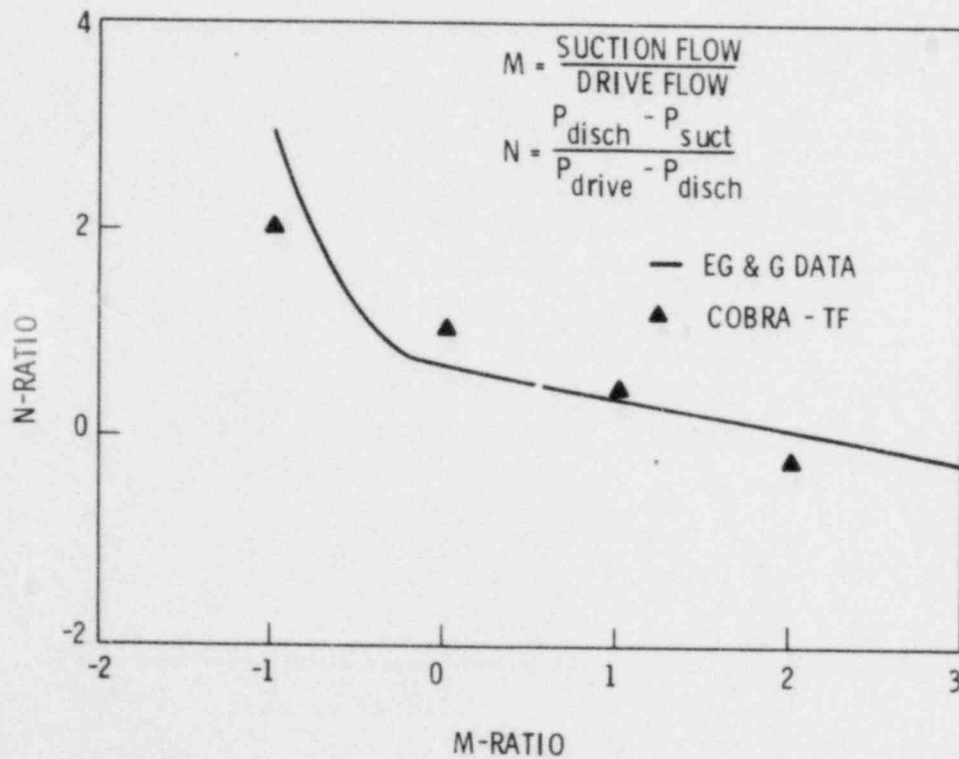
FIGURE 15. M-N Jet Pump Characterization Curve

21
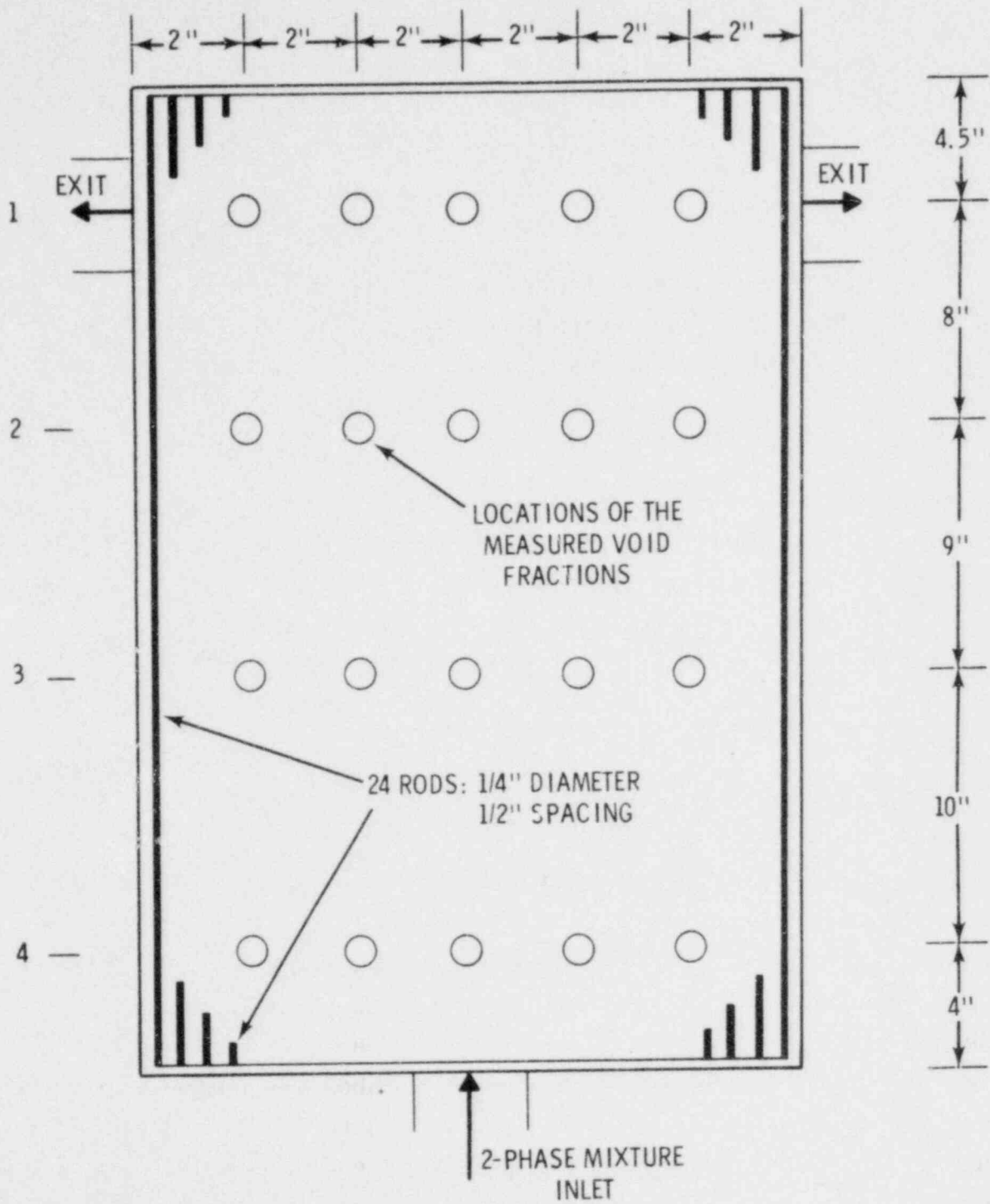
FIGURE 16. Rod Position Indicator Two-Dimensional Phase Separation Experimental Apparatus

Runs were made both with and without 24 simulated fuel rods of 1/4 in. diameter and 1/2 in. pitch. In addition, the mass withdrawal method was varied: in some cases all mass was removed from one side of the test section; in others it was equally split between the two outlets.

COBRA/TRAC MODEL

Two of the symmetric experiments were chosen for initial COBRA/TRAC simulation, although some nonsymmetric cases will also be simulated in the future. One run was made with the rods in and the other with rods out. Inlet conditions were a total mass flowrate of 206.53 lbm/min and an inlet quality of 0.257% (α_v = 0.6058).

The COBRA/TRAC noding is shown in Figure 17. The experiment was modeled using the vessel component, a short pipe at the exit, and a break. The air and water mixture was simulated using saturated steam and water at 40.7 psia. At this pressure, the vapor/liquid density ratio is the same as in the actual experiment. A transient was run from a standing start, with initially no vapor in the test section, until the change in the dependent variables was sufficiently small.

DATA COMPARISON

Figure 18 shows the computed and experimental void fraction distributions at four axial levels for the case with rods in. In order to compare data, the continuous RPI void distribution curves were visually averaged to obtain channel average values. The experimental results clearly show the affinity of the vapor phase for the high velocity region near the jet centerline. Unfortunately, the computed void distribution does not show the same behavior. In fact, the computed solution shows just the opposite trend at the middle axial levels. Also noteworthy is the underprediction of the void fraction in all channels at the lowest axial level.

Figure 19 shows results for the rods-out case. Experimentally, it appears that the absence of rods allows the void distribution to spread out quite rapidly downstream of the inlet, with the void fraction being slightly higher

23
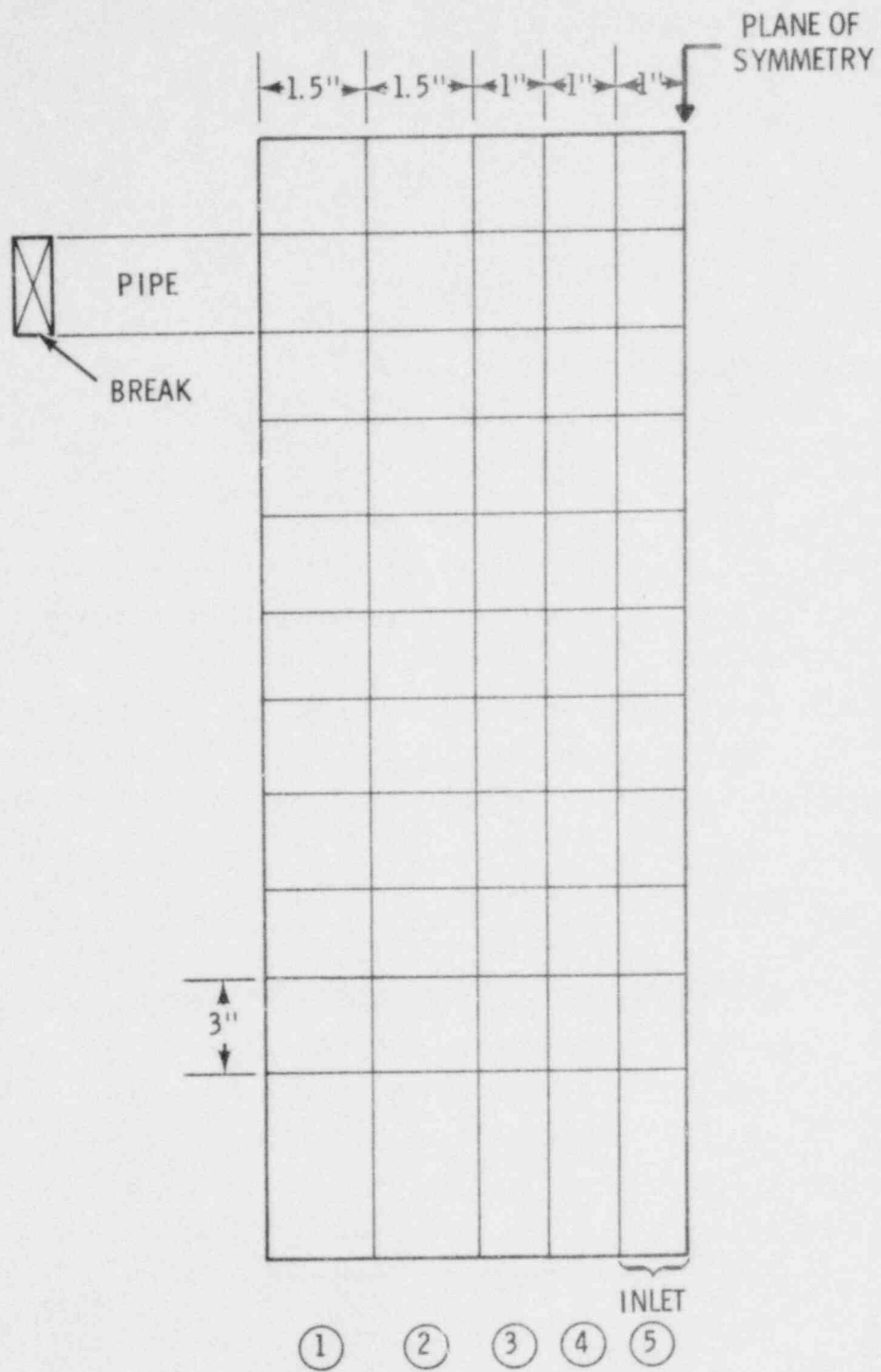
FIGURE 17. COBRA/TRAC Model of Rod Position Indicator Phase Separation Experiment
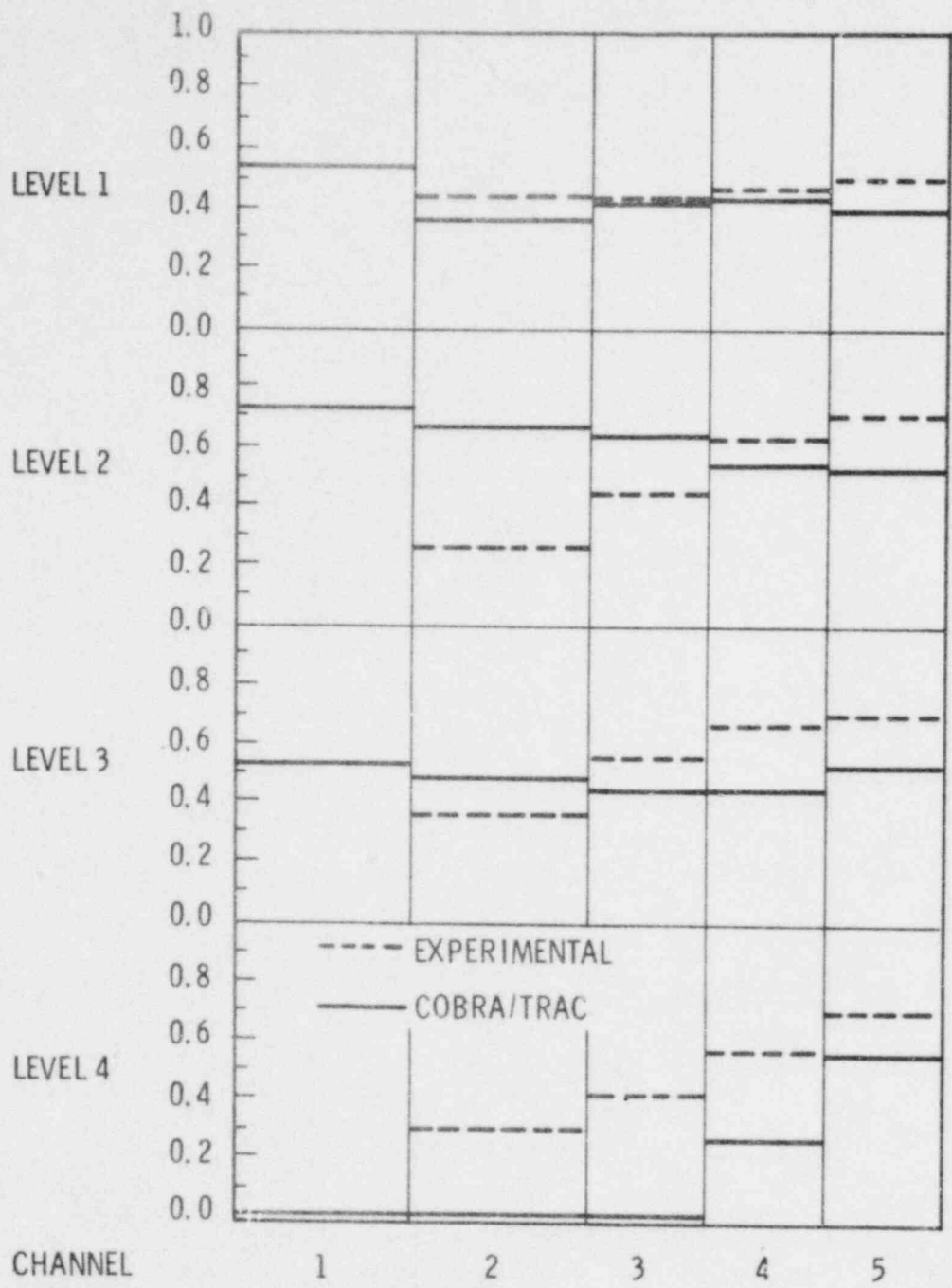
FIGURE 18. Void Fraction Distributions for Case with Rods In
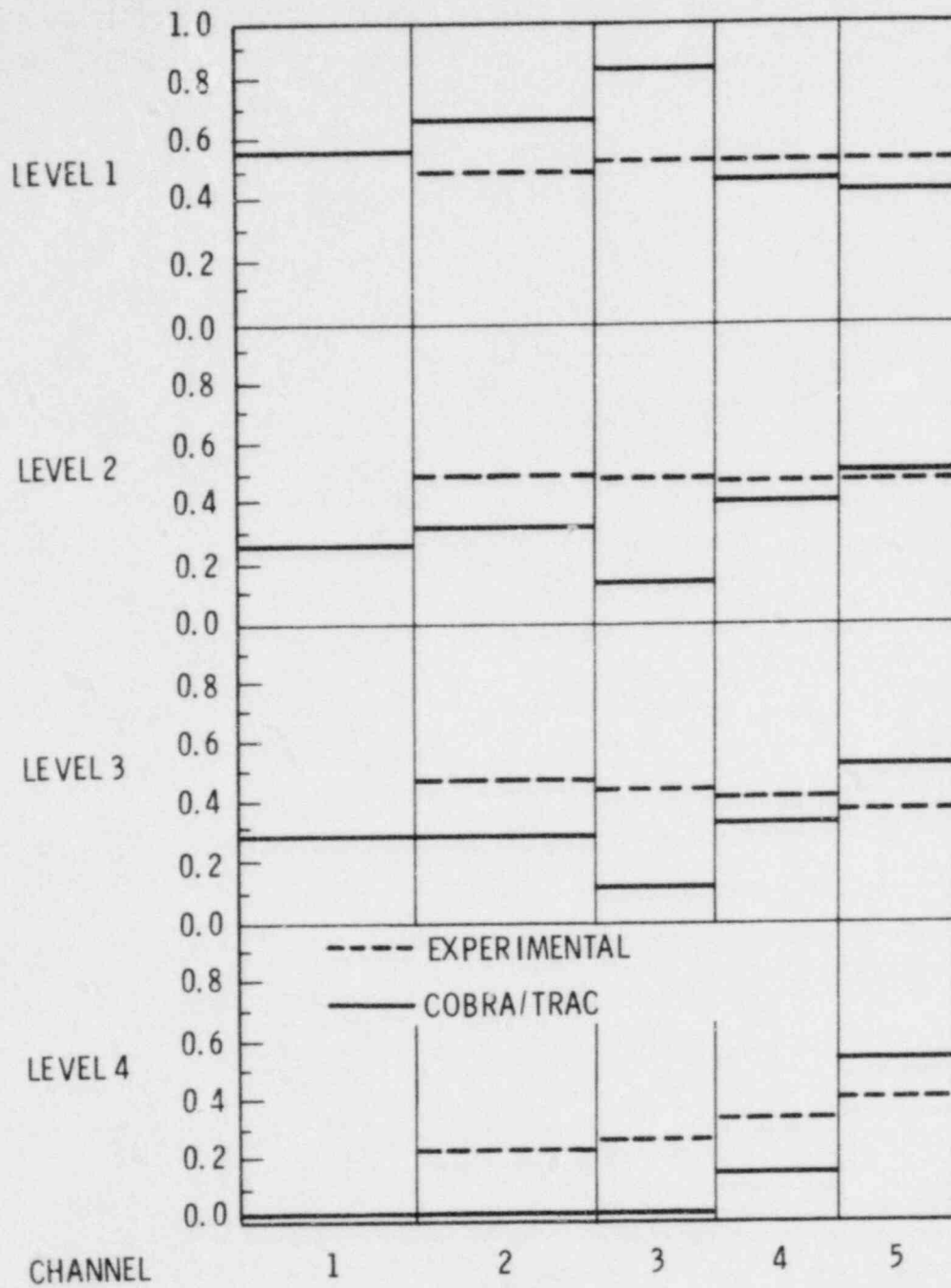
FIGURE 19. Void Fraction Distributions for Case with Rods Out

near the wall than at the jet centerline. A somewhat different trend appears in the computed solution. The void distribution is highly nonuniform at every axial level with generally a higher void fraction near the jet centerline. Also, the highly voided region centered in channel 3 near the top of the test section is not in agreement with the experimental data.

DISCUSSION OF RESULTS

Although there may be several reasons for the disagreement between computed and measured results, the most important is probably the lack of a turbulence model in the code. Experiments[7,8] have shown that the dispersed phase tends to migrate toward regions of high intensity continuous phase turbulence. It has been theorized[9] that the turbulent normal stresses are responsible for this behavior. Thus, by including a valid two-fluid turbulence model in the code, the calculations for both the rods-in and rods-out cases should improve.

The results should also be improved by including the viscous shear stresses on the continuous phase. In a rod bundle, these stresses may be negligible compared to the wall shear, but in other configurations they could be important. Their inclusion should definitely improve results for the rods-out case.

Future efforts will be directed to the formulation of turbulent and viscous stress models for the code. The models will be tested on the two experiments discussed above and also on some of the nonsymmetric RPI phase separation experiments.

The execution speed for these calculations was 0.0032 sec/Δt-cell on the CDC-7600. The steady state was achieved after 10 seconds of transient time, in each case using an average time step size of 0.00497 for the case with rods in and 0.00449 for the case with rods out.

EXPERIMENTAL DATA COMPARISONS - FLECHT REFLOOD TESTS

A series of FLECHT forced reflood experiments was simulated to assess the combined performance of the heat transfer, quench front, and "hot-wall"

27

entrainment model. Two of the tests (#3541 and #4321) were from the original FLECHT series[10] and had been simulated previously using the two-fluid version of COBRA-TF. The third test (#00904) is from the FLECHT low flooding rate cosine test series;[11] flooding rate is 1.5 in./sec. Attempts to model test #00904 with the two-fluid model were unsuccessful and resulted in the development of the "hot-wall" entrainment model.

COBRA/TRAC MODEL

The operating conditions for these tests are given in Table 1. Figure 20 details the noding used in the COBRA/TRAC model of the FLECHT facility. Two channels were used in the core section with a flow rate boundary condition applied at the beginning of the heated length. No attempt was made to model the details of the upper plenum and upper plenum de-entrainment. COBRA-TF was used to model all of the vessel/rod-bundle, and RAC-P1A components (a pipe and a break) were used to supply the pressure boundary condition in the upper plenum.

COMPARISON WITH DATA

Figure 21--clad temperature versus time for the hot rod, midplane--shows a comparison of the predicted and measured temperature histories for test #3541. Both turnaround time and peak temperature were predicted well; however, later in the transient the heat transfer was underpredicted, which resulted in higher clad temperatures and a later quench time. This discrepancy was not seen in the simulation of test #4321 and has since been determined to result from a discontinuity in the calculated critical heat flux as a function of mass

TABLE 1. Flecht Forced Reflood Tests

Run	TCLAD (^{O}F)	Peak Power (kw/ft)	Flooding Rate (in./sec)	TFLUID (^{O}F)	Pressure (psia)
3541	1598	1.24	5.9	148	57
4321	1608	1.24	3.9	151	58
00904	998	0.85	1.48	128	41

PRESSURE B.C.

FLOW B.C.
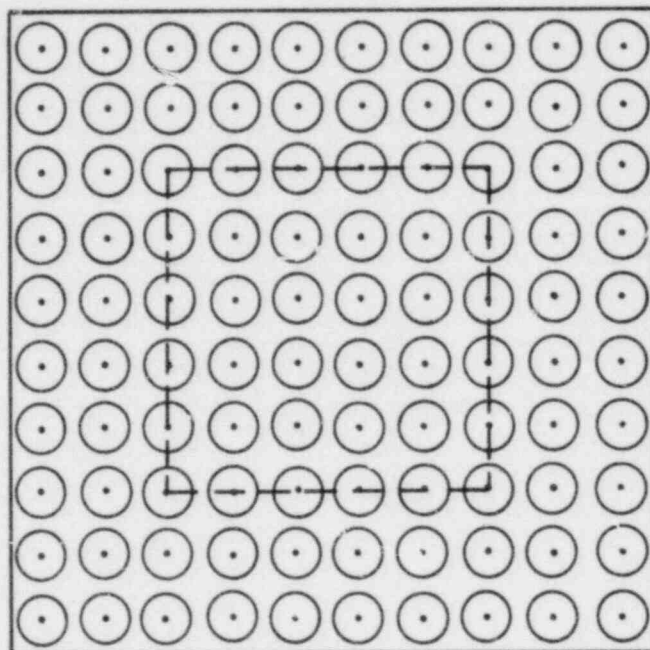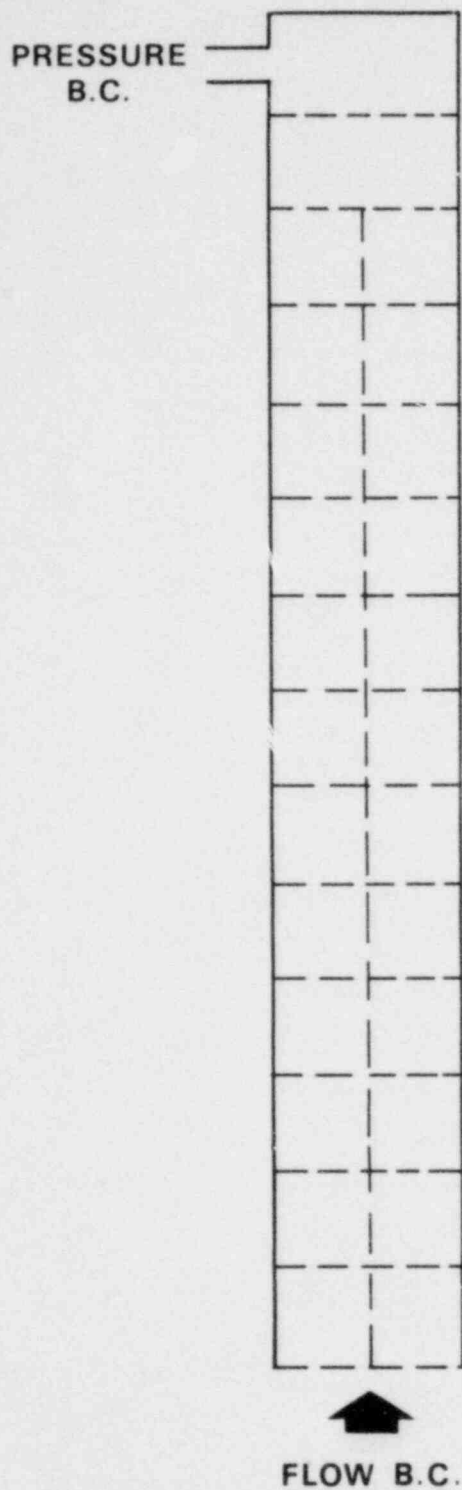
- TWO CHANNELS
  - 1 FOOT FLUID NODES

- FOUR HEAT TRANSFER SURFACES
  - CENTER CHANNEL
    - HOT ROD (10)
    - AVERAGE ROD (11.5)

  - EXTERIOR CHANNEL
    - AVERAGE ROD (69.5)
    - FLOW HOUSING

FIGURE 20. COBRA Flecht Model

29
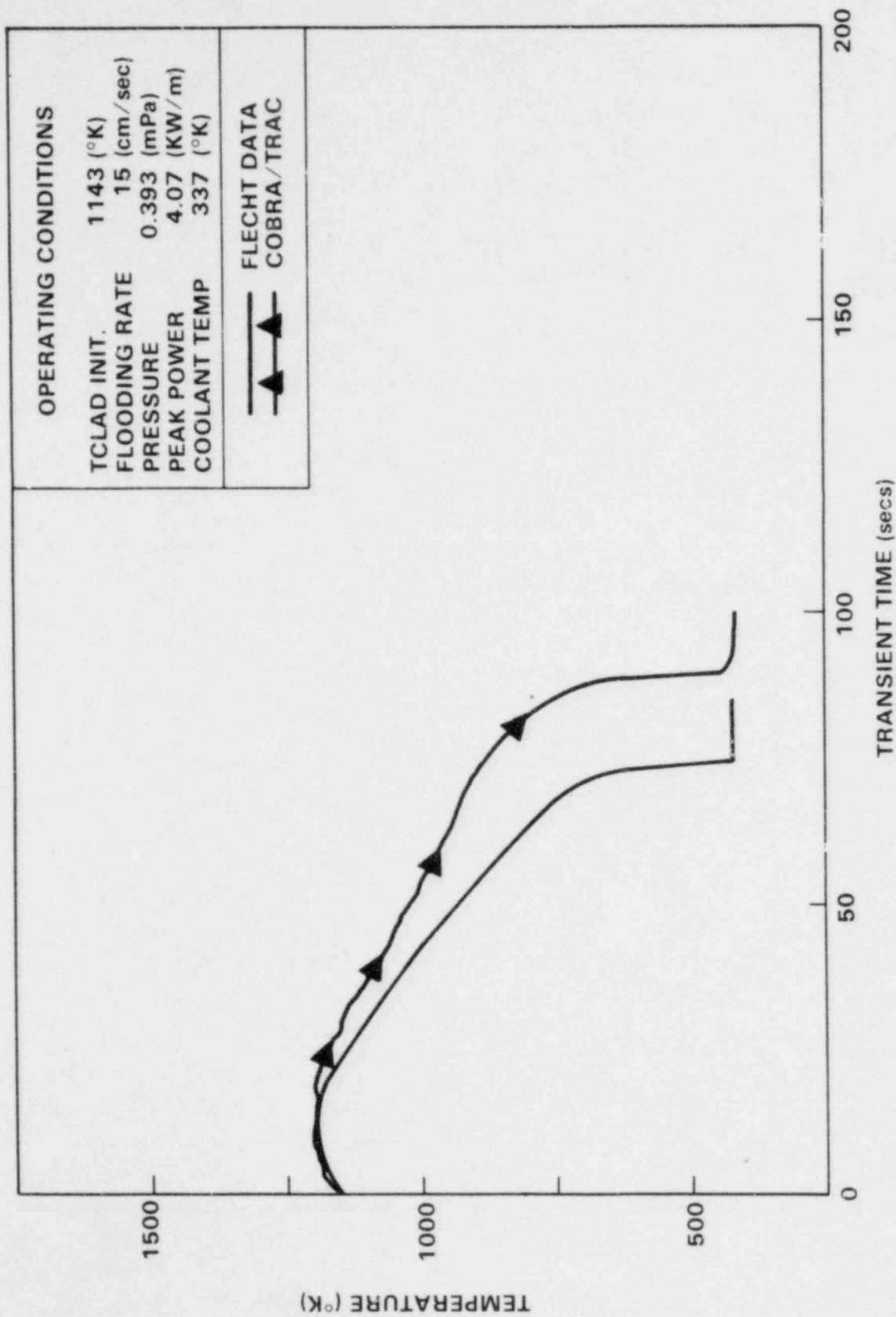
FIGURE 21. FLECHT Test 3541: Clad Temperature versus Time (hot rod, midplane)

30

flow rate. The mass flow rate in test #3541 was such that near the quench front the mass flux had approximately the same value as the logic switch between the two equations of the Biasi critical heat flux (CHF) correlation. Consequently, switching between equations resulted in oscillations that caused too much carryover and led to the poorer heat transfer.

Test #4321 is illustrated in Figure 22. Comparison between calculation and experiment is very good for the entire transient. As noted above, because the flooding rate of test #4321 was lower than that of test #3541, the CHF correlation switching oscillations were not present in this simulation.

Test #00904, shown in Figure 23. is a low flooding rate test (1.5 in./sec). It is differentiated from the two previous tests in that the major mode of heat transfer is dispersed flow film boiling rather than inverted annular film boiling. During the first 75 seconds of the transient, the rod heatup is predicted well; however, between 75 and 150 seconds during a period of dispersed flow film boiling, the heat transfer was seriously underpredicted. At this time the quality was approximately 40 to 50% and the void fraction was 0.996. After 150 seconds, the froth level reached the 6-ft elevation and inverted annular film boiling was established until 190 sec, when rewet occurred and the rod quenched.

There was a discrepancy in cladding temperature histories during the precursory cooling period. However, the excellent agreement between measured and predicted void fractions depicted in Figures 24 through 26 illustrates the ability of the "hot-wall" entrainment model, coupled with the three-field formulation, to model reflood entrainment. The experimental void fractions were determined from the output of pressure difference cells located every two feet along the bundle. These void fractions are an indicator of the liquid mass inventory in the bundle and are especially important in low reflood rate tests. For example, in test #00904, approximately 25% of the inlet mass flow is boiled off and another 60% is carried over as entrained liquid droplets, which leaves just 15% of the inlet flow to contribute to the liquid mass inventory. Consequently, a small error in the entrainment can, when integrated over time, lead to a large discrepancy in the mass inventory and result in predicted quench times that are very different from the experiment results.

31
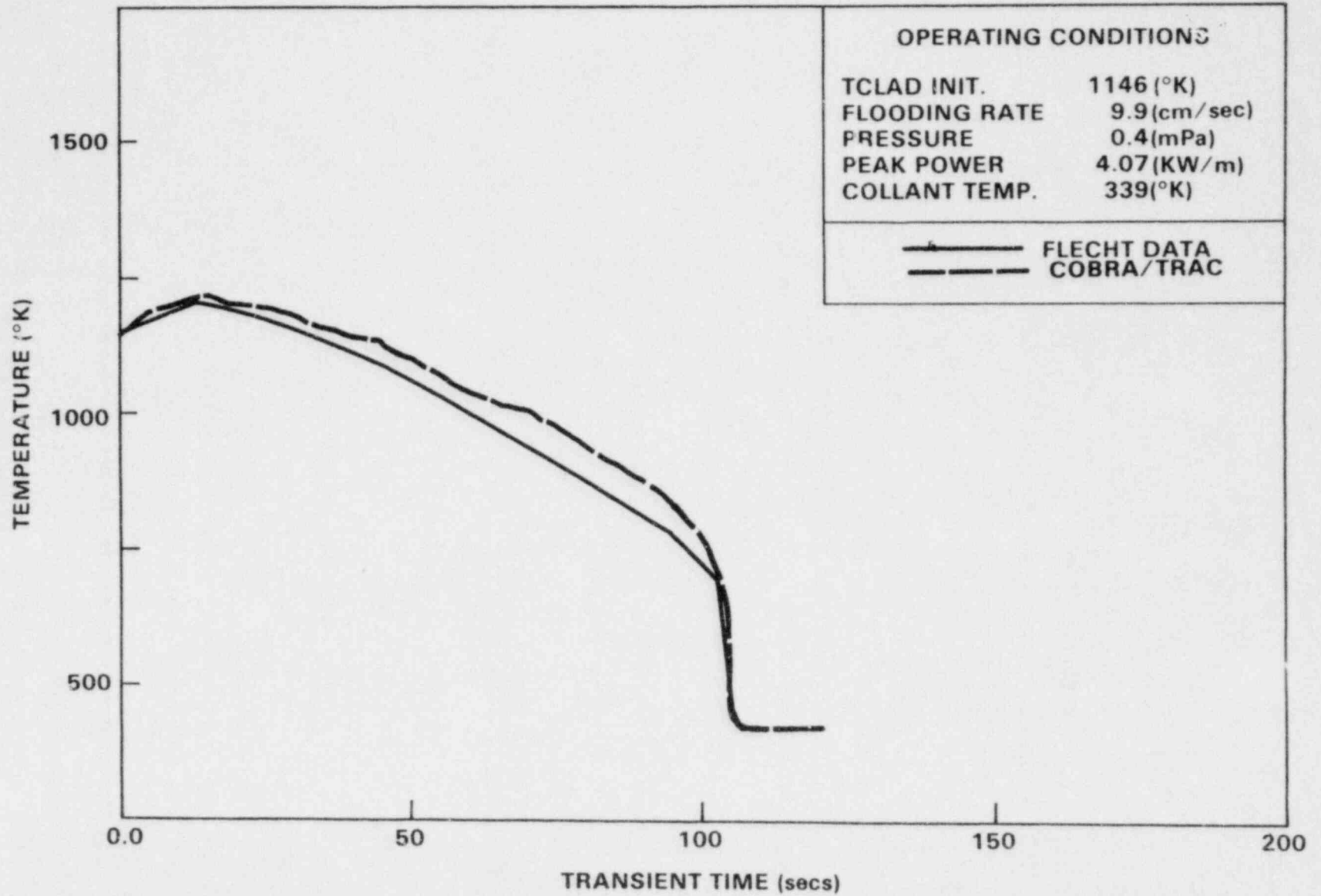
FIGURE 22. FLECHT Test 4321: Clad Temperature Versus Time (hot rod, midplane)
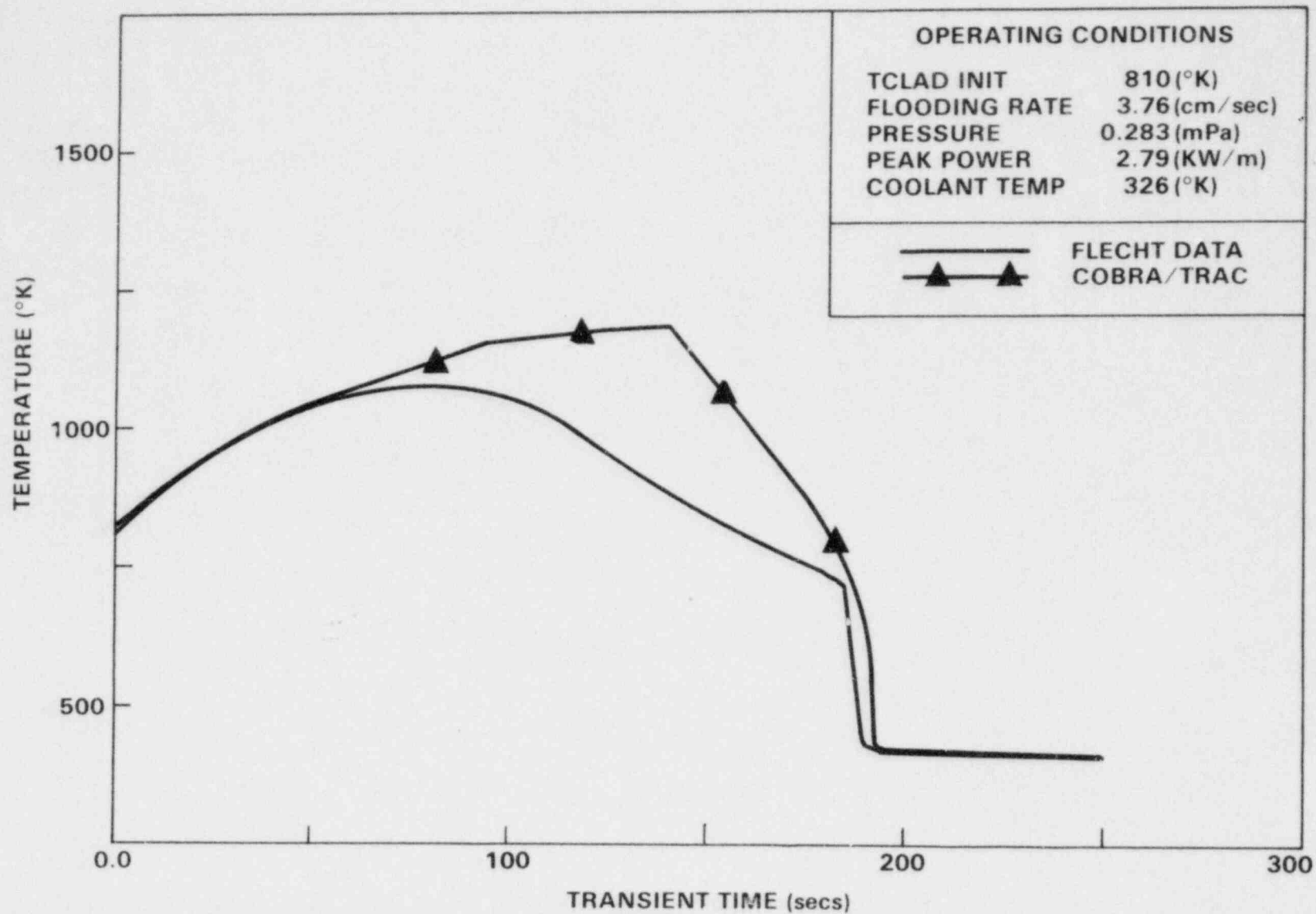
FIGURE 23. FLECHT Test 00904: Clad Temperature Versus Time (hot rod, midplane)
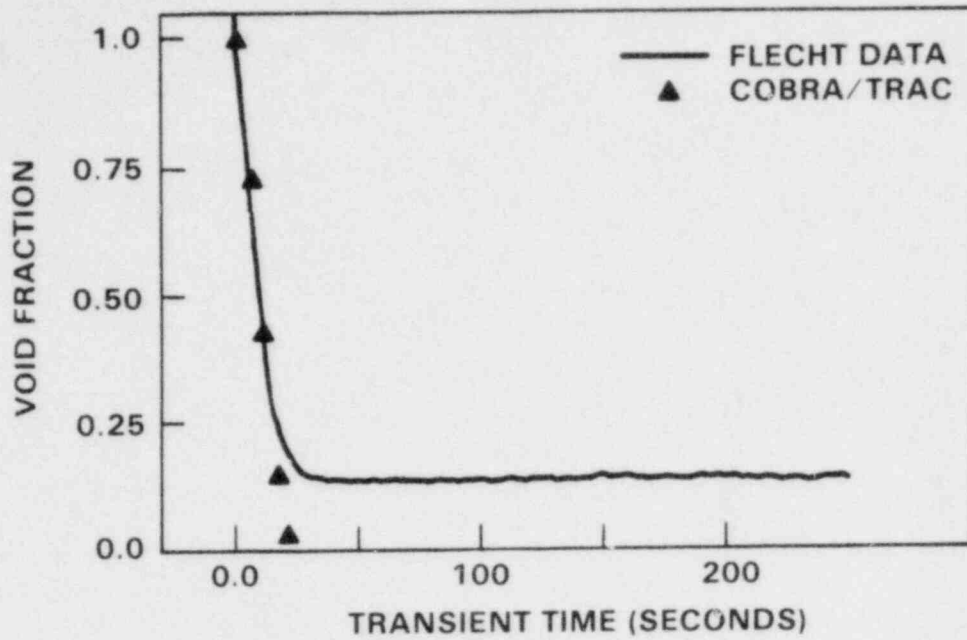
FIGURE 24.   FLECHT-Low Flooding Rate Test 00904 - Void
Fraction Versus Time for 0-2 ft Level
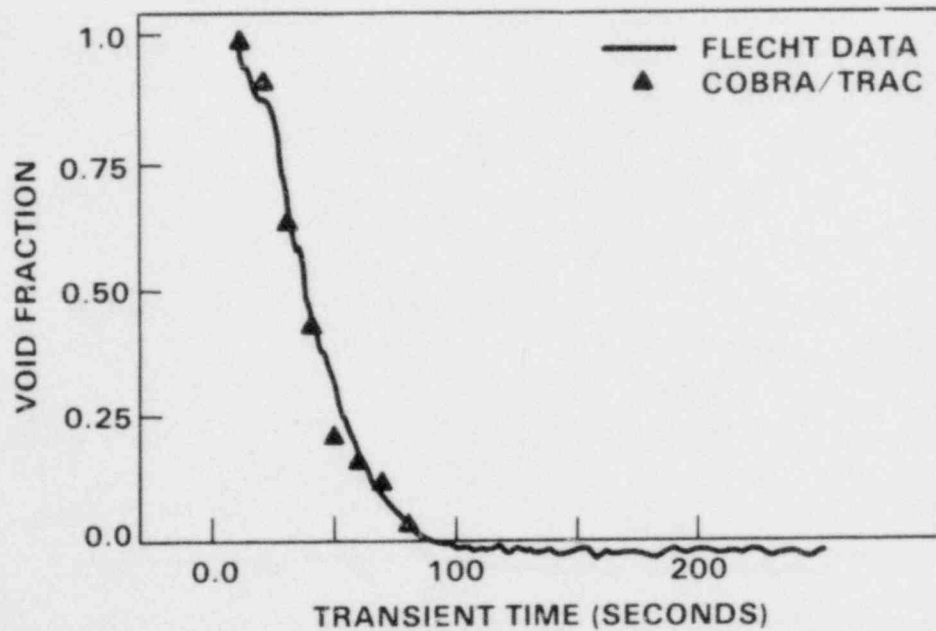
FIGURE 25.   FLECHT-Low Flooding Rate Test 00904 - Void
Fraction Versus Time for 2-4 ft Level
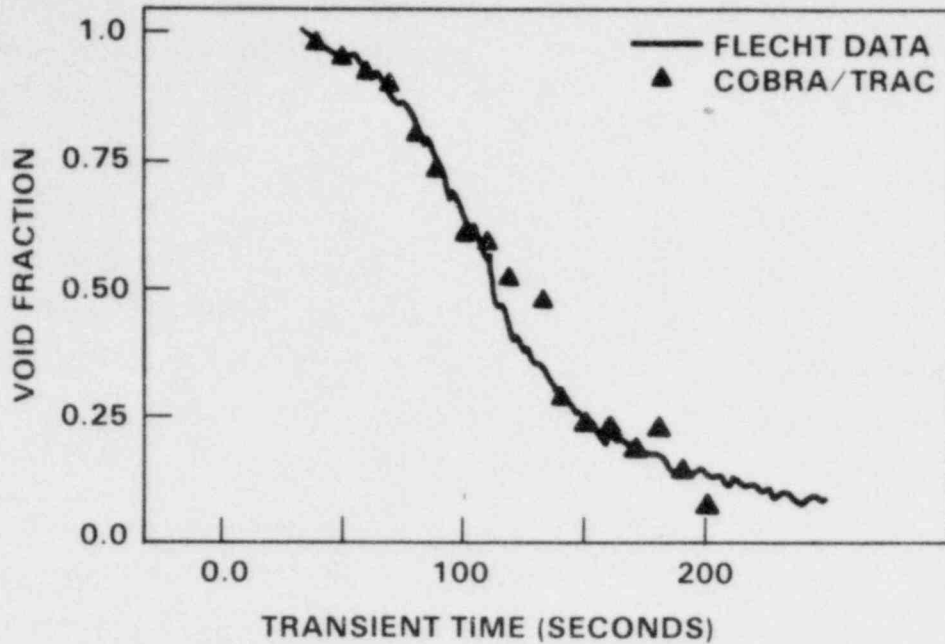
FIGURE 26. FLECHT-Low Flooding Rate Test 00904 - Void
Fraction Versus Time for 4-6 ft Level

It was felt that the fluid conditions for test #00904 were predicted quite
well and that the discrepancy in dispersed flow heat transfer rates during the
75 to 150-sec period was due to not enough credit being taken for droplet heat
transfer mechanisms. Upon closer examination it was discovered that:

- an error existed in the equation that calculated radiation to
  droplets

- use of the Goeneveld-Hadaller steam convection equation was
  inappropriate for lower mass flowrates.

In fact, during the simulation of test #00904, the calculated radiative heat
transfer was negligible, but when the correction was made, approximately 20 to
25% of the total rod heat flux was due to droplet radiation. The Groeneveld-
Hadaller correlation is based on data taken from mass fluxes greater than 30
$(gm/cm^2 sec)$; whereas the mass flux was approximately 3 $(gm/cm^2 sec)$, and
for these conditions the Groeneveld-Hadaller correlation predicted convective
heat transfer coefficients of less than the single-phase vapor (Dittus-Boelter)

flowing alone in the channel. Consequently, for low mass flow rates, the Groeneveld-Hadaller correlation was replaced with the Chen low flow-rate film-boiling correlation.

After the above changes were implemented, a new single-channel (12 nodes in the core, 2 nodes in the upper plenum) model of the FLECHT test section was set up and test #00904 was rerun. The comparison between measured and predicted clad temperature histories (Figure 27) at the 6-ft elevation showed significant improvement over the previous simulation. As a result of this simulation, the "hot-wall" entrainment model and heat transfer fixes are being implemented in the latest version of the code.

An example of the enhanced entrainment modeling capability of the three-field model is shown in Table 2, which is a copy of code output for test #00904. The treatment of the fluid in the froth region as a two-group drop model (large and small droplets) results in the maintenance of a sharp liquid level interface virtually eliminating numerical diffusion and predicted void fractions and droplet sizes (0.9⁵ and 0.050 in., respectively) in the range of those observed in the FLECHT movies.

For the test simulation (#00904), the CPU time compared to real transient time was 11.8 sec. to 1.0 sec.

FUTURE WORK

Additional developmental assessment calculations will be performed during the next quarter. The physical models used in the code will be improved as the results of data comparisons dictate. Further work on the JAERI reflood experiments will also be reported.
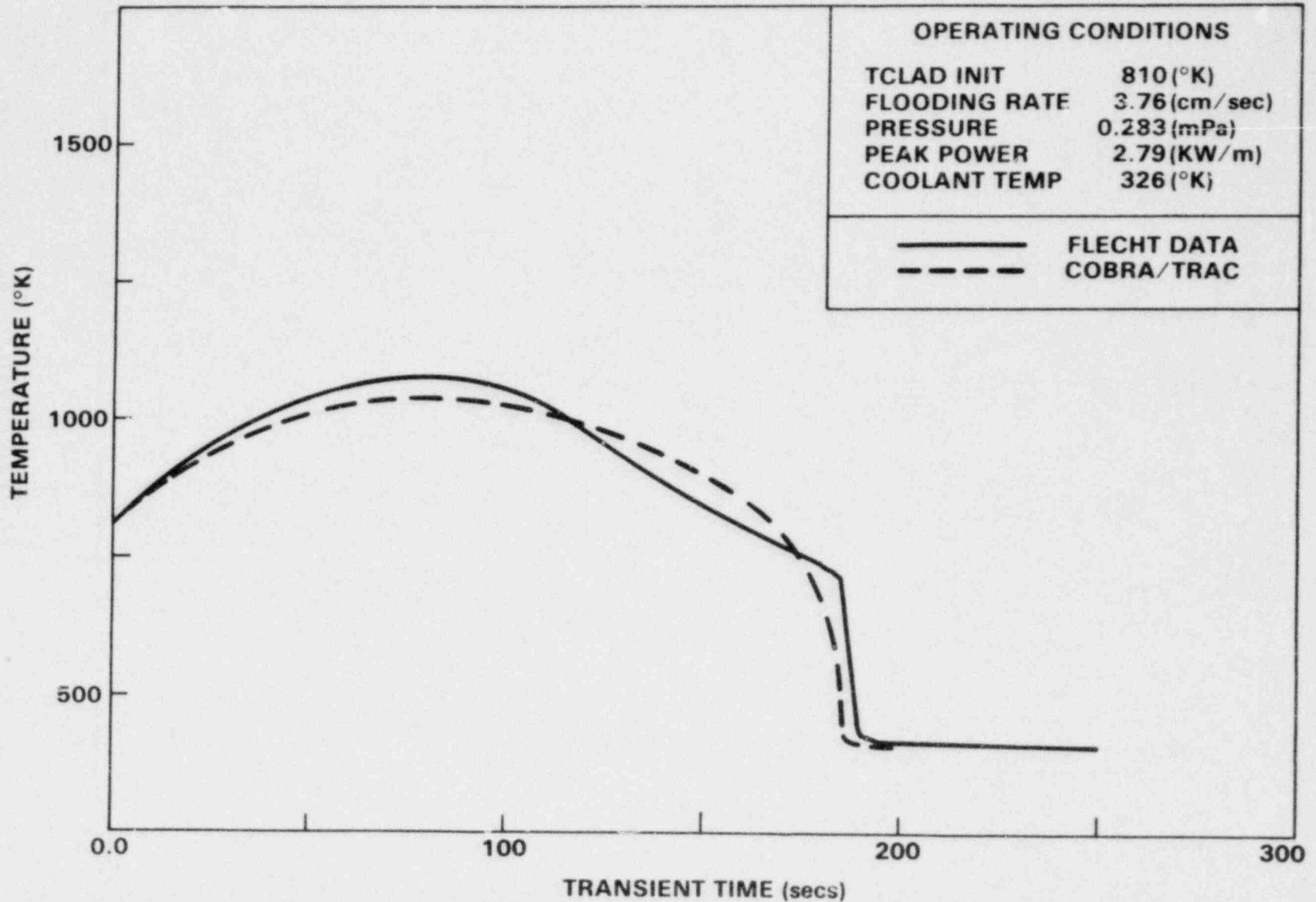
FIGURE 27. FLECHT Test 00904: Clad Temperature Versus Time (hot rod, midplane)

TABLE 2. Output for Test Number 00904
(Simulation Time = 49.99405 Seconds)

NDDF No.	Dist. (ft)	Pressure (psi)	Velocity (ft/sec)			Void Fraction		
			Liquid	Vapor	Entr.	Liquid	Vapor	Entr.
14	13.00	41.014	0.00	66.28	31.38	0.0000	0.9968	0.0032
13	12.00	41.051	0.00	64.76	33.31	0.0000	0.9969	0.0031
12	11.00	41.086	0.00	63.93	32.11	0.0000	0.9967	0.0033
11	10.00	41.108	0.00	62.73	30.78	0.0000	0.9964	0.0036
10	9.00	41.142	0.00	61.64	29.44	0.0000	0.9962	0.0038
9	8.00	41.166	0.00	58.59	28.14	0.0000	0.9959	0.0041
8	7.00	41.198	0.00	54.50	27.22	0.0000	0.9957	0.0043
7	6.00	41.224	0.00	46.39	26.64	0.0000	0.9955	0.0045
6	5.00	41.212	0.00	38.55	26.74	0.0552	0.9402	0.0045
5	4.00	41.443	0.00	79.27	29.59	0.6783	0.3182	0.0035
4	3.00	41.833	0.12	38.98	39.64	0.9870	0.0130	0.0000
3	2.00	42.244	0.13	0.13	0.13	0.9979	0.0021	0.0000
2	1.00	42.666	0.12	0.12	0.12	1.0000	0.0000	0.0000
1	0.00	41.010	0.12	0.00	0.12	1.0000	0.0000	0.0000

REFERENCES

1. A. E. Dukler, Two-Phase Interactions in Counter-Current Flow Studies of the Flooding Mechanism, Progress Report, NUREG-0214, June 1977.*

2. Lovell, T. W., The Effect of Scale on Two-Phase Counter-Current Flow Flooding in Vertical Tubes, M.S. Thesis, Thayer School of Engineering, Dartmouth College, June 1977.

3. Richter, H. J., et al., The Effect of Scale on Two-Phase Counter-Current Flow Flooding, NUREG/CR-0312, June 1978.*

4. C. J. Crowley, J. A. Block and C. N. Cary, Downcomer Effects in a 1/15-Scale PWR Geometry, Experimental Data Report, CREARE, Inc., NUREG-0281, May 1977.*

5. H. S. Crapo, Code Assessment and Applications Program, Quick-Look Report for Jet Pump Tests, CAAP - TR-78-030, October 1978.

6. R. T. Lahey, Jr., Two-Phase Phenomena in Nuclear Reactor Technology, Quarterly Progress Report No. 8, NUREG/CR-0418, October 1978.*

7. A. Serizawa, et al., "Turbulent Structure of Air/Water Bubbly Flow," International Journal of Multiphase Flow, Vol. 2, 1976.

8. R. T. Lahey, Jr., et al., Subchannel and Pressure Drop Measurements in a Nine-Rod Bundle for Diabatic and Adiabatic Conditions, GEAP-13049, March 1970.

9. S. K. Sim, Analysis of Phase Distribution Mechanisms in Turbulent Two-Phase Pipe Flow, M.S. Thesis, Rensselaer Polytechnic Institute, Troy, NY, 1977.

10. J. O. Cermak, et al., PWR Full Length Emergency Cooling Heat Transfer (FLECHT) Group 1 Test Report, WCAP-7435, 1970.

11. E. R. Rosal, et al., FLECHT Low Flooding Rate Cosine Test Series Data Report, WCAP-8651, December 1975.

---

*Available for purchase from the NRC/GPO Sales Program, U.S. Nuclear Regulatory Commission, Washington, DC 20555, and the National Technical Information Service, Springfield, VA 22161.

FUEL SUBASSEMBLY PROCUREMENT AND IRRADIATION TEST PROGRAM[a]

C. L. Mohr, Program Manager
E. L. Courtright, Project Manager
R. L. Goodman
G. M. Hesson
L. L. King
R. F. Klein
D. D. Lanning
R. R. Lewis
R. K. Marshall
J. D. Rising
R. E. Schreiber

SUMMARY

Substantial progress was made on the detailed core region design for the 9-rod test train. Interface arrangements were made with EG&G, Idaho, regarding schedule, design parameters, and the scope of the program. Long lead items, including major instrumentation and materials, are on order, and negotiations have begun with the potential component suppliers.

Arrangements were made with EG&G to evaluate scram data obtained during the preconditioning phase of LOC-3. This data will be analyzed to determine the thermal resistance of rods containing internal centerline thermocouples.

Preliminary planning for the ESSOR Reactor Test Support Program was completed. Schedules and milestones for developing the conceptual hardware to meet program objectives were established.

INTRODUCTION

The Fuel Subassembly Procurement and Irradiation Test Program has been divided into four tasks for FY 1980. The objectives of these tasks are:

- Task A - <u>Power Burst Facility (PBF) Test Train Hardware</u>. This task will provide instrumented test train hardware for selected PBF

---

[a] RSR Fin. Budget No: B2084; RSR Contact: R. Van Houten

experimental programs. Assembly hardware will include replacement quadrants for RIA type 4-rod test trains and a fully instrumented 9-rod test assembly for the RIA 1-7 and OPTRAN 1-3 experiments.

- Task B - Gap Conductance Test Analysis. This task will provide testing methodologies and analysis techniques for obtaining fuel rod thermal performance data from PBF experiments. Post-test analysis and data interpretation of experimental results will be provided.

- Task C - Dual Purpose Assemblies. This task is responsible for transferring IFA-513 dual purpose test rods currently under steady-state irradiation in Halden to PBF for subsequent transient testing.

- Task D - Multi Rod Test Trains - ESSOR Project. The scope of this project includes provisions for supplying fully instrumented and fueled test assemblies, analytical services, and engineering support for the ESSOR Reactor Test Program at Ispra, Italy. The program is designed to yield important experimental data related to fuel rod deformation and post-accident coolability of damaged fuel rod clusters after small-break, medium-break, or large break loss-of-coolant accidents.

PBF TEST TRAIN HARDWARE

4X QUADRANTS

Five 4X strongback assemblies--complete with pads, SPND mounting brackets, and high-pressure connector mounting brackets--were completed. The strongback assemblies have been through receiving inspection and are released for assembly and outfitting of the individual quadrants.

Calibration of the turbine flowmeters for the replacement quadrants were completed. The calibration data collected at Pacific Northwest Laboratory (PNL) show excellent agreement with the calibration curves supplied by the manufacturer. Also, the lower instrumentation packages were assembled.

All machined components for the quadrant assemblies have been received from off-site shops and have been through receiving inspection and released for final quadrant assembly and outfitting. Fabrication of high-pressure connector components was started with the replacement of a purchase order to an outside vendor.

A preliminary fit up of hardware and strongbacks complete with hanger tubes was performed. The results of the fit up indicate that there are no major problems in quadrant interchangeability.

9-ROD ASSEMBLY

A preliminary design review for the 9-rod RIA 1-7 and OPTRAN 1-3 test assembly was held at PNL. A Design and Fabrication Plan and a QC Planning Document were issued. Interface agreements between PNL and EG&G were also established.

Detailed design of the core region components was nearly completed and design work on other modules of the test train initiated. The decision was made to subcontract major component fabrication and instrument installation with a single source. Potential suppliers were invited to examine the preliminary designs for an expression of interest and agreement with the proposed schedule. Follow-up discussions of design details and visits to fabrication facilities were initiated. Long-lead instrumentation items were ordered, and critical materials have been located for early order placements.

GAP CONDUCTANCE TEST ANALYSIS

Discussions with EG&G indicate that scram data from LOC-3 and programmed "mini-transient" data from LOC-5 would be suitable for gap conductance data analysis work. These data will be sent to PNL for analysis during the next quarter.

43

MULTI-ROD TEST TRAINS - ESSOR PROJECT

Detailed task structures, objectives, and scheduled milestones for FY 1980 were prepared. A subcontract was placed with EG&G, Idaho, to determine the radiant and convective heat transfer energy losses for a 36-rod bundle in the SUPERSARA test loop, exposed to both small-break and large-break test conditions. This contract also provided consultation services to assist the ISPRA staff in obtaining facility approval for ESSOR to operate under fission power during a blowdown.

FUTURE PLANS

TASK A - PBF TEST TRAIN HARDWARE

Final assembly of the 4X replacement quadrants will be completed upon receipt of the differential Copper-Constantan thermocouples.

Decisions will be made regarding on-site or off-site grid fabrication and hydraulic testing of the 9-rod test train and its components. The in-cell and in-canal remote handling ___, fixtures, and handling tools will be developed. Detailed test train design will be completed by March 1, 1980.

TASK B - GAP CONDUCTANCE ANALYSIS

Scram data obtained from LOC-3 and GC-2 will be reviewed. A characterization of initial steady-state data will be established first and then the thermal resistance versus power curves prepared from the transient data.

TASK C - DUAL PURPOSE ASSEMBLIES

The IFA-513 assembly is currently under irradiation at Halden. No further work is planned until this assembly is ready for discharge near mid CY 1981.

TASK D - MULTI-ROD TEST TRAINS - ESSOR PROJECT

Radiation heat transfer calculations to determine the pressure vessel and shroud temperatures in the SUPERSARA test loop during the most severe

small-break and large-break conditions will be completed. Estimates of steam temperature super heat will also be made for the postulated test conditions. A conceptual assembly design capable of handling program objectives will be proposed and discussed with members of the Ispra Staff.

EXPERIMENTAL SUPPORT AND DEVELOPMENT OF SINGLE-ROD FUEL CODES:

TASK A - IRRADIATION EXPERIMENTS[a]

D. D. Lanning, Program Manager
D. D. Lanning, Task Leader
M. E. Cunningham
R. E. Williford

SUMMARY

This task is concerned with coordination of the test fuel irradiations on instrumented fuel assemblies (IFAs) performed for the Nuclear Regulatory Commission (NRC) at Halden, Norway. The purpose of these tests is to obtain reliable independent data on the thermal/mechanical behavior of fuel for fuel modeling code development.

The irradiation test (IFA-431) has been completed. Currently, two other test assemblies are under irradiation (IFA-513 and IFA-432). The fourth and final test in the program (IFA-527) is under construction and will begin irradiation in early 1980.

Progress this quarter has centered on finalizing plans for the post-irradiation examination of IFA-432.

INTRODUCTION

This program is the continuation of the Experimental Support and Verification of Steady-State Fuel Codes program (begun in 1974). The program now has the following general objectives:

- collecting and analyzing in-reactor data on fuel rod thermal/ mechanical behavior, especially as a function of burnup

- correlating the irradiation data with detailed post-irradiation data and with ex-reactor tests on mechanical and thermal parameters of fuel rods

---

- integrating all this information into the FRAPCON and FRAP-T series
  of fuel modeling codes.

The Halden Reactor in Norway was chosen as the site for the irradiation tests. Task A of this program is concerned with the conduct of those tests and the necessary coordination activities (test rig design, safety analysis, fuel shipments, post-irradiation examination procedures, fuel disposal, etc.). Considerable coordination is required because post-irradiation examination will be performed at Kjeller, Norway, and Harwell, UK, and all test fuel rods will be returned to the United States either for transient testing or disposal.

Table 1 summarizes the design and instrumentation of the four 6-rod test assemblies in the program. A matrix has been established covering the effects of fuel-cladding gap size, fuel density, and resistance to densification. Note that IFA-431 has completed irradiation and post-irradiation examination; IFA-513 and IFA-432 are still under irradiation; and IFA-527, specifically designed to study the effects of fuel cracking and relocation, will begin irradiation in March 1980.

TECHNICAL PROGRESS

The IFA-432 and IFA-513 fuel assemblies continued an uneventful irradiation this quarter. However, there has been some failure of instrumentation in both assemblies. The current status of the instrumentation is summarized in Table 2.

The fuel rods and assembly hardware for IFA-527 have been prepared, and the instruments are undergoing calibration. The construction is on schedule.

Arrangements were finalized by Pacific Northwest Laboratory (PNL), Halden, and Harwell for the discharge, shipment, and mechanical compliance testing of Rod 8, IFA-432 at Harwell, UK. This rod will be shipped from Halden to Harwell in March or April 1980 together with EG&G fuel at an overall cost savings to the NRC. It has been concluded that the main group of IFA-432 rods will not be discharged until August 1981 and that all of the IFA-432 rods will be destructively examined. Rods 2, 3, 4, and 9 will remain at Kjeller, and Rods 1, 5, 6, 8 and (unirradiated) Rod 7 will go to Harwell, UK.

48

TABLE 1. Experimental Matrix for NRC/PNL Halden Fuel Assemblies

Assembly & Rod	Power,(a) kW/m	Fuel(b) Type	Diametral Gap, μm			Initial Fill Gas			Detectors(c)				
			50-75	230	380	100% He 0.1 MPa	100% He >0.1 MPa	Xe 0.1 MPa	UTC	LTC	ES	PT	SPND
IFA-431	35/25												7
1		95S		x		x			x	x	x	x	
2		95S			x	x			x	x	x		
3		95S	x			x			x	x	x		
4		95S		x				100%	x	x	x		
5		92S		x		x			x	x	x	x	
6		92U		x		x			x	x	x	x	
IFA-432	50/35												7
1		95S		x		x			x	x	x	x	
2		95S			x	x			UT	x	x		
3		95S	x			x			x	x	x		
4		95S		x				100%	x	x	x		
5		92S		x		x			x	x	x	x	
6		92U		x		x			x	x	x	x	
IFA-513	40/28												9
1		95S		x		x			x	x	x	x	
2		95S		x			0.3 MPa		x	x	x	x	
3		95S		x		x			x	x	x	x	
4		95S		x				8%	x	x	x	x	
5		95S		x		x			x	x	x	x	
6		95S		x				23%	x	x	x	x	
IFA-527(d)	10/14												9
1		95S	x					100%	x	x	x	x	
2		95S		x				100%	x	x	x	x	
3		95S		x				100%	x	x	x	x	
4		95S		x				100%	x	x	x	x	
5		95S		x				100%	x	x	x	x	
6		95S		x				100%	x	x	x	x	

(a) Linear power is given for upper and lower thermocouple positions, respectively.
(b) Three fuel types are used, all enriched to 10% U-235.
  95S = 95% TD, Stable
  92S = 92% TD, Stable
  92U = 92% TD, Unstable
(c) UTC = Upper Thermocouple
  LTC = Upper Thermocouple
  ES = Elongation Sensor
  PT = Pressure Transducer
  SPND = Self-Powered Neutron Detector
  UT = Ultrasonic Thermometer
(d) IFA-527 will be positioned in the upper portion of the core. As a result, the assembly's peak linear heat rate will be at the lower thermocouple position.

TABLE 2. Instrument Status[a]

Assembly Rod	Pressure Transducers	Upper Thermocouples	Lower Thermocouples	Elongation Sensors	Neutron Detectors
IFA-432					
Rod 1	R	X	R	X	All ok except Co-detector
Rod 2	-	-	U	R	
Rod 3	-	U	R	X	
Rod 4 (8)	-	-	-	R	
Rod 5	R	X	R	X	
Rod 6	U	X	U	R	
IFA-513					
Rod 1	X	R	R	R	All ok
Rod 2	U	X	R	R	
Rod 3	R	X	R	R	
Rod 4	R	R	R	X	
Rod 5	X	X	R	R	
Rod 6	R	U	R	X	

(a) Symbols: R = Reliable
             U = Unreliable
             X = Not Functioning
             - = Not Installed

A supplement to BSA-963 (PNL-Halden agreement) was completed this quarter that details the cost for construction, irradiation, and special handling for IFA-527, as well as post-irradiation costs for IFA-432. In addition, the project planning document for the program was completed and approved.

FUTURE PLANS

The major events of next quarter in this task will be the startup of IFA-527, the shipment of Rods 7 and 8 (IFA-432), and the compliance testing of Rod 8 at Harwell, UK.

EXPERIMENTAL SUPPORT AND DEVELOPMENT OF SINGLE-ROD FUEL CODES:

TASK B - DATA QUALIFICATION AND ANALYSIS[a]

D. D. Lanning, Program Manager
M. E. Cunningham, Task Leader
E. R. Bradley
C.   Nealy
W. N. Rausch
R. E. Williford

SUMMARY

A major objective of the Experimental Support and Development of Single-Rod Fuel Codes is the irradiation of instrumented fuel assemblies (IFAs) to obtain well-characterized data. Task B of this program is responsible for qualifying and analyzing this data. This quarter, a data tape covering the period July-August 1979 was received and corrected, three reports were published, and work continued on the four major areas of analysis: fuel relocation, transient temperatures, error propagation, and fission gas release.

INTRODUCTION

The Experimental Support and Development of Single-Rod Fuel Codes Program is a continuation of the Experimental Support and Verification of Steady-State Codes Program (begun in 1974). This program now has the general objectives of collecting and analyzing in-reactor data on fuel rod temperatures, fission gas release, and cladding elongation as a function of irradiation history; correlating post-irradiation examination with the in-reactor data; utilizing ex-reactor testing for a better understanding of fuel rod mechanical behavior; and integrating all of this information into the FRAPCON computer code. The qualification and analysis of the data obtained from in-reactor testing of fuel rods is the responsibility of Task B of this program.

The work in this task is divided into three subtasks:

- Subtask B-1: Data Processing

This subtask is responsible for receiving, correcting, characterizing, and presenting the data obtained from the fuel assemblies.

- Subtask B-2: Data Reports

This subtask is responsible for preparing reports on the precharacterization of the fuel assemblies, the data obtained from the assemblies, and the post-irradiation analysis of the assemblies.

- Subtask B-3: Data Analysis

This subtask is responsible for providing in-depth analysis of the in-reactor fuel rod data obtained. Specific areas of interest for FY 1980 are analysis of data for inferring fuel relocation and its effect, use of transient temperature data to better understand fuel behavior, analysis of statistical variations and error propagation, and analysis of fuel rod fill gas pressure data for inferring fission gas release.

The activities related to these subtasks are discussed below.

SUBTASK B-1: DATA PROCESSING

During this quarter, one data tape (covering the period July 6 - August 29, 1979) was received, corrected, and made available for analysis.

SUBTASK B-2: DATA REPORTS

Two reports were published this quarter. The first dealt with analysis of the xenon-filled fuel rods in IFA-431 and IFA-432 (Cunningham, Lanning and Williford 1979). The second report reviews the irradiation of IFA-431 and correlates the post-irradiation examination results with the in-reactor data (Neally et al. 1979).

SUBTASK B-3: DATA ANALYSIS

Fuel Relocation Analysis

A complete discussion of the basic concepts used in fuel relocation and mechanical response modeling have appeared in previous NRC-RSR quarterly reports. In addition, a formal report is now being published (Williford et al. 1980).

The primary results of these effects can be summarized as follows:

- The concept of a concentric gap between the fuel and cladding is erroneous since the cracked fuel is always in contact with the cladding.

- The effective elastic modulus and thermal conductivity of the cracked fuel is significantly reduced from values for solid pellets.

- Out-of-pile tests have confirmed the reduction in fuel elastic modulus. Analysis of transient temperature data has confirmed the reduction in effective thermal conductivity (Cunningham, Lanning and Montgomery 1979).

These results are demonstrated by Rods 1, 2, 3 (IFA-432) and Rod 6 (IFA-513), which had initial diametral gaps of 230, 380, 75, and 230 μm, respectively. Rods 1, 2, and 3 were backfilled with pure helium at 1 atm, while Rod 6 was backfilled with a mixture of 77% helium/23% xenon (resulting in a gas thermal conductivity 50% of pure helium) at 1 atm. Figure 1 shows that the reduced fuel effective thermal conductivity is dependent on the initial crack void, the fill gas, and the hydrostatic pressure on the fuel. The conductivity factor approaches 1.0 as increasing power levels result in increased fuel thermal expansion, which closes the cracks. This results in a feasible integral to melt. The dependence of radial elastic modulus on the crack void is shown in Figure 2. As the cracks close, the cracked fuel system becomes more rigid, thus increasing the elastic modulus. Figure 3 shows that the cracked fuel column also exhibits a slight anisotropy.

These models have been inserted into intermediate versions of FRAPCON-2 and are presently being tested against in-pile thermal and mechanical response
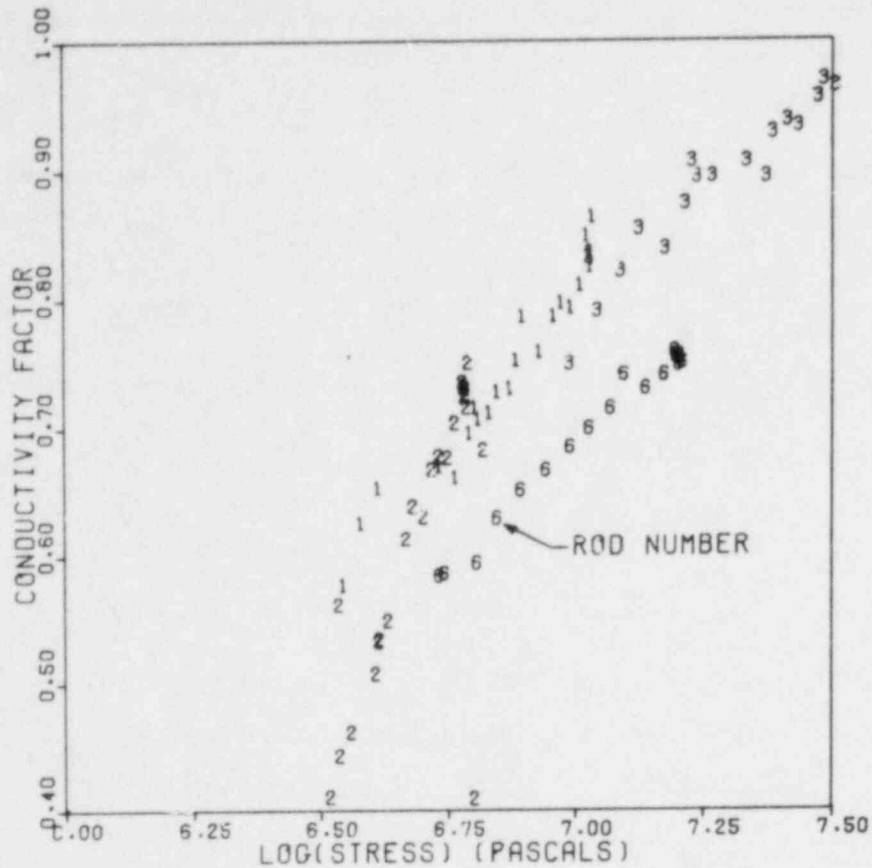
FIGURE 1. Thermal Conductivity as a Function of Fuel Stress

of Halden rods. Future work includes the pretest prediction of IFA-527 (xenon-filled rods) mechanical response during startup. This assembly should yield valuable data concerning the effects of axial fuel-cladding slippage on the effective elastic modulus.

Transient Temperature Data Analysis

Analytical efforts in this quarter have probed the usefulness and limitations of the "fast drop" and "scram" fuel centerline temperature data taken from Halden test assemblies. During the fast drops, the reactor power decreases from 100% of full power to 80% in 10 to 15 seconds. Full scrams, on the other hand, are decreases from 100% of full reactor power to approximately 5% in less than 1 second. An explanation of our analysis procedures for fast drops was

54
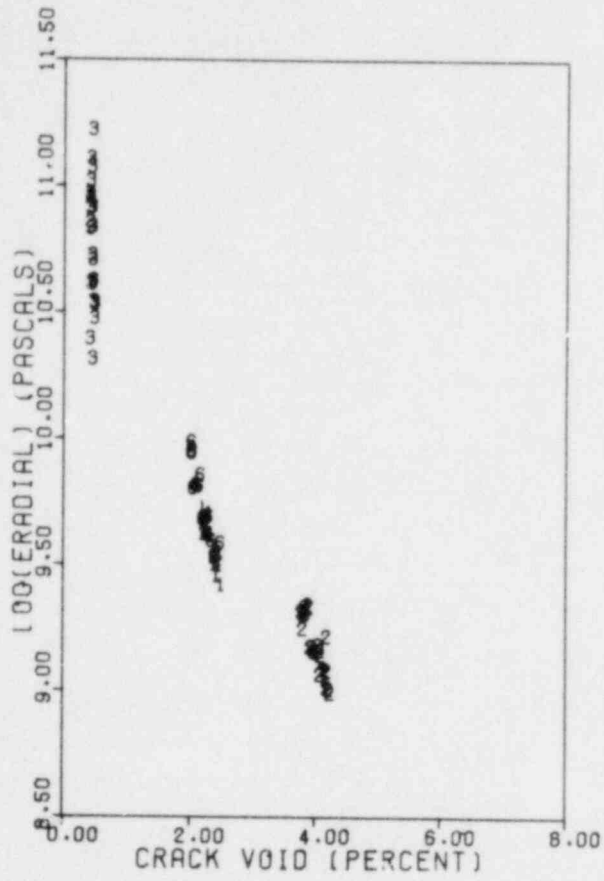
FIGURE 2. Fuel Radial Elastic Modulus as a Function of Crack Void

FIGURE 3. Anisotropy of Fuel Elastic Modulus

published this quarter (Cunningham, Lanning and Montgomery 1979). Analysis of scram data is being developed and will be published later in FY 1980.

The following conclusions, which apply to both fast drops and scrams, have been drawn:

- During computer simulations of transient centerline temperature response, clear divergence is seen in the predictions based on two extreme models of fuel rod heat transfer.[a]

- The computer simulations of centerline temperature are insensitive to variations in the fuel thermal conductivity crack factor as a function of radius.

- The simulations of centerline temperature are insensitive to azimuthal heat flow effects, such as an eccentrically positioned fuel pellet or a severe neutron flux tilt across the fuel rod.

- The apparent general applicability of Model 2 as opposed to Model 1, which was observed during fast drops, extends to full scrams (except at the extreme low-temperature end of the scram).

Figures 4 and 5 illustrate the first two conclusions above. Figure 5 shows typical Model 1 and Model 2 results for an idealized fast drop of 20% and also shows the effect of various crack factor radial distributions upon Model 2 predictions. The clear separation of the model predictions is not affected by drastic variations of the crack factor distribution. This is taken to mean that conclusions drawn about the appropriateness of one model over another are not compromised by possible random variations in the crack pattern. In support of this idea is the close similarity of both steady-state and transient temperature response for the three identical rods in IFA-513

(a) The models being considered are: (1) the fuel thermal conductivity is presumed to be equal to values determined from ex-reactor testing on solid pieces and adjusting the gap conductance to match steady-state fuel center temperature data; and (2) the gap conductance is held steady at its inferred pre-transient value and modifying the fuel thermal conductivity (by a multiplicative crack factor) to account for steady-state temperature-versus-power data over the full range of power.
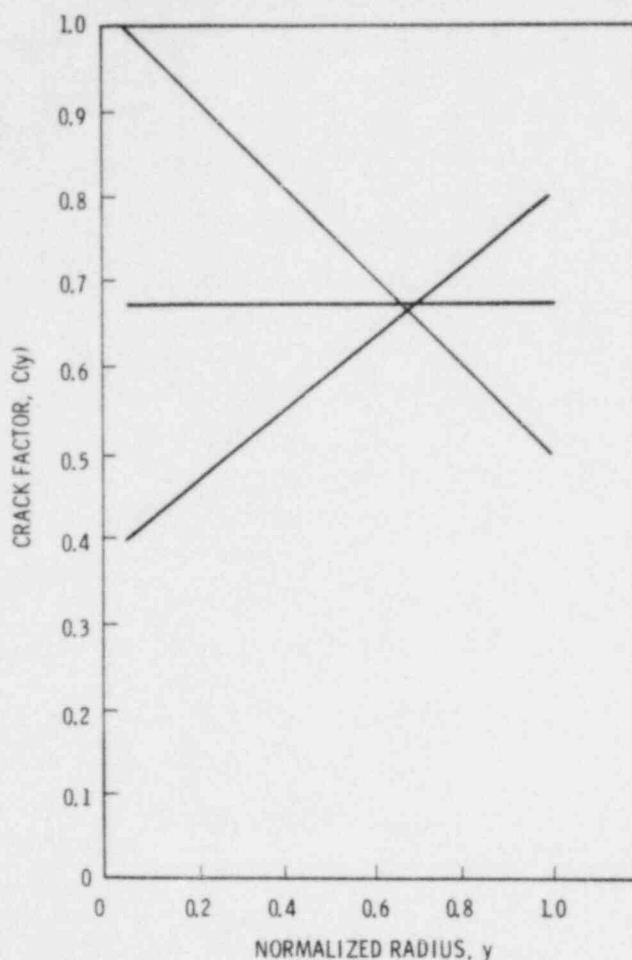
FIGURE 4. Crack Factor Distributions

(Lanning and Cunningham 1979). At beginning of life, the major potential cause of dissimilarity should be crack pattern variations.

Figure 6 provides support for the third conclusion. This figure shows that both fuel pellet eccentricity and severe flux tilting have little effect on the normalized centerline temperature transient response. Therefore, conclusions drawn about effective fuel thermal conductivity or gap conductance, based on fuel centerline transient temperature response, apply only in an azimuthally averaged sense.

The last conclusion is supported by Figure 7. This shows typical data and Model 1 and Model 2 predictions for a full scram experienced by IFA-513 on

57

SYMBOL	MODEL	CRACK FACTOR
□	2	Constant
Δ	2	Linear, decreasing
+	2	Linear, increasing
X	1	Constant
◇	1	Linear, decreasing
✦	1	Linear, increasing
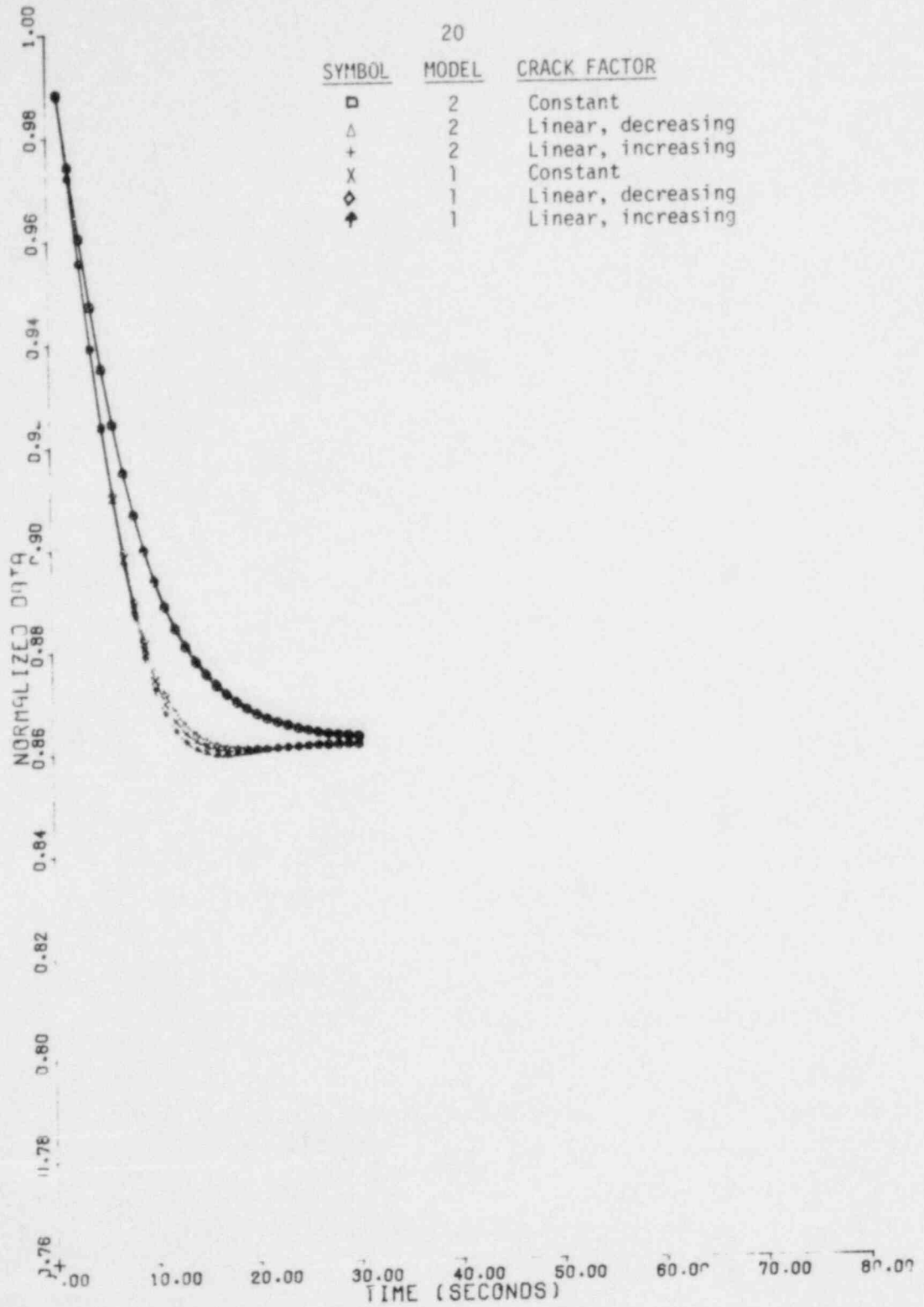
FIGURE 5. Effect of the Distributions Upon Typical Calculated Transient Responses to 20% Step Power Decreases
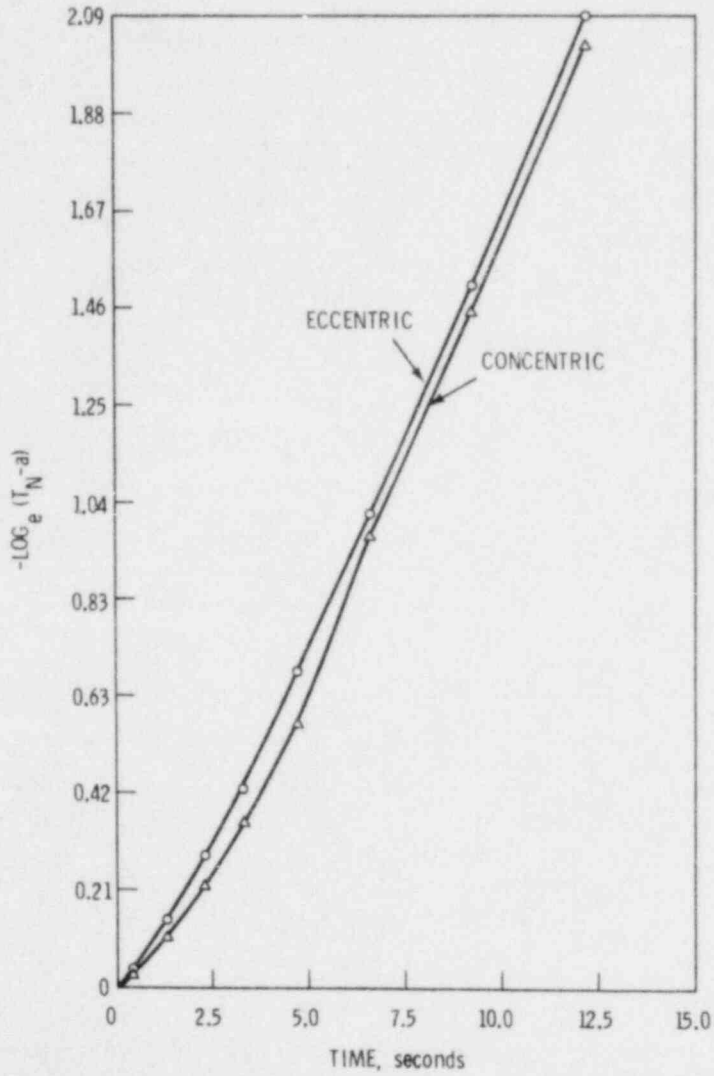
FIGURE 6a. Typical Response of Concentric and Fully Eccentric Pellets to a 100% Power Decrease (helium-filled rod)

59
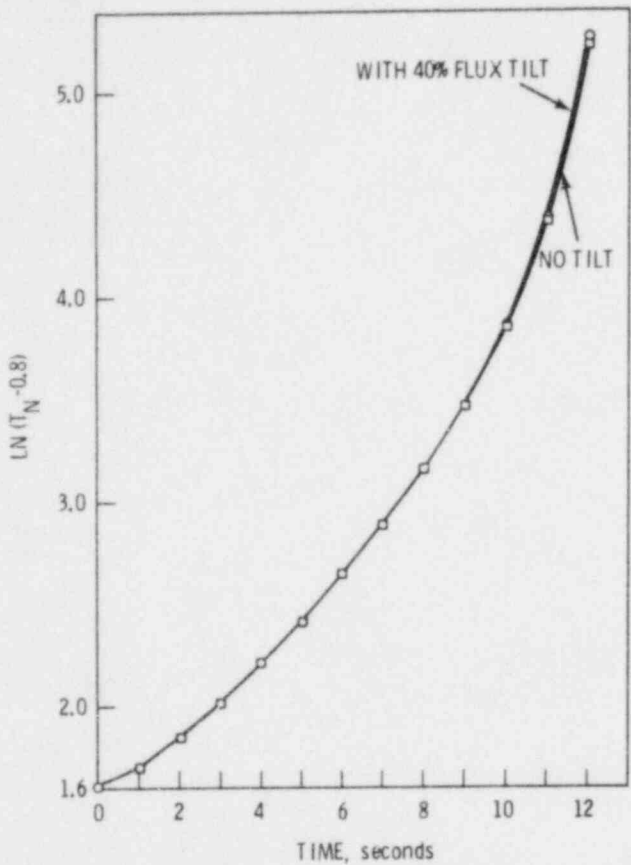
FIGURE 6b. Response of Fuel Centerline Temperature to a Step 20% Power Decrease (with and without flux tilt of 40% edge-to-edge)

60
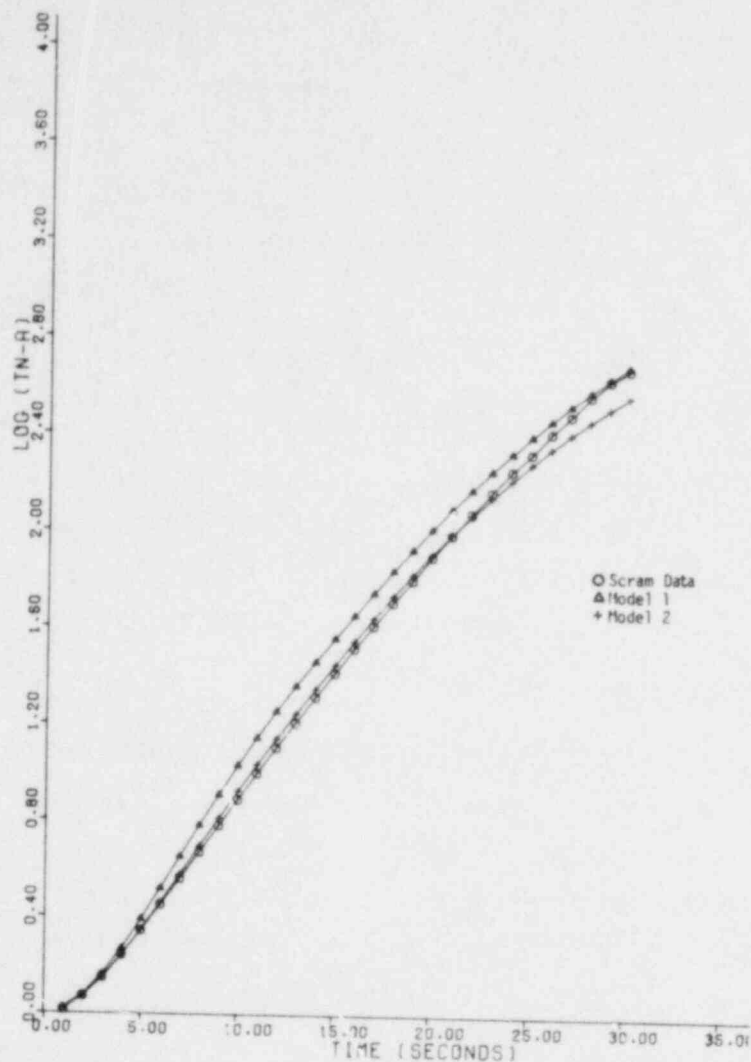
FIGURE 7. IFA-513, TF11 (Rod 6, Bottom)

August 23, 1979. Model 2 is clearly more successful than Model 1 in predicting the centerline temperature response throughout most of the time range. This is startling because it implies that the fuel is almost totally incapable of shrinking away from the cladding.[a] This has far-reaching implications, among them the following:

(a) Constant gap conductance is a major feature of Model 2. Constant gap conductance implies a constant fuel-cladding gap size, which in turn implies that the fuel does not shrink away from the cladding and widen the gap upon power decrease.

61

- The fuel is probably in at least light contact with the cladding all along the length of the rod at all power levels (due to pellet cracking and relocation).

- Because of cracks, the effective thermal conductivity of the fuel at low powers (below 20 kW/m) is probably much less than normally predicted.

- The fuel pellet column is in no sense monolithic in its thermal and mechanical behavior.

In summary, the measured centerline transient temperature responses appear to be useful in pointing out the qualitative nature of fuel rod heat transfer, but these responses are not capable of yielding quantitative confirmation of gap conductance, crack patterns, or azimuthal heat flow effects.

Modeling and Data Error Analysis

This work has the objective of evaluating errors and uncertainties in computer code predictions of steady-state fuel behavior. The current work is concentrating on evaluating stored energy uncertainty for different fuel rod designs (boiling and pressurized water reactors), examining the bias between data and code predictions, and evaluating the effect on temperature prediction uncertainty using a cracked and relocated fuel model.

During this last quarter, a journal article entitled, "Uncertainty Analysis and Thermal Stored Energy Calculations in Nuclear Fuel Rods" was accepted for publication by Nuclear Technology. This article discusses the use of linear propagation of errors to estimate the uncertainty in temperature predictions by steady-state fuel performance codes.

Five fuel rod types have been chosen for a study examining the differences in uncertainty predictions as a function of fuel rod design. The rod types being evaluated are BWR 7x7, BWR 8x8 (0.1 and 0.3 MPa initial fill gas pressure), PWR 15x15, and PWR 17x17. Table 1 lists the design assumptions. Two single-cycle power histories assuming a constant neutron flux throughout the

TABLE 1. Parameters for Fuel Rod Type Comparison

Parameter	Rod Type			
	BWR 7x7	BWR 8x8	PWR 15x15	PWR 17x17
Fuel diameter, mm	12.37	10.57	9.31	8.19
Cladding ID, mm	12.68	10.80	9.50	8.36
Cladding OD, mm	14.30	12.52	10.77	9.50
Fuel enrichment, % U-235	2.2	2.2	2.6	2.8
Fuel density, % TD	94	95	94	95
Initial fill gas	Helium	Helium	Helium	Helium
Initial gas pressure, MPA	0.10	0.10 0.30	2.38	2.03 0.10

irradiation are used.[a] For the first power history, each rod type has an initial peak linear heat rate typical of its design. Those linear heat rates are: BWR 7x7 - 34 kW/m, BWR 8x8 - 29 kW/m, PWR 15x15 - 32 kW/m, and PWR 17x17 - 25 kW/m. The second power history assumes that all rods have an initial peak linear heat rate of 35 kW/m.

Analysis of bias between GAPCON-THERMAL-3 (GT3) and data from IFA-513 was begun this quarter. This analysis is based on comparing the average response and variance of Rods 1, 3, and 5 of IFA-513 to the predicted behavior and uncertainty. Figure 8 shows the results of this analysis for the first rise to power of IFA-513. For powers greater than 30 kW/m, GT3 significantly over-predicts the data; i.e., the variance band for the data and the uncertainty band for GT3 do not overlap.

(a) These power histories assume a constant neutron flux results in a decreasing linear heat rate because of fuel depletion. A peak burnup of 2590 GJ/kgU (30,000 MWd/MTM) is also assumed.
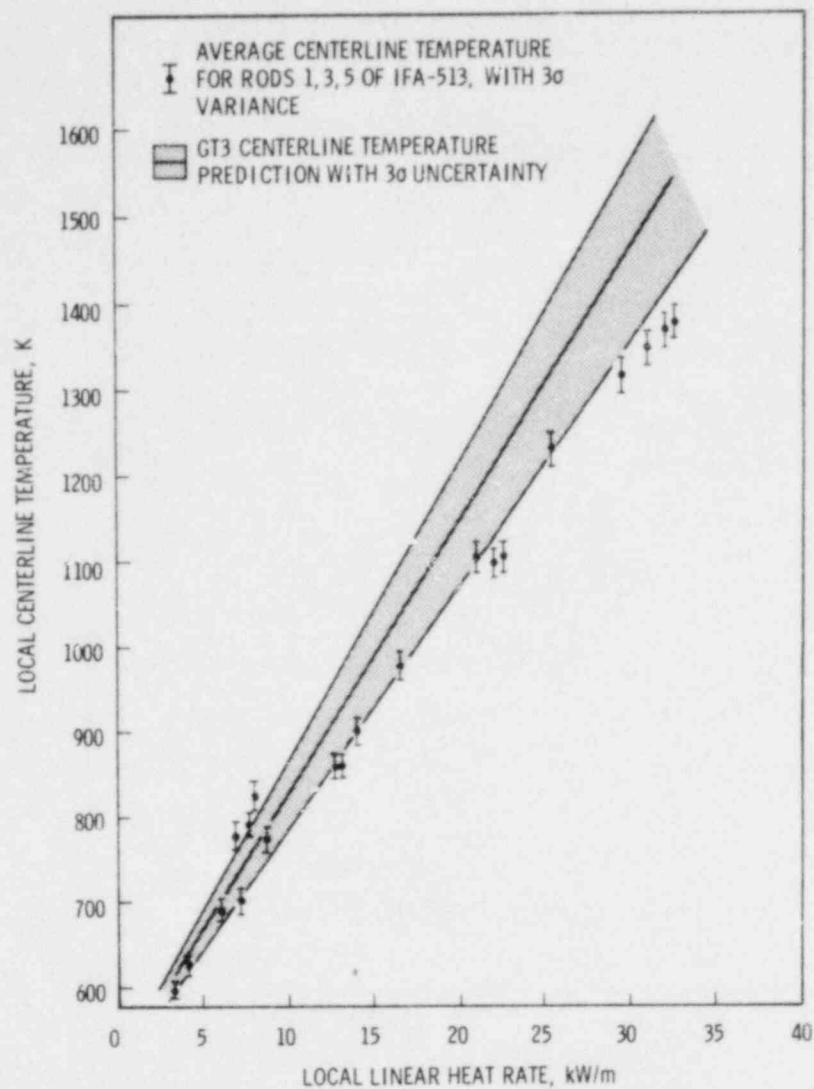
FIGURE 8. Comparison of Bias Between Data and Prediction
for First Rise to Power of IFA-513

Fission Gas Release Analysis

A paper entitled "Burnup Dependent Fission Gas Release" was presented at
the American Nuclear Society's (ANS) Winter Meeting. The paper was well
received and generated considerable interest both at the meeting and there-
after, as evidenced by written requests for copies of the paper. The paper
compares the fission gas release as deduced from the IFA-432 pressure data to
predictions from the burnup-dependent gas release model recently developed by

ANS working group 5.4 and concludes that the model over-predicts fission gas release in fuels irradiated to 1700 GJ/kgU (20 GWd/MTM).

A more detailed analysis of the pressure data from IFA-431 and IFA-432 is included in an interim NUREG/PNL report (Bradley et al.). The primary conclusion from this analysis is that burnup enhanced release of fission gases does not occur in UO_2 fuels irradiated to 1700 GJ/kgU (20 GWd/MTM). This report is in the final stages of preparation and will be published next quarter.

The pressure data from IFA-513 through August 1979 has been received from Halden and examined at PNL. The data show a small, gradual pressure increase with increasing burnup. However, there are indications that some of the pressure changes may be associated with instrument changes rather than a real pressure change. We are currently trying to determine the cause of the observed pressure changes and to establish the sensitivity and reliability of the bellows-type pressure transducers that were used in IFA-513.

REFERENCES

Bradley, E. R., et al. 1979. An Evaluation of the In-Pile Pressure Data from Instrumented Fuel Assemblies IFA-431 and IFA-432. NUREG/CR-1139, PNL-3206, Pacific Northwest Laboratory, Richland, Washington.*

Cunningham, M. E., D. D. Lanning and S. D. Montgomery. 1979. A Procedure for the Qualitative Inerpretation of Fuel Centerline Thermocouple Response to Step-Power Decreases. NUREG/CR-1012, PNL-3096, Pacific Northwest Laboratory, Richland, Washington.*

Cunningham, M. E., D. D. Lanning and R. E. Williford. 1979. The Thermal and Mechanical Behavior of a Xenon-Filled Fuel Rod as a Function of Burnup. NUREG/CR-0749, PNL-3075, Pacific Northwest Laboratory, Richland, Washington.*

Lanning, D. D., and M. E. Cunningham. 1979. Startup Data Report for NRC/PNL Halden Assembly IFA-513. NUREG/CR-0862, PNL-2948, Pacific Northwest Laboratory, Richland, Washington.*

Neally, C., et al. 1979. Post-Irradiation Data Analysis for NRC/PNL Halden Assembly IFA-431. NUREG/CR-0797, Pacific Northwest Laboratory, Richland, Washington.*

Williford, R. E., et al. 1980. The Analysis of Fuel Relocation for the NRC/PNL Halden Assemblies, IFA-431, IFA-432, and IFA-513: An Interim Report. NUREG/CR-0588, PNL-2709, Pacific Northwest Laboratory, Richland, Washington.*

---

*Available for purchase from the NRC/GPO Sales Program, U.S. Nuclear Regulatory Commission, Washington, DC 20555, and the National Technical Information Service, Springfield, VA 22161.

EXPERIMENTAL SUPPORT AND DEVELOPMENT OF SINGLE-ROD FUEL CODES:

TASK C - CODE COORDINATION AND EX-REACTOR TESTING(a)

D. D. Lanning, Program Manager
R. E. Williford, Task Leader
W. N. Rausch
M. E. Cunningham
J. Hofweber
E. Greenwell
J. L. Daniel
L. Inaba
R. T. Lansiedel
L. R. Bunnell
K. A. Hsieh

SUMMARY

During the first quarter, this task was restructured to reflect the increased emphasis on mechanistic relocation and pellet-cladding interaction (PCI) models that have resulted from Task B relocation analysis of the in-pile data. There are now four subtasks: code coordination and development, mechanical testing of short rods, PCI model development, and model verification. Refinements in the relocation model have been implemented in FRAPCON-2 and are being evaluated against in-reactor data. Code structure improvements are nearing completion as progress toward the combined Pacific Northwest Laboratory (PNL)-Idaho National Engineering Laboratory (INEL) version of FRAPCON-2 continues. The design phase of the experimental support efforts nears completion.

INTRODUCTION

The primary objectives of the code development and experimental support efforts are to provide verified analytical models for implementation into FRAPCON-2 and FRAP-T and to coordinate code structure improvements and verification between PNL and INEL.

Efforts in FY 1979 have resulted in the definition of fuel performance models that more closely represent physical reality and in a preliminary code structure to facilitate the implementation of these models. The fact that operating nuclear fuel is cracked resulted in significant reductions in effective thermal conductivity and elastic moduli from those for solid UO_2. The state of the cracked fuel was described by three primary mechanical parameters: crack roughness, gap roughness, and crack pattern. However, those parameters are presently inferred from thermal results. Efforts in FY 1980 will focus on establishing a firm physical foundation for the cracked fuel model and the implementation of these models into a combined PNL-INEL version of FRAPCON-2.

TECHNICAL PROGRESS

Progress has been made in the following four subtasks:

SUBTASK C-1 - CODE COORDINATION AND DEVELOPMENT

Refinements in the relocation model have been implemented into the joint PNL-INEL version of FRAPCON-2. The models and code are currently in the testing and debugging stage. The PNL mechanical model PELET was inserted into the joint version of FRAPCON-2 and debugged. Some code structure changes are being made to improve conveyance characteristics and core requirements. Visits to PNL by EG&G personnel resulted in mutually agreeable milestones for the code verification and documentation.

SUBTASK C-2 - MECHANICAL TESTING OF SHORT RODS

Equipment designs are nearing completion for experiments designed to obtain out-of-pile data on the diametral and axial PCI behavior of short length UO_2-Zircaloy rods. Emphasis is placed on simulation of in-pile loading conditions. Simultaneous experiments are being conducted at PNL on unirradiated rods and at Harwell, UK, on unirradiated and irradiated rods.

SUBTASK C-3 - PCI MODEL DEVELOPMENT

An advanced method is under development to economically model the effects of asymmetric pellet cracking that result in fuel column anisotropy and PCI. Efforts expended on fuel fragment and crack shape descriptions, compatibility equations, and ratcheting mechanisms are beginning to yield a consistent description of the behavior of cracked fuel systems. Understanding gained from these efforts has been useful for designing model verification experiments.

SUBTASK C-4 - MODEL VERIFICATION

Experimental verification of the three primary mechanical parameters and two major assumptions for the relocation models is nearing the end of the design stage. An integrated set of three experiments is being implemented at PNL to provide data quantifying the circle and gap roughnesses, the hydrostatic stress state assumption, and the axial fuel-cladding nonslippages assumption. A data base for crack patterns has been assembled and is under analysis. A method for generating representative crack patterns in prototype pellets has been developed.

FUTURE PLANS

The past quarter was the planning and design stage. The second quarter will be the implementation and experimentation phase. Verification runs for FRAPCON-2 will begin, the new PCI model will be put in the form of a computer algorithm, and data from the short rod mechanical tests and model verification experiments will commence. Experimentation and analysis will overlap in the third quarter, and reporting will occur primarily in the fourth quarter.

69

ULTIMATE HEAT SINK PERFORMANCE MEASUREMENT[a]

R. K. Hadlock, Project Manager

SUMMARY

A measurement effort of approximately four weeks was completed at the Department of Energy's (DOE) San Francisco Operations Office (DOE/SAN) Geothermal Component Test Facility, East Mesa, California, in early October. Thermal performance and water utilization data were obtained for four episodes of cooling pond and spray pond cooling from an initially warm temperature in the range 105 to 130°F. These data complement those obtained previously at the Raft River site in southern Idaho. Efforts are underway to acquire data from a thermally hot cooling/spray pond at East Mesa prior to program completion at the end of CY 1980.

INTRODUCTION

The present scope of the Ultimate Heat Sink Program at Pacific Northwest Laboratory (PNL) includes continuation and completion of cooling pond and spray pond measurements, formulation of data volumes, and suggestions for modeling improvements. The measurement effort was initiated at the Raft River, Idaho, geothermal facility and has been continued at the East Mesa, California, Geothermal Component Test Facility, managed by WESTEC Services, Inc., for DOE. The geothermal retention basins have provided analogs to Ultimate Heat Sinks of Emergency Core Cooling Systems in both cooling po   nd spray pond modes. The measurement efforts have produced data of thermal performance and water utilization for vari us conditions including short-term worst case combinations of meteorological influences. Work completed early in the past quarter has produced comparative data of cooling pond and spray pond performance for warm (105 to 130°F) initial pond temperature. The East Mesa facility will be used again in CY 1980 to study performance for initially hot pond temperature.

TECHNICAL PROGRESS

The East Mesa experiment series, which resulted in cooling pond and spray pond data for moderately warm water temperatures, was completed in early October.

The Raft River data for warm and hot water in the cooling pond mode were transmitted to the Nuclear Regulatory Commission (NRC), in usable but not publishable format, in early November.

Initial planning for the 1980 measurements has proceeded with WESTEC Services, Inc., and DOE/SAN at a meeting in Oakland, California. The required rate of available hot water, to ensure a hot initial pond temperature, will not likely be met. PNL has, as a result, provided options/techniques to enable a hot pond with the available rate for NRC consideration. These include ways to cover the pond surface during pond filling to significantly reduce heat loss through evaporation and radiative exchange.

The 1979 East Mesa data have been partially organized similar to the Raft River data from 1978. These data, in usable but not publishable format, will be transmitted when the organization is complete.

FUTURE PLANS

PNL intends to produce the required hot spray pond data at the East Mesa site prior to termination of the contract on December 31, 1980. Special techniques will be required to take into account a less than desired rate of available hot water at the site. These techniques will reduce heat loss due to evaporation and radiative exchange during pond filling. The NRC and PNL are considering the options, and a concurrence will be reached shortly for action to be accomplished in the spring. This action will include a small-scale test prior to mounting the actual measurement program. Data volumes and suggestions for modeling improvements will be provided to the NRC prior to January 1, 1981.

72

ACOUSTIC EMISSION - FLAW RELATIONSHIP FOR IN-SERVICE MONITORING OF NUCLEAR PRESSURE VESSELS[a]

P. H. Hutton, Project Manager
R. J. Kurtz

SUMMARY

A fatigue crack growth test of a heavy section cylindrical bend specimen was begun. Initial testing was performed in room temperature air or 550°F water at 1350 psig. The initial results indicated that acoustic emission (AE) was detected under conditions relevant to the nuclear reactor operating environment.

Extensive planning for an off-reactor structural test was conducted. This test was designed to provide a semi-realistic simulation of reactor pressure vessel conditions, including AE from growing fatigue cracks as well as various noise sources.

A conceptual application methodology for in-service flaw assessment of nuclear pressure vessels during hydrotest by AE was developed. This application methodology was developed as a response to a Nuclear Regulatory Commission (NRC) branch position paper on AE.

INTRODUCTION

The purpose of this program is to provide an experimental evaluation of the feasibility of detecting and analyzing flaw growth in reactor pressure boundaries on a continuous basis using AE. Type A533B, Class 1 steel is being used in all experimental testing. The objectives of this program are:

- characterize AE from defects under material property conditions recognized as being of primary concern to reactor pressure vessel integrity and characterize acoustic signals from representative innocuous sources

---

73

- develop criteria for distinguishing significant flaw AE from innocuous acoustic signals

- develop an AE-flaw damage model to serve as a basis for relating in-service AE to pressure vessel integrity

- make available a characterized high-temperature AE sensor

- develop a continuous surveillance AE data acquisition and analysis system.

Progress relative to these objectives is discussed in the following sections. These include AE/fracture mechanics tests, off-reactor structural tests, a review of NRC branch position paper on AE, and reports. The final section describes the work planned for the next quarter.

AE FRACTURE MECHANICS TESTING

This section describes the experimental procedure used in fatigue crack growth testing a heavy section cylindrical bend specimen and is followed by a discussion of the initial test results.

PROCEDURE

A fatigue crack growth test of a heavy section cylindrical bend (HSCB) specimen was initiated. The HSCB specimen, shown in Figure 1, is an 8-in. OD by 2-in. ID cylindrical section of A533B, Class 1 steel with a circumferential ID notch 0.875-in. wide by 1-in. deep. The specimen is being sinusoidally loaded in tension-tension bending at a cycle rate of 0.5 Hz and an R-ratio approximately equal to 0.1. Figure 2 shows a drawing of the test specimen welded to the loading frame. During fatigue cycling, the specimen was internally exposed to either room temperature (RT) air or 550°F water at 1350 psig. Figure 3 shows the specimen and loading frame connected to the high temperature-pressure water loop. Figure 4 shows a close-up of the HSCB specimen and the relative location of the AE sensors.

74
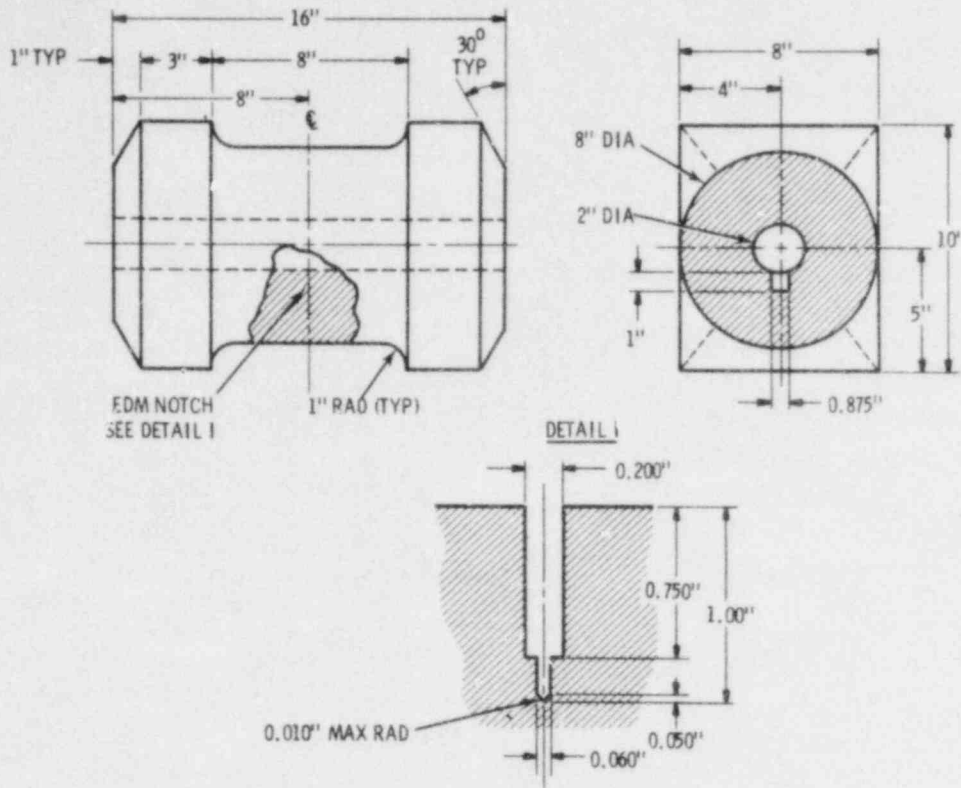
FIGURE 1. Heavy Section Cylindrical Bend Specimen and Electro-Discharge Machined Notch Dimensions

The AE system being used on the HSCB test is the same monitor system used on previous laboratory tests. It uses zone isolation to focus on signals originating from the defect area in the specimen. In this application, three waveguide sensors (1/8 in. dia by 2 ft long) are used to establish an area approximately 2 in. by 6 in. surrounding the defect from which "valid" signals are accepted. In addition to the three waveguide sensors, a Westinghouse high temperature surface mounted sensor is also used to evaluate comparative AE detection ability and to supply AE waveforms for digital recording. These waveforms, together with AE waveforms from the waveguide and noise signals from both types of sensors, are being used for further pattern recognition development to characterize AE signals from crack growth. Effective sensitivity of the AE system was approximately 0.15 μ bar.
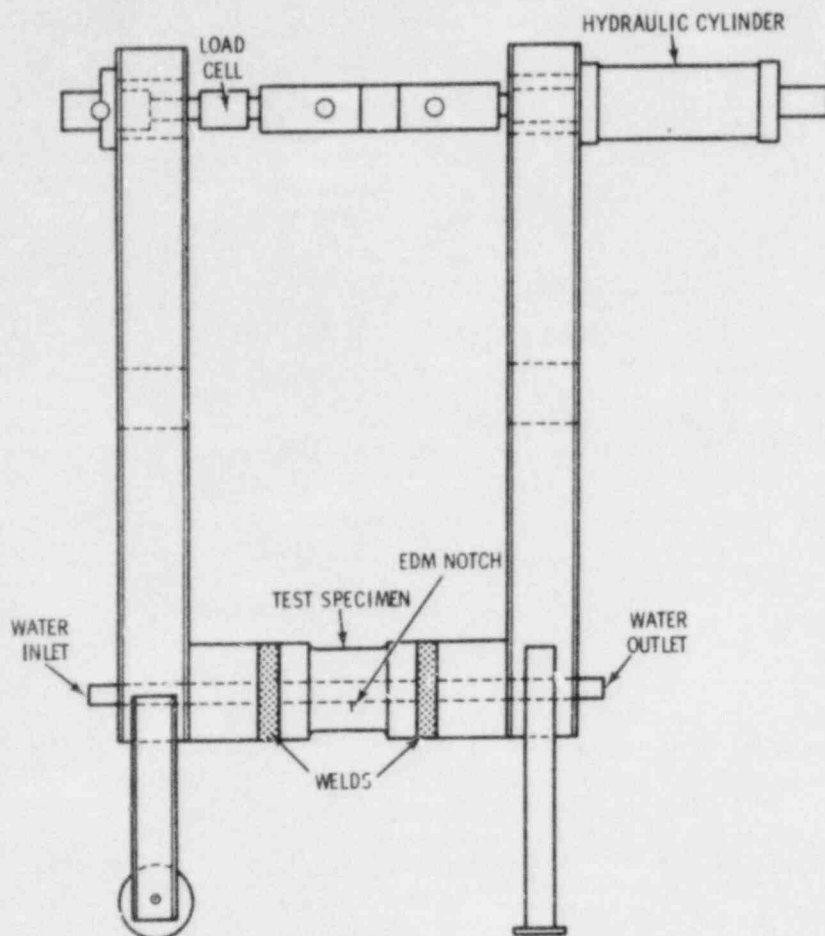
FIGURE 2. Test Specimen and Bending Equipment

An ultrasonic "pitch-catch" technique is being used to measure crack growth from the ID flaw. A 5 MHz ultrasonic signal is injected at a 45° angle on the OD surface. The reflected signal from the ID surface received by a second transducer is then examined for attenuation by the growing crack as the system is translated along the specimen. When a position is reached where 50% of the energy is being attenuated by the crack, the angular path of the beam is used to calculate crack length.

RESULTS

Initial test results are plotted in Figure 5. These data show that introduction of pressurized high temperature water did not significantly affect AE
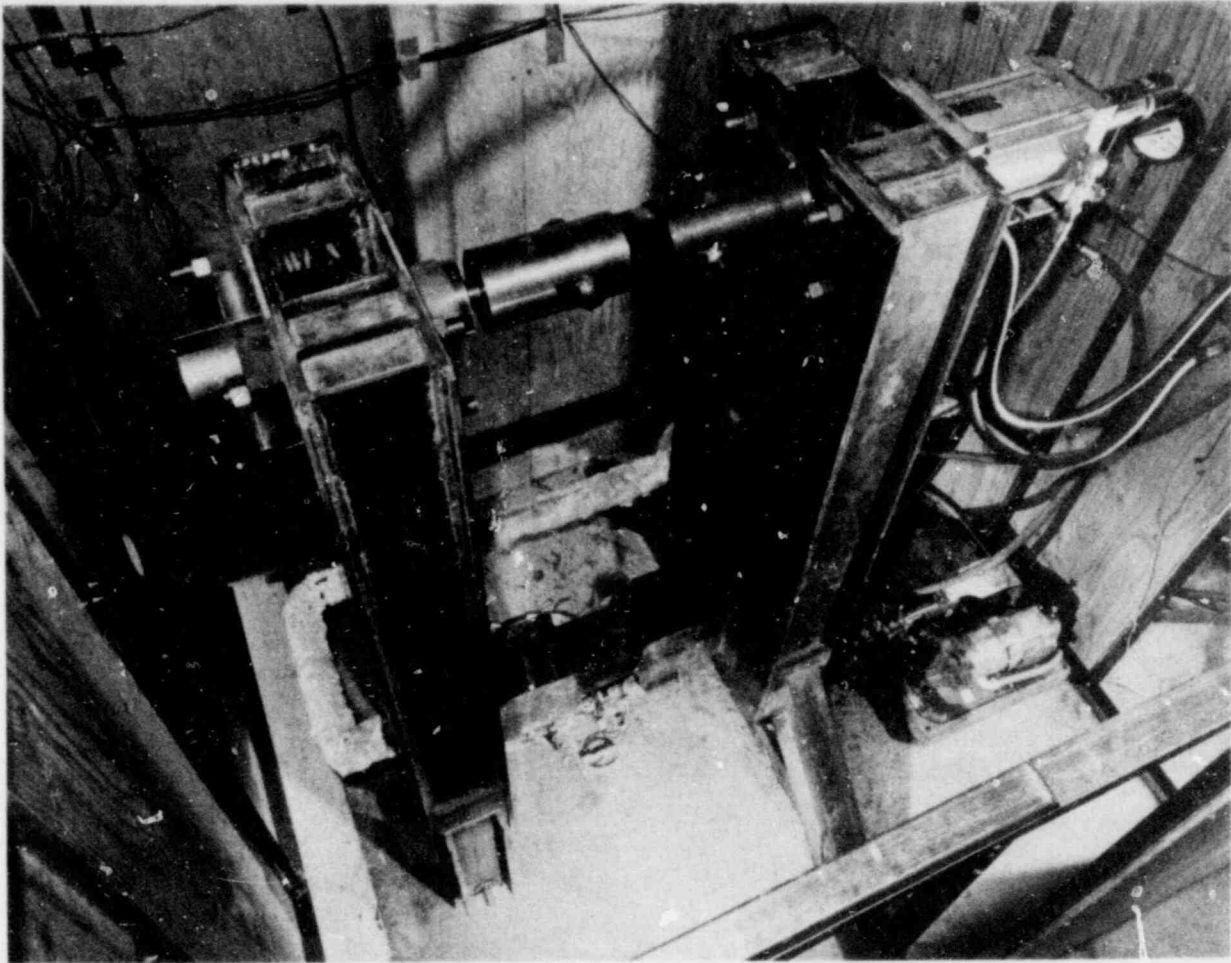
FIGURE 3. Heavy Section Cylindrical Bend Specimen and Loading Frame
Connected to High Temperature-Pressure Water Loop

detection. The AE data shown in Figure 5 include unpartitioned and peak-time
partitioned data. The two curves are very similar during fatigue testing in
RT air but with the introduction of 550°F water, apparent abnormal signals
are included in the validated data. Eliminating these long rise time signals
produces a data curve at 550°F that is consistent with the RT data. The
source of the abnormal signals is not clear; however, it has been established
that they are a function of increasing temperature. The most significant
aspect of these results is that AE was detected under conditions relevant to
the nuclear reactor operating environment.
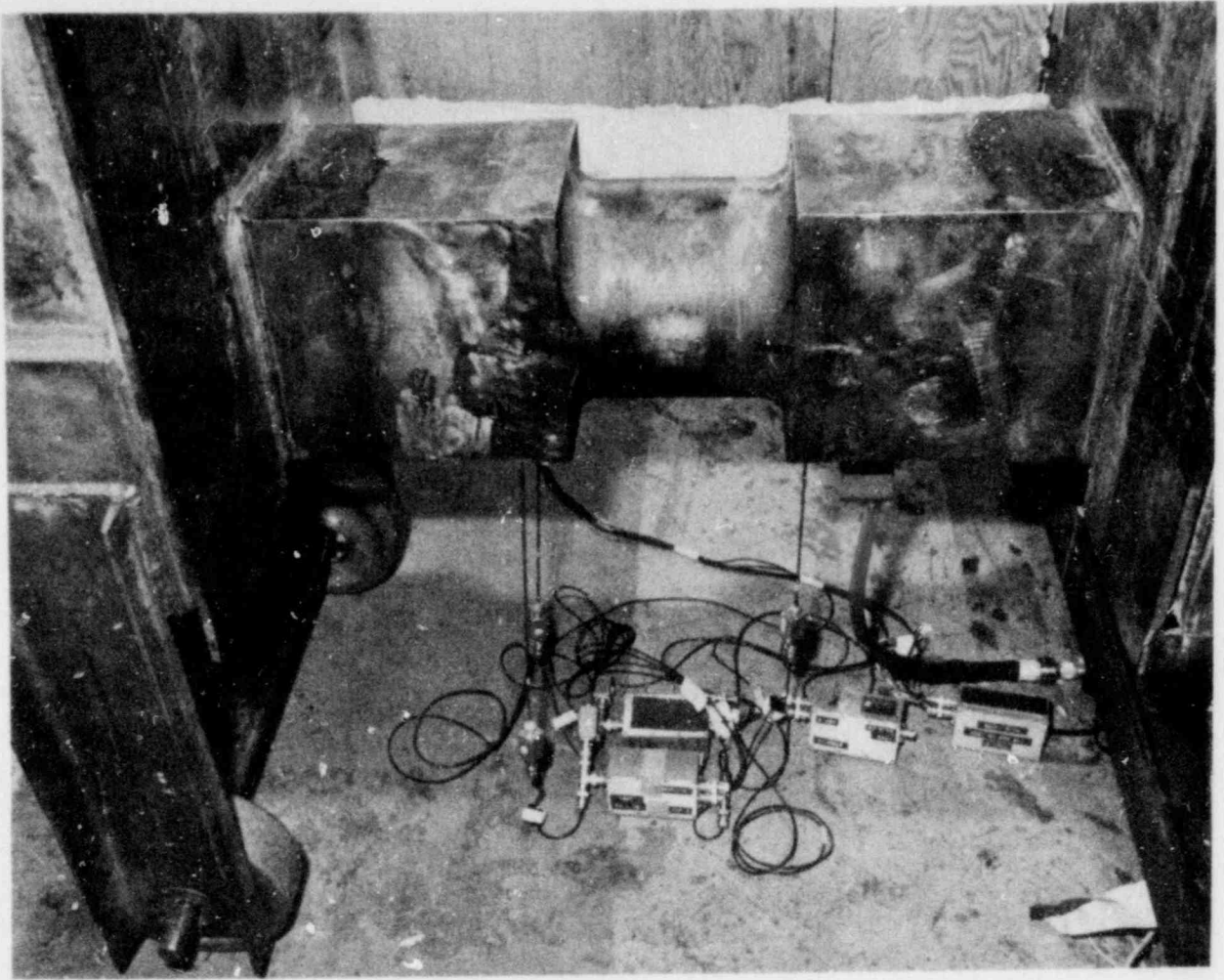
FIGURE 4. Close-up of the Heavy Section Cylindrical Bend
Specimen Showing the Relative Location of the
Acoustic Emission Sensors
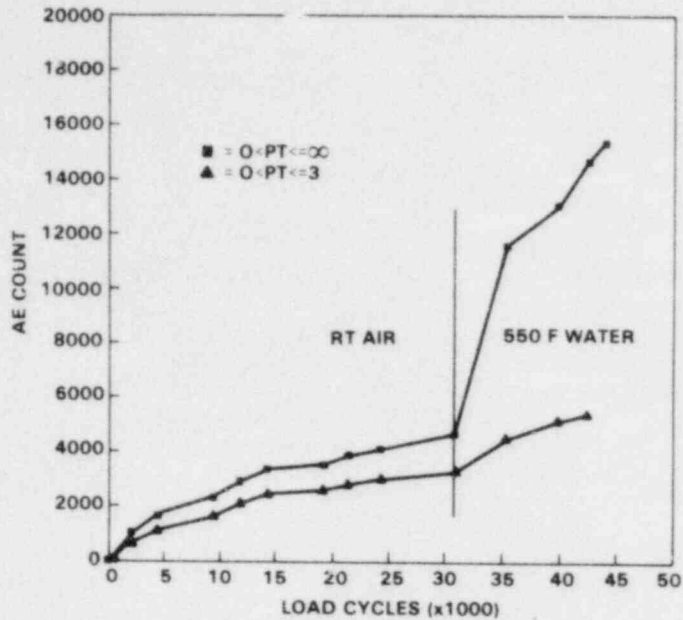
FIGURE 5. Summation Acoustic Emission Event
Count Versus Load Cycles for
Fatigue Cycling of the Heavy
Section Cylindrical Bend Specimen

OFF-REACTOR STRUCTURAL TEST

One of the goals of the FY-80 AE/Flaw Characterization Program is to AE monitor a large-scale vessel test. The test specimen and environmental and loading conditions should be designed to provide a semi-realistic simulation of reactor pressure vessel conditions, including AE from growing fatigue cracks and various noise sources. This section describes the work performed this quarter to locate a test vessel and associated equipment.

Analyses of the feasbility of performing the current off-rector vessel test matrix (see Appendix A) have been performed at both Pacific Northwest Laboratory (PNL) and Oak Ridge National Laboratory (ORNL). These analyses were based upon using the Heavy Section Steel Technology Program (HSST) ITV-7 repaired to meet test specimen needs.

79

Two major technical limitations have been identified by both laboratories. The first of these limitations is concerned with the cyclic frequencies that were specified in the test matrix. With equipment presently available at either laboratory, the room temperature phase of the proposed test matrix would require about 240 eight-hour working days to complete. Based on this finding, discussions were initiated with various hydraulic equipment suppliers to obtain estimates for the cost and delivery time required to construct equipment suitable for hydraulically pressure cycling the entire vessel, piping, immersion heaters, and circulating pump at a frequency of 0.25 Hz. The results from these discussions indicated that appropriate equipment would cost as much as $150K, with a 6- to 9-month delivery time.

The second major limitation is concerned with the intermediate test vessel. The vessel closure was designed for 100 cycles to 16,000 or 20,000 psi, depending on the temperature. ORNL staff believe that the closure studs would be the critical component susceptible to fatigue damage. Consequently, a fatigue analysis, as well as an inspection and replacement schedule, would be necessary if the number of cycles applied to the vessel became very large.

In view of these limitations, two alternatives are under consideration. One is to reduce the number of pressurization cycles to a number that is attainable in a reasonable time with currently available equipment. A range of ΔKs would be obtained by employing multiple flaws of different geometries. The second option is to combine constant vessel pressure loading with cyclic notch pressurization. Cyclic notch pressurization would allow more flexibility in the choice of loading parameters; however, it may not be possible to measure crack opening displacement at the notch opening, and a significant increase in atypical background noise may be introduced.

Capability and limitations of testing the vessel at PNL are being rigorously defined. With this information, the plan is to meet with ORNL staff the second week in January 1980 to arrive at specific conclusions on the final test format, test location, and vessel repair procedure. This is a critical step leading to definition of vessel repair requirements so the repair work ca. be initiated.

REVIEW OF NRC BRANCH POSITION PAPER ON ACOUSTIC EMISSION

A conceptual application methodology for in-service flaw assessment of nuclear pressure vessels during hydrotest by AE was developed during this reporting period. This application methodology was developed as a response to an NRC branch position paper on AE. This section describes the concepts that were formulated.

PURPOSE

The purpose of this paper is to provide an initial framework for the application of AE as a basis for locating and assessing regions of structural degradation in a pressure vessel during a hydrotest.

INTRODUCTION

Section XI of the American Society of Mechanical Engineers Boiler and Pressure Vessel Code contains rules and procedures for performing pre-service and periodic in-service inspections of nuclear power plant components and for evaluating flaw indications detected during the inspections. This paper discusses a possible method for flaw assessment, based on in-service AE monitoring during a hydrotest. It is presented as a basis for a possible future adjunct to flaw evaluation procedures contained primarily in a non-mandatory appendix (Appendix A) of Section XI.

BACKGROUND

The flaw evaluation procedures of Section XI are based on the concepts and principles of linear elastic fracture mechanics (LEFM). The potential application of AE to flaw assessment, described here, is also based on LEFM using Section XI, Appendix A, as a foundation for developing the method of application.

Although the concept of LEFM is well known, a brief review of the basic features may be useful. The significant quantity is the stress intensity factor, K_I, for the opening mode loading of a sharp-tipped crack. K_I is related to the stress, σ, remote from the crack and a characteristic dimension, a, of the crack through an equation of the form:

$$K_I = C\sigma\sqrt{a} \qquad\qquad (1)$$

where C is a numerical factor whose value depends on the geometry of the crack, the ratio of the crack size to the section size of the component containing the crack, and the type of loading. As a simple example, $C = \sqrt{\pi}$ for the case of tensile loading of a very wide plate containing a through-thickness crack of length 2a. The brittle fracture criterion is that initiation of unstable crack propagation occurs when K_I attains a critical value. This critical value is denoted as K_{IC} and is identified as the fracture toughness of the material. Thus, fracture mechanics principles enable the formulation of a fracture analysis methodology in terms of applied stress, flaw size, and a material property.

Although extremely useful, LEFM is properly limited to characterizing non-ductile failures. These limitations may be minimized by advanced techniques of elastic-plastic fracture mechanics. To date, these advanced techniques have not been incorporated into Section XI analysis procedures.

Acoustic emission denotes a phenomenon whereby transient elastic waves are generated by the rapid release of energy from a localized source or sources within a material under strain. In metals, deformation and crack growth can produce AE. As an emerging nondestructive testing technique, AE has a unique feature for flaw surveillance: the capability to detect and locate flaws during a hydrotest by using a fixed array of AE sensors. Also inherent in this capability is the potential for continuous long term surveillance during service operations.

Acoustic emissions are usually discrete, discontinuous in nature, usually inaudible, and are sensed as minute displacements at a material's surface. A common method of detecting AE employs a piezoelectric sensor mounted on the surface of the object. The piezoelectric material generates an electrical pulse that is dependent on the strain wave passing under the sensor. The resulting AE analog signals are amplified, conditioned, and analyzed to measure parameters such as signal counting, signal energy, etc.

The AE signal voltage varies with time, usually in a complex manner believed to depend upon such factors as the AE source mechanism, the sensor couplant, the sensor mechanical to electrical conversion, the AE path length,

and geometry of the body (specimen or structure) between the AE source and the sensor. This complex relationship is not yet clearly understood because critical problem areas associated with the detected AE signal remain to be solved. These problem areas include:

- identification of the relationship between AE analog signals and the causative mechanisms

- quantification of a wave propagation process through the material structure

- characterization of the sensor response and its relationship to propagating elastic waves.

Because of these limitations, primary standards for calibrating AE systems do not exist, and unambiguous separation of AE from innocuous noise signals has not been achieved. In addition, experiments conducted by different investigators on nominally the same test material have yielded divergent results.

In spite of the foregoing difficulties, AE techniques are being successfully used to detect and locate flaws during pressure system testing (e.g., hydrotesting of pressure vessels and piping). Progress in the areas of pattern recognition and signal deconvolution may permit an empirical segregation of AE from other transient acoustic signal sources (i.e., mechanical and electrical noise.) We believe the long term potential of AE technology far outweighs the present limitations and with adequate investigation, these problems can be overcome.

POTENTIAL APPLICATION METHOD

To relate AE to K_I during hydrotest requires that experimental AE-K_I data exist for the relevant material conditions anticipated during pressure vessel service. This implies that the influence of environmental and loading conditions upon the material--and, hence, the AE response from that material--are known. Data from surface notch flaws in 6-in. thick HSST vessel hydrotests have been obtained and are shown in Figure 6 in terms of AE event count versus K. These data, while showing the positive potential for vessel flaw assessment by AE, represent a limited data base for flaw severity assessment. Only a

83
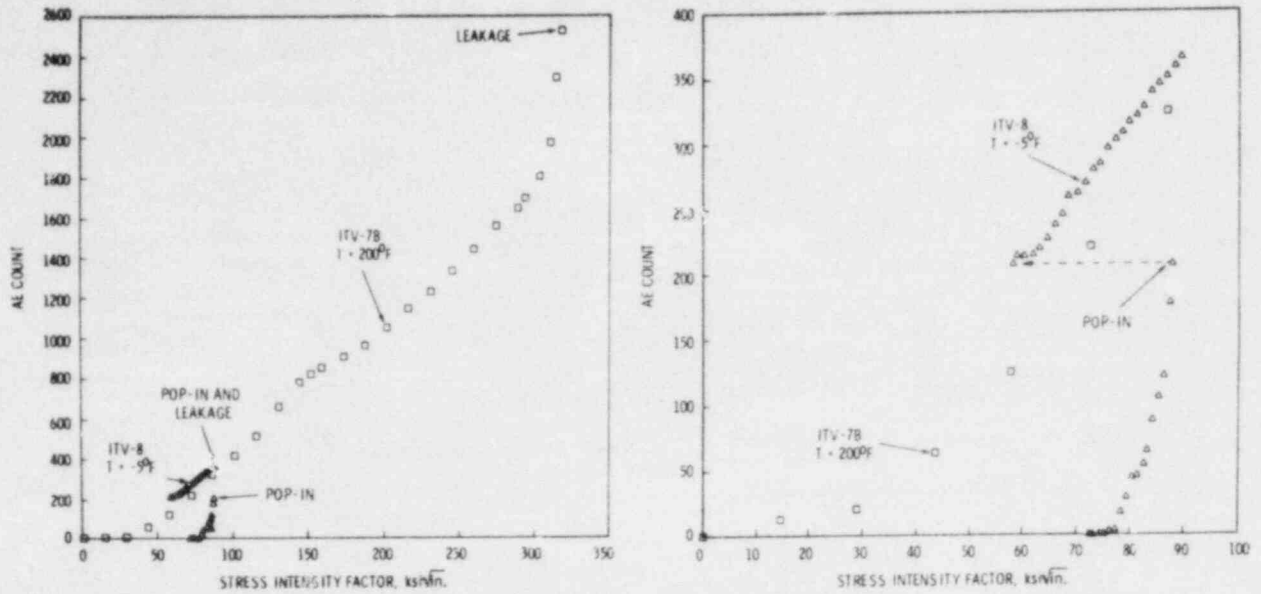
FIGURE 6. Acoustic Emission Versus Stress Intensity Factor for Heavy
Section Steel Technology Program Vessels V-7B and V-8

limited range of test conditions are represented by the curves shown in Figure 6. Nevertheless, a concept for a quantitative flaw evaluation procedure during hydrotest can be delineated from the HSST vessel test data if the following assumptions are made:

- Separation of AE from noise signals may be achieved.

- The response of the AE monitoring system is known and is similar to that used in the HSST tests as determined by the following criteria:

$$\frac{T.H.}{G.} \Big/ \frac{1 \text{ volt}/\mu \text{ bar}}{S} = 0.1 \text{ to } 0.15 \text{ } \mu \text{ bar}$$

where T.H. is system detection threshold in volts, G. is system gain, and S is sensor peak sensitivity in the frequency range of 150 to 300 KHz in terms of dB re 1 volt/μ bar.

- The flaw dimensions remain essentially constant during a hydrotest, such that the K_I descriptor is valid up to the hydrotest pressure.

84

- Figure 1 depicts the experimental relation between flaw severity and AE for the pressure vessel material under consideration and adjustment factors to compensate for flaw distance from the AE sensors and for geometric disturbances in the transmission path have been determined.

Using Equation 1, the stress intensity factor resulting from a stressed flaw in a reactor pressure vessel during a hydrotest may be expressed as:

$$K_I = C_1 P_h \tag{2}$$

where P_h is the maximum hydrotest pressure, taken as 115% of the nominal reactor operating pressure, and C_1 is a constant that includes all flaw and vessel geometry terms and structural loading (e.g., conversion of pressure to stress) type factors. Equation 2 may be rearranged to yield:

$$K_I = C_1 P_o + C_1 (P_h - P_o) \tag{3}$$

where P_o is the nominal reactor operating pressure.

Figure 7 shows a hypothetical AE versus test pressure curve for a hydrotest. The number of AE count obtained from a particular flaw during the hydrotest, δN, may be used in conjunction with the data in Figure 6 to determine the change in stress intensity factor, δK_I, of the flaw due to changing the pressure from P_o to P_h.

The change in stress intensity factor due to the overpressure of the hydrotest is given as the second term in Equation 3 or:

$$\delta K_I = C_1 (P_h - P_o) \tag{4}$$

Hence, for a particular quantity of AE from a flaw at a given location, that relation can be expressed:

85
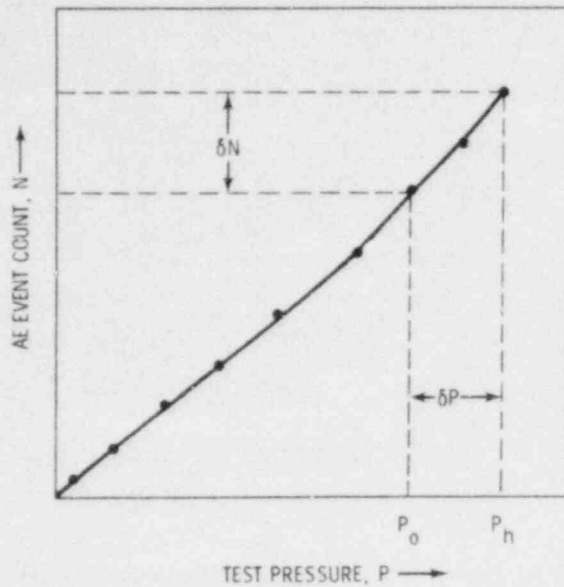
FIGURE 7. Hypothetical Acoustic Emisssion
Versus Test Pressure Curve for a
Nuclear Pressure Vessel Hydrotest

$$\delta N = f(\delta K_I) \tag{5}$$

where $f(\delta K_I)$ represents the mathematical relationship for the flaw severity -
AE data shown in Figure 6. Over the range of expected values for K_I (i.e.,
15-200 ksi$\sqrt{in.}$), this relationship may be taken as an equation of the form:

$$\delta N = C_2 \delta K_I \tag{6}$$

where C_2 is the slope of the nearly linear relationship between AE and K_I.

Substituting the right hand side of Equation 4 into Equation 6 produced:

$$\delta N = C_2 C_1 (P_h - P_o) \tag{7}$$

Solving for C_1 and substituting back into Equation 2 produces the final result:

$$K_I = \frac{\delta N}{C_2} \frac{P_h}{P_h - P_o} \qquad (8)$$

The resulting stress intensity factor represents a quantitative measure of the flaw severity, which may be used to calculate the degree of structural degration. Furthermore, this K value may be used in a fatigue crack growth analysis to predict end of life for a given structural element.

This analysis has illustrated in principle how an assessment of flaw severity based upon AE data alone may be obtained. The analysis is based upon a very limited amount of experimental data and should not be construed as anything more than a qualitative measure of flaw severity at this time.

REPORTS

The quarterly progress report for July 1 to September 30, 1979 was prepared during this period.

WORK PLANNED FOR NEXT QUARTER

Work plans for the period January 1 to March 31, 1980, include:

- finalize arrangements for preparing a vessel test to simulate AE monitoring under reactor operating environment

- complete the HSCB specimen test

- initiate preparation of a new analysis-before-test document

- finalize preparations for installing high temperature AE sensors on N Reactor

- finalize preparations for monitoring HSST irradiated 4T fracture specimens

- initiate design of an AE system to apply the developed AE/flaw relationships and AE characterization method to a vessel test

- continue development of AE characterization by pattern recognition.

87

APPENDIX A

PRELIMINARY TEST MATRIX FOR THE FY-80
OFF-REACTOR STRUCTURAL TEST

GENERAL REQUIREMENTS

This section lists the specimen, environmental, and loading conditions required to perform a quasi-realistic simulation of reactor pressure vessel (RPV) loadings.

Test Specimen Requirements	Purpose
1. Cylindrical geometry	Simulate RPV
2. 4 in. (10.16 cm) min. wall thickness	Heavy section effects
3. A533B Cl. 1 steel	Vessel material
4. Longitudinal seam weld	Locate flaw in weld material
5. $1/2 \pm 1/4$ in. $(1.27 \pm 0.64$ cm) slag inclusion located in the long weld	Innocuous noise source
6. I.D. flaw	"Blind" flaw
7. O.D. flaw	Flaw without coolant contact
8. Stainless steel cladding ~0.2 in. (.51 cm) thick by ~4 ft.^{2} (.37 m^2)	Innocuous noise source
9. Flaw geometry: part-circular designed to provide constant stress intensity factor along the crack front	Simulate semi-embedded flaws in a RPV

Environmental Conditions	Purpose
1. RT-550°F (287°C) water	Simulate RPV
2. 20 ft/sec. (6.10 m/sec) coolant flow velocity in inlet and outlet	Flow noise
3. Thermal insulation should cover the exterior of the vessel	Innocuous noise source

4. Methods for producing electrical   Innocuous noise source
   transients are required

Loading Conditions	Purpose

1. Fatigue Crack Growth

   Obtain crack growth under simulated
   RPV conditions

   The water pressurization system
   should be capable of providing
   cyclic mechanical stressing of
   the vessel at frequencies ranging
   between 0.01 and 1.0 Hz. In
   addition, the pressurization
   system should be capable of pro-
   viding loadings up to 30 ksi
   (207 MPa). Finally, pressure
   cycling at R-ratios of 0.1 and
   0.9 must also be included.

   Fatigue crack growth will be
   conducted at 550°F (287°C) and
   room temperature

2. Thermal Fatigue

   Innocuous noise source simulation
   as well as crack progagation
   mechanism

   There are two types of thermal
   fatigue: high cycle and low
   cycle. The high cycle thermal
   fatigue originates from unstable
   turbulent mixing of relatively
   cold feed-water introduced into
   the hot reactor through nozzles.
   It is felt by some investigators
   that this fatigue damage mechanism
   will not drive the cracks beyond
   the vessel clad depth. Thus, it
   may be argued that it may not be
   necessary to model this mechanism,
   since the resultant cracks do not
   become significant until operated
   on by another mechanism. It
   should be recognized, however,
   that this mechanism may be impor-
   tant in the sense that weld clad-
   to-base metal interfacial noise
   may be generated.

Thus, it is necessary to produce temperature fluctuations (ΔT water $\sim 200^\circ F$, $111^\circ C$) in a localized region at a cycle rate of about 1 Hz.

Low cycle thermal fatigue arises principally from thermal and mechanical stress generated during start-up and shutdown of the reactor vessel. This mechanism will be simulated as one of the reactor transients.

3. Reactor Transients

    A. Heatup and cooldown
    B. Normal variations $\pm$ 10% power excursions
    C. Leak test

Simulate RPV pressure and temperature loadings

4. Blind Tests

Test the operation of the AE monitoring system during periods when no crack growth is produced and when the crack is growing both with and without background noise

Blind test of the AE monitoring system shall be performed at randomly selected times during the test sequence after the first five crack growth increments and associated marking cycles at $550^\circ F$. The first method simulates the effects of $\pm$ 10% power variations and is produced by cycling the pressure between 9.5 and 10.5 ksi (65.5 and 72.4 MPa) at a rate of 1.0 Hz. The second method attempts to simulate the Kaiser effect and shall consist of cycling the pressure between 1.1 and 5.3 ksi (7.6 and 36.5 MPa) at a rate of 1.0 Hz. Third, the influence of high cycle thermal fatigue on a localized region of the weld cladding shall be imposed at arbitrary times during the high temperature crack growth increments. Little, if any, crack

90

growth is expected to occur during
these testing periods. In addi-
tion, these methods plus high
temperature crack growth incre-
ments shall be applied at times
when background noise is present
and when no background noise is
present.

5. Fracture

Simulate RPV pressure loadings
which might be encountered during
emergency or faulted transients

Pressurize vessel to failure
at 200°F (93.3°C).

PROPOSED TEST SEQUENCE

The following test sequence was based upon a series of assumptions, which
are:

1. Vessel dimensions: 27-in. (68.6-cm) I.D. by 6-in. (15.2-cm) wall
   thickness.

2. Initial flaw geometry: part-circular, with an initial depth of 0.5 in.
   (1.27 cm) and an initail surface length of 1.35 in. (3.43 cm).

3. Flaw location: stress intensity factor calculations were based on an O.D.
   flaw located in the beltline region of the vessel.

4. Loads: the pressure and temperature versus time histories for the
   heat-up/cooldown, normal power variations, and leak test transients were
   modeled after a PWR reactor vessel (see pp. F-29 - F-68, Reference 1 for
   details).

The detailed test sequence is given in Table A.1 and Figures A.1 and A.2:

Notes:

1. All 550°F crack growth and crack marking increments shall be preceeded
   by the heatup transient detailed in Figure 1. Similarly, upon completion
   of a crack growth or crack marking increment, the vessel shall be cooled
   and depressurized as per the Figure 1 cooldown transient. Thus, a total
   of 54 heatup/cooldown transients will be performed.

2. Following some of the crack marking cycling, there shall be a leak test
   simulation (designated L.T. in the table). The pressure and temperature
   history for this transient is shown in Figure 2.

91

2. Upon completion of all fatigue crack growth, the vessel shall be pressurized to failure (approx. 30 ksi, 207 MPa maximum) at a temperature of 200°F (93.3°C).

REFERENCES

1. Marston, T.U. 1978, Flaw Evaluation Procedures: ASM,E XI, EPRI-NP719 SR, Special Report, Electric Power Research Institue, Palo Alto, California.

TABLE A.1. Test Sequence for FY-80 Off-Reactor Structural Test

Pressure, ksi		Crack Growth in.	Freq., Hz	No. of Cycles	Environ.	Crack Growth Rate	Comments
Pmax	Pmin						
10.5	1.1	0.10	1.0	40,000	RT, air	5.1×10^{-6}	Initiation
10.5	3.2	0.05	1.0	15,000	"	3.4×10^{-6}	Mark
10.5	1.1	0.10	1.0	16,000	"	6.4×10^{-6}	
10.5	3.2	0.05	1.0	12,000	"	4.2×10^{-6}	Mark
10.5	1.1	0.10	1.0	13,000	"	7.9×10^{-6}	
10.5	3.2	0.05	1.0	10,000	"	5.2×10^{-6}	Mark
10.5	1.1	0.10	1.0	10,000	"	9.7×10^{-6}	
10.5	3.2	0.05	1.0	8,000	"	6.1×10^{-6}	Mark
10.5	1.1	0.10	1.0	9,000	"	1.1×10^{-5}	
10.5	3.2	0.05	1.0	7,200	"	6.9×10^{-6}	Mark
10.5	1.1	0.10	1.0	7,900	"	1.3×10^{-5}	
10.5	3.2	0.05	1.0	6,400	"	7.8×10^{-6}	Mark
10.5	1.1	0.10	1.0	7,900	$550, H_2O$	1.3×10^{-5}	See Note (1)
10.5	4.2	0.05	1.0	9,000	"	5.6×10^{-6}	Mark
10.5	1.1	0.10	1.0	7,000	"	1.4×10^{-5}	
10.5	4.2	0.05	1.0	8,200	"	6.1×10^{-6}	Mark
10.5	1.1	0.10	1.0	6,500	"	1.5×10^{-5}	
10.5	4.2	0.05	1.0	7,500	"	6.6×10^{-6}	Mark
10.5	1.1	0.10	1.0	6,000	"	1.7×10^{-5}	
10.5	4.2	0.05	1.0	6,900	"	7.2×10^{-6}	Mark
10.5	1.1	0.10	1.0	5,500	"	1.8×10^{-5}	
10.5	4.2	0.05	1.0	6,400	"	7.8×10^{-6}	Mark, then L.T. see Note (2)
10.5	1.1	0.10	1.0	5,000	"	2.0×10^{-5}	
10.5	5.3	0.05	1.0	9,100	"	5.5×10^{-6}	Mark
10.5	1.1	0.10	1.0	4,700	"	2.1×10^{-5}	
10.5	5.3	0.05	1.0	8,500	"	5.9×10^{-6}	Mark
10.5	1.1	0.10	1.0	4,400	"	2.3×10^{-5}	
10.5	5.3	0.05	1.0	8,000	"	6.3×10^{-6}	Mark
10.5	1.1	0.10	1.0	4,100	"	2.4×10^{-5}	

TABLE A.1. (cont'd)

Pressure, ksi Pmax	Pmin	Crack Growth in.	Freq., Hz	No. of Cycles	Environ.	Crack Growth Rate	Comments
10.5	5.3	0.05	1.0	7,400	550,$H_2$0	6.6×10^{-6}	Mark
10.5	1.1	0.10	1.0	3,800	"	2.6×10^{-5}	
10.5	5.3	0.05	1.0	7,000	"	7.2×10^{-6}	Mark, then L.T.
10.5	1.1	0.10	1.0	3,600	"	2.8×10^{-5}	
10.5	6.3	0.05	1.0	10,400	"	4.8×10^{-6}	Mark
10.5	1.1	0.10	1.0	3,300	"	3.0×10^{-5}	
10.5	6.3	0.05	1.0	9,700	"	5.1×10^{-6}	Mark
10.5	1.1	0.10	1.0	3,100	"	3.2×10^{-5}	
10.5	6.3	0.05	1.0	9,000	"	5.5×10^{-6}	Mark
10.5	1.1	0.10	1.0	2,900	"	3.4×10^{-5}	
10.5	6.3	0.05	1.0	8,500	"	5.9×10^{-6}	Mark
10.5	1.1	0.10	1.0	2,700	"	3.7×10^{-5}	
10.5	6.3	0.05	1.0	7,900	"	6.3×10^{-6}	Mark, then L.T.
10.5	1.1	0.10	0.01	2,500	"	4.0×10^{-5}	
10.5	7.4	0.05	1.0	14,400	"	3.5×10^{-6}	Mark
10.5	1.1	0.10	0.01	2,300	"	4.3×10^{-5}	
10.5	7.4	0.05	1.0	13,300	"	3.8×10^{-6}	Mark
10.5	1.1	0.10	0.01	2,200	"	4.6×10^{-5}	
10.5	7.4	0.05	1.0	12,300	"	4.1×10^{-6}	Mark
10.5	1.1	0.10	0.01	2,000	"	5.1×10^{-5}	
10.5	7.4	0.05	1.0	11,100	"	4.5×10^{-6}	Mark
10.5	1.1	0.10	0.01	1,800	"	5.6×10^{-5}	
10.5	7.4	0.05	1.0	10,200	"	4.9×10^{-6}	Mark, then L.T.
10.5	1.1	0.1	1.0	1,600	"	6.1×10^{-5}	
10.5	7.4	0.05	1.0	9,300	"	5.4×10^{-6}	Mark
10.5	1.1	0.1	1.0	1,500	"	6.8×10^{-5}	
10.5	7.4	0.05	1.0	8,100	"	6.2×10^{-6}	Mark
10.5	1.1	0.1	1.0	1,300	"	7.8×10^{-5}	
10.5	7.4	0.05	1.0	7,100	"	7.1×10^{-6}	Mark
10.5	1.1	0.10	0.01	1,050	"	9.6×10^{-5}	

94

TABLE A.1. (cont'd)

Pressure, ksi		Crack Growth in.	Freq., Hz	No. of Cycles	Environ.	Crack Growth Rate	Comments
Pmax	Pmin						
10.5	8.4	0.05	1.0	14,000	550,H_2O	3.5×10^{-6}	Mark
10.5	1.1	0.1	0.01	1,000	"	1.0×10^{-4}	
10.5	8.4	0.05	1.0	11,000	"	4.5×10^{-6}	Mark
10.5	1.1	0.1	0.01	780	"	1.3×10^{-4}	
10.5	8.4	0.05	1.0	10,000	"	5.2×10^{-6}	Mark
10.5	1.1	0.1	0.01	620	"	1.6×10^{-4}	
10.5	8.4	0.05	1.0	7,800	"	6.4×10^{-6}	Mark, then L.T. see Note (3)
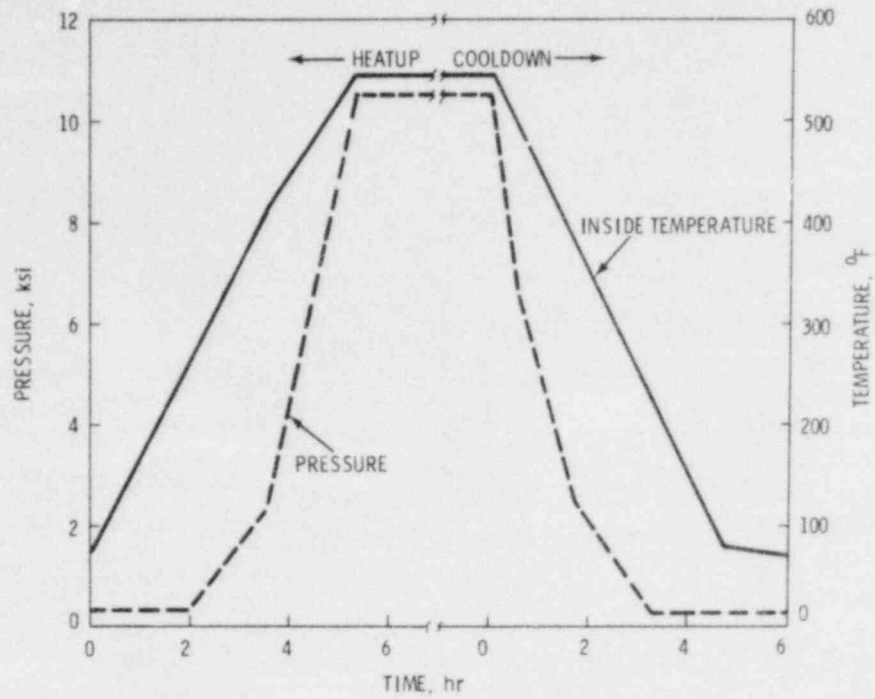
FIGURE A.1. Heatup/Cooldown Transient
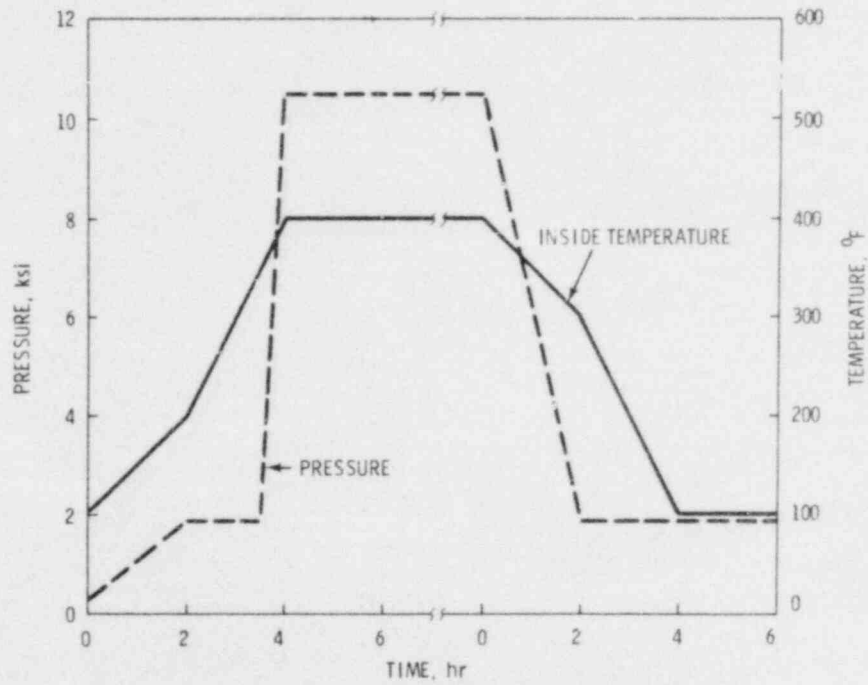
FIGURE A.2. Leak Test Transient

96

INTEGRATION OF NONDESTRUCTIVE EXAMINATION
RELIABILITY AND FRACTURE MECHANICS[a]

G. J. Posakony, Program Manager
F. L. Becker, Project Manager
S. H. Bush, Project Manager
S. R. Doctor
G. B. Dudder
P. G. Heasler
F. A. Simonen
G. P. Selby

SUMMARY

Major accomplishments during the past quarter included:

- completion of material acquisition and initiation of sample fabrication

- completion of a program review and the finalization of the round robin (industrial verification of inspection reliability) test matrix.

INTRODUCTION

The progress and accomplishments of the past quarter are described by task below.

TASK 1:   DRAFT "WHITE PAPER"

The white paper is a critical review of published and unpublished documents dealing with the impact of inspection reliability on reactor system safety. Seven of the proposed 15 chapters of the white paper have been drafted, and final publication of the document is planned for late 1981. In the interim, summaries will be published in the quarterly reports as they become available. Chapters 1 and 2 are summarized below.

CHAPTER 1: JUSTIFICATION, PURPOSE, AND SCOPE

This white paper, "Reliability of Nondestructive Examination," will ultimately consist of 15 chapters on the reliability of various nondestructive examination (NDE) techniques, the significance of the lack of reliability in probabilistic terms, and factors and procedures that could enhance reliability. The reliability of detecting, locating, and sizing flaws will be an input into a probabilistic fracture mechanics model that highlights the significance of failing to detect flaws or inaccurately locating and sizing them in the context of component failure probability.

The emphasis of the white paper will be on nuclear systems; however, relevant NDE data on a spectrum of materials and applications will be examined to determine the applicability of the information to nuclear reactor systems.

The purpose of this exercise is not to generate a series of white papers on NDE practices. Rather, it is to pinpoint strengths and weaknesses as input into experimental programs aimed at increasing the reliability of flaw detection. The hoped-for output of the combined detection reliability-probabilistic fracture mechanics program is improved examination procedures for incorporation into the Boiler Pressure Vessel Codes, American Society of Mechanical Engineers (ASME), Sections III, V, and XI and a better insight into component failure probabilities as they are influenced by improved reliability in detecting, locating, and sizing flaws.

Nondestructive examination, particularly ultrasonic, has been quite controversial. Its proponents claim high levels of flaw detection sensitivity and accuracy of flaw sizing, while its opponents denigrate ultrasonics as a viable examination procedure. As is usually the case with exaggerated claims, the truth lies somewhere in between.

The purpose of the white paper is to assess the significance of flaws at various locations in pressure boundary components and to optimize the NDE procedures accordingly. If the presence of a flaw in a given location results in a very high stress intensity factor due to location and loads, rigorous NDE procedures with a high detection reliability should be applied. On the other hand, much less rigorous criteria could be applied to innocuous defects such as slag, laminations, or deeply embedded (small) flaws. Since the concern is

with flaws in operating reactors, exposure of NDE operators to radiation is a critical factor, and every effort should be made to reduce the time spent on geometric indications or in regions of minor safety significance so the time can be spent in the areas of major safety significance.

Emphasis will be on an integrated program. If component design and/or fabrication procedures adversely affect NDE detection of flaws, changes should be made. Where possible, materials should be selected that are amenable to NDE. Fracture mechanics and component failure statistics should be used to pinpoint critical locations where enhanced NDE may be required. Potential failure mechanisms should be examined to optimize the NDE for the types of cracks anticipated.

Present plans are to divide the white paper into 15 chapters. Consideration will be given to all pressure boundary components where failures have safety or substantial economic significance. Emphasis will be given to piping and to the reactor pressure vessel since much of the data relevant to these components can be applied to pumps, valves, steam generators, etc. Steam generator tubing may or may not be covered since there are extensive NDE efforts relevant to tubing, and the information has been well reported to the relevant organizations.

CHAPTER 2: NATIONAL AND INTERNATIONAL REGULATORY AND CODE REQUIREMENTS RELEVANT TO INSPECTION AND ACCEPTANCE/REJECTION OF FLAWS IN NUCLEAR PRESSURE BOUNDARY COMPONENTS

The detection, sizing, and acceptance/rejection of flaws are sensitive to the particular national codes, standards, and regulations. For examination requirements typical of thick-walled components used in light water reactors, two codes are pre-eminent and differ sufficiently to permit excellent comparisons. These codes are: (1) The Federal Republic of Germany (FRG) Arbeitsgemeinschaft Druckbehalter (AD) - Markblatter, specifically manufacturing/inspection HP series;[1,2] and (2) the ASME Codes, specifically ASME-III Construction,[3] ASME V Nondestructive Examination,[4] and ASME XI In-Service Inspection.[5] Since both the FRG and USA codes are compulsory, the differences have a greater impact than do non-mandatory standards or codes in draft status.

Some idea of the use made of the various codes can be obtained from Table 1. The emphasis on ASME XI may be due in part because it has been in effect longer.

Ultrasonic equipment represents a significant difference in philosophy between the FRG codes and ASME. Both require the use of single probe pulse height equipment; however, in the FRG code, the tandem technique is required in addition to single probe for wall thicknesses greater than 100 mm.

Equipment frequency range is similar under both codes; however, the FRG codes are more specific. For example:

Angle Beam
    Thickness < 25 mm   2 - 5 MHz
    Thickness > 25 mm   1 - 2.5 MHz
Longitudinal Beam   2 - 5 MHz

Beam angles are similar. A longitudinal beam, 40-55° (usually 45°) and 55-70° (usually 60°), is cited with the proviso that at least 15° must separate the two used. The German requirements are more explicit for testing cladding, depending on whether it is done from the clad side or the opposite side. They require a longitudinal wave at a defined angle. The same procedure is in use in the U.S., but there is no mandatory requirement.

Transducer requirements are similar in definition of shape and size. In Germany, the near fields are fixed as functions of wall thickness: for t < 25 mm, the near field is < 50 mm; for t > 25 mm, the near field is > 50 mm.

Calibration requirements represent the major difference in philosophy. Since calibration establishes sensitivity and may set acceptance/rejection criteria, many of the claims and counterclaims for the superiority of one ultrasonic testing (UT) technique can be traced to the calibration criteria. The marked effect has been discussed by Meyer,[16,17] and his data will be described in detail in a later section of this chapter. The ASME procedure uses a series of side-drilled holes varying in size as a function of calibration block thickness. The block(s) should compare in thickness to the component being tested, and the acoustic properties of block and component should

100

IMAGE EVALUATION
TEST TARGET (MT-3)

6"
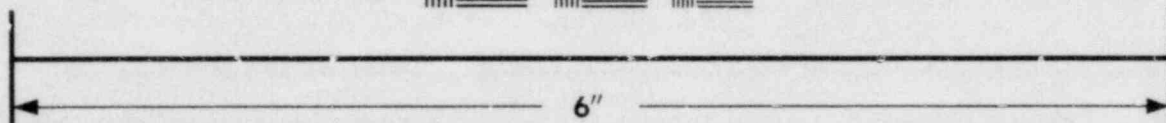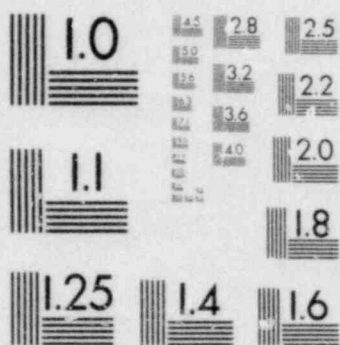
MICROCOPY RESOLUTION TEST CHART

IMAGE EVALUATION
TEST TARGET (MT-3)
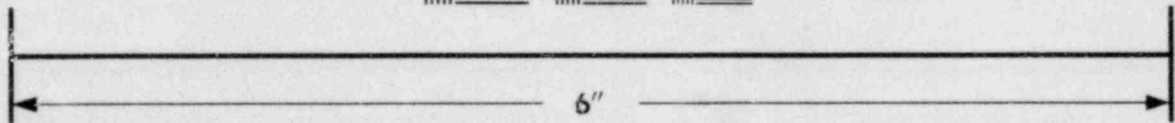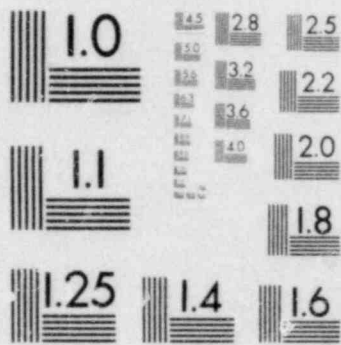
MICROCOPY RESOLUTION TEST CHART
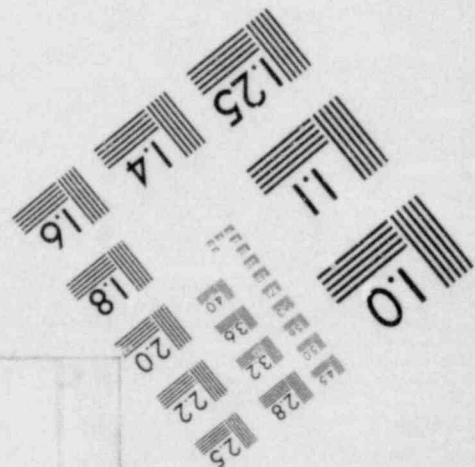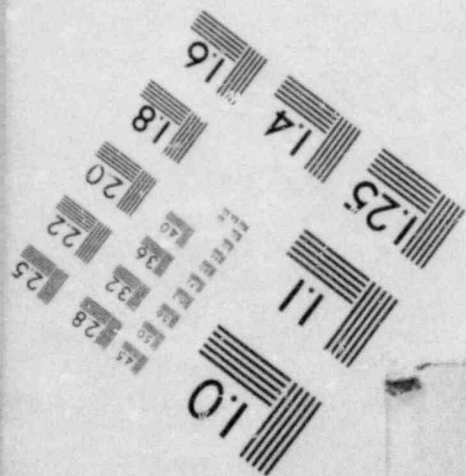
TABLE 1. Examples of Use of Codes and Regulations
by Various Countries (not complete)

(Periodic Inspection of Light Water Reactors)

Country	Code			Regulations		Comment	Ref.
	ASME XI	FRG-AD-M	Other	Yes	No		
Austria	X	X	X	X		Austrian Code	6
Belgium	X					Relies on ASME and AD-M - Parital	7
France	X			X		Ministry Order Feb. 26, 1974 No. 33-19	8
FRG		X		X		RSK	1,2
India	X			X			9
Italy	X						10
Japan	X			X		MITI Technical Standards, Electric Utility Act	11
Netherlands	X						6
Spain	X			X			6
Sweden	X		X			RPV follows ASME XI; Piping - special requirements	12
Switzerland	X		X	X		Writing code based on ASME XI	13
U.S.	X			X			14
IAEA			X			Modeled on ASME XI	15

be essentially the same. The side-drilled hole sizes range from 3/16 and 1/4 in. to thicknesses of 6 inches. Additional holes, increasing in diameter by 1/16 in., are added for every additional two inches of block thickness.

German blocks use flat-bottom holes for calibration with a diameter of either 3 mm or 10 mm used for accept/reject. Major emphasis is placed on use of the Kraut-kramer AVG (DGS) diagram, which can be used in lieu of calibration blocks. Both ASME and DGz fP (German Association for NDE Methods) or AD-RHP 5/3 define linearity, control, screen height, and calibration intervals; while there are differences, they are not considered major.

Surface finish requirements are more severe in Germany. A surface finish of <10 µm mean value is designated. ASME is more vague, simply requiring that the surface be smooth and free of weld spatter, scale, etc. Both require that the weld region have no excessive elevations or depressions leading to probe tilt.

Rate of travel of the probe is limited to 6 in./sec in ASME. The German codes appear to be moot; however, this could be due to an inadequate search of the literature.

UT weld examinations vary in degree. The differences are best seen by selecting a reactor pressure vessel such as a pressurized water reactor (PWR) where the wall is about 250 to 300 mm thick. For pre-service examinations, the German requirements include examination from both inside and outside, if possible, versus one or the other or both required by ASME XI. Examinations should be from both sides of the weld on the same surface where possible in both countries. German requirements include moving the probe in both directions along the weld plus rotating the probes to detect transverse cracks. For electroslag welds, an added beam traverse must be made at 45° to the weld. ASME XI requires examination of base metal to a distance t/2 from the weld.

The FRG in-service examination must include at least 50 mm strips parallel to the weld for submerged-arc and manual welds and >100 mm for electroslag welds. In the case of in-service examination, which is usually limited to either the inner or the outer surface but not both, there is a German requirement to coordinate single probe and tandem examinations from the inner surface

102

to permit coverage of the most probable flaw orientations. At the pre-service stage, the German requirement is to examine 100% of the reactor pressure vessel surface. In essence this is done on PWRs due to the nature of the UT examination; however, it is not a code requirement. It is a requirement at the plate or forging stage.

Overlap coverage of the probe is the same, >10%.

Cladding examination differs to a major degree. For example, the ASME code finds surface indications acceptable while the German codes do not. The German codes (D G(z) fP; AD-RHP 5/3; RSK Directive for DWR-design April 24, 1974) permit no cracks at the clad-base metal interface (same as ASME III), require angled longitudinal wave >2 MHz from the side opposite the clad, or dual transmit receive probes >2 MHz on the clad side. It is an RSK requirement that the required sensitivity be maintained through cladding. Sensitivity is set by using either a 2-mm diameter drill hole parallel to the test surface at the interface with adjustment to full screen height or a 2-mm flat-bottomed hole with bottom at the interface with the signal adjusted to 3/5 screen height. Added requirements include random examination with 70° angle probes (RTD - BAM 70°) for detecting crack-like defects at the interface.

Recording levels tend to be more specific in the FRG compared to ASME XI. The ASME XI requirement depends upon the edition and addenda. The requirement was 20% distance amplitude correction (DAC) of the primary reference level initially, which was changed to 50% DAC because of the large number of geometric indicators.

Acceptance-rejection limits depend on both codes on whether the vessel is under the construction code or in the preoperational or operational stage. Neither construction code (FRG or ASME III) will accept cracks or crack-like defects. Both will accept UT indications below certain sizes.

ASME XI defines a spectrum of acceptable flaws (not indications) at both the preservice and in-service stages. The reader is directed to ASME XI for the complete picture. For an operating vessel where the flaw exceeds the acceptable value, it is permissible to do a fracture mechanics analysis according to Appendix A of ASME XI and, if the analysis indicates the flaw

does not exceed the criteria of IWB-3600, the vessel need not be repaired. However, the flaw must be monitored at several subsequent examinations.

Flaw sizing and locating procedures are generally similar. The ASME code requires sizing by measuring the maximum DAC value then measuring the two ends on the basis of 50% of the maximum DAC value.

Multiple flaws or indications are considered to be additive if they occur at the same depth and are closer than some specific value. ASME XI defines elaborate criteria; the German code states that indications are added unless separated by more than the length of the largest indication.

Presumed Limitations--ASME XI Versus FRG Codes

Trumpfheller [18,19] argues that the ASME XI approach to flaw sizing is less thorough than the German code rules, primarily because the ASME code contains no criteria establishing when an indication should be interpreted as emanating from a crack-like defect. The preceding was based on the 1971 edition of ASME XI, which did not contain the mandatory Appendix I covering UT procedures. Presumably, Appendix I in part supplies the missing criteria. A more pertinent claim concerns the recording and action levels of ASME XI. These levels have varied from 20% to 100% DAC, depending on the Code edition and addendum..

One further difference in code philosophy is cited by Trumpheller.[18] A statistical or probabilistic approach is used in establishing the size and number of acceptable defects per specified volume of weld. The ASME codes emphasize size rather than numbers.

Meyer[16,17] conducted a series of experiments that highlight the similarities and differences of the FRG HP 5/3 and ASME V and XI codes. Table 2 from Reference 17 compares these differences when applied to the examination of a weldment. The author[16,17] conducted a testing program on different types of reference blocks of various thickness, containing natural and artificial reflectors of known size, location, and orientation. He rigorously applied ASME and HP 5/# for calibration, testing, recording, and reject/repair.

Meyer's conclusions in Reference 16 are more understandable after reading Reference 17 since some of the conclusions are not obvious from the report contents. These were:

TABLE 2. Comparison of Weld Examination According to to HP 5/3 (Level C) and ASME Code Section V for Wall Thicknesses Over 4 Through 6 Inches

Sensitivity Setting	HP 5/3	ASME
Calibration method	+	0
Transfer correction	+	0
Recording level	+	0
Unacceptable level L	+	0
Higher sensitivity according to test results	+	-

Examination Technique	HP 5/3	ASME
Longitudinal Flaws		
Two different beam angles	+	+
Straight beam technique	+	+
Examination from both sides of the weld	+	+
Tandem technique	+	+
Transverse Flaws		
Two different beam angles	+	+
Examination from one surface	+	+
Tandem technique	+	-
Evaluation of Flaws		
Evaluation of flaw amplitude	+	0
Length of flaw	+	0
Depth of flaw	+	+
Height of flaw	+	0
Number of flaws	+	-
Distance between flaws in same depth	+	-
Distance between flaws in direction of thickness	+	-

- It is necessary to use different probe angles (70°, 45°, etc.) and to scan from different directions to ensure flaw detection.

- The tandem technique affords added reliability in evaluating defects, compared to the single probe technique.

- Defect/rejection criteria should be in terms of the number of defects per meter of weld to minimize unnecessary repair (this is the same point made by Trumpfheller).[18]

- HP 5/3 is more severe than ASME V for rejection using echo amplitude as the criterion.

- For detection, the two codes yield essentially comparable results.

Meyer[17] argues that the ASME procedure where UT equipment is calibrated with notches or edges is essentially unsatisfactory, based on experience, whereas excellent correlations have been obtained with cylindrical boreholes (flat-bottomed holes). He notes that most national codes use flat-bottomed holes for calibration.

Meyer[17] cites several factors adversely influencing the detection of flaws by UT:

- An adverse angle resulting from probe angle and flaw orientation may prevent a majority of the UT beam from being reflected back to the probe (UT from both sides of the weld helps).

- Small planar defects normal to the surface are difficult to recognize from either side because most of the UT beam is reflected in different directions (the tandem technique may help).

- Laminations may shadow planar defects.

- Lack of fusion between weld beads will lead to curved surfaces that cause UT beam scatter.

- Shrinkage stresses may result in compressive loads on the crack rendering it transparent to the UT beam (with smooth surfaces and low frequencies, complete transparency is probable at >20 N/mm^2 compressive stress).

- There is an interaction between defect size and its orientation; small reflectors can be detected at steeper angles than large reflectors because such small reflectors behave as if they are spheres. As reflector size increases, the UT beam is deflected in the opposite direction so that even at small angles of defect orientation, no part of the beam is reflected back to the probe; this pertains to the tandem technique also.

Acceptance/Rejection Criteria

The ASME UT rejection criteria is quite straightforward. If the amplitude exceeds 100% DAC, the defect is rejectable. The situation is somewhat more complicated for HP 5/3. A definite dB value (6 or 12 dB) above the recording level is the general criterion for repair. Between the recording level and the repair level there may exist a definite number of reflectors, depending on both length and number of indications using a one meter weld length as the basis. If combined indications occur, the rejection level is usually reduced from 12 dB to 6 dB. A comparison is made with ASME V; however, it would be more relevant to use ASME XI, where clustered defects are considered.

Governmental Regulations

The government, whether in the United States or elsewhere, can have either a positive or a negative impact on the applicable codes covering NDE procedures and flaw acceptance levels. Emphasis will be given to the U.S. regulations because of greater familiarity. Examples of how positive changes may come about are contained in the Code of Federal Regulations, Title 10 (10 CFR)[20] specifically in Appendix A and Appendix B and in 10 CFR Part 50.55(a), which deals specifically with ASME codes. Positive actions are also promulgated through Regulatory Guides and Branch Technical Positions. Negative actions occur by failure to take action. For example, as late as mid-1979, 10 CFR Part 50.55(a) approved ASME Section III, Division I, through the 1977 edition of this code including the summer 1977 addenda, while ASME Section XI is approved only through the 1974 edition including the summer 1975 addenda. This difference is due to reservations in the Regulatory staff on specific but limited items within the Section XI code.

107

Summary

Principal differences in NDE philosophy exist between the ASME XI Code and the FRG HB 5/3 Code. These differences have been discussed in this chapter. It appears that the major difference is the acceptance/rejection thresholds for indications rather than in the detection of flaws.

The following paragraphs are an attempt to orient the reader to the scope of each chapter.

Chapter 1

This chapter is discussed above.

Chapter 2

This chapter is discussed above.

Chapter 3: Detection, Location, and Sizing - The PVRC Program

The Pressure Vessel Research Committee (PVRC) Industrial Cooperative Program complemented the U.S. Atomic Energy Commission/Nuclear Regulatory Commission Heavy Section Steel Technology Program and concentrated on NDE flaw detection and sizing reliability. The results from the PVRC and European Plate Inspection Steering Committee Program represent a major body of data on thick steel sections as plates, forgings, and nozzles in plates or forgings. The use of a round robin testing program highlights team variability as well as indicating the sensitivity of detection reliability to the NDE procedure followed.

Chapter 4: Flaw Detection

The emphasis is on the factors influencing flaw detection, such as material characteristics, surface characteristics, coupling efficiency, geometry, etc. Results with commercial state-of-the-art and advanced equipment are emphasized.

Chapter 5: Flaw Sizing and Location - with NDE

This is a review of the literature relevant to errors in sizing of natural and artificial flaws and assessment of factors such as external loads, flaw roughness, beam spread, size of focal spot, etc., as they influence sizing.

Chapter 6: Ultrasonic Testing

Emphasis on UT, with literature pertaining to focused probes, acoustic holography, adaptive learning networks, and a review of other NDE techniques that were examined.

Chapter 7: Ultrasonic Equipment - Characteristics and Limitations

Both theoretical upper bound limits and variability typical of the electronic circuitry and transducers are considered. This chapter also covers existing limitations and the possibilities for improvement.

Chapter 8: Flaw Detection and Sizing - Theoretical Background

Several excellent papers have been written on wave behavior in solids. Some of the work should lead to new approaches in flaw location and sizing.

Chapter 9: NDE - For Measurement of Physical and Mechanical Properties

The intent here is to concentrate on those properties directly pertinent to failure potential. Obvious choices include residual stress levels and distribution, approach to end of life by fatigue, properties such as internal friction that may correlate with toughness, and stress intensity. Ideally, one would like to measure parameters directly relevant to fracture mechanics.

Chapter 10: Failure Statistics and Flaw Significance

Types and probability of failure by component size, specific location, etc., are assessed to benchmark the probabilistic fracture mechanics task.

Chapter 11: Relevant Statistical and Probabilistic Models

This chapter is an assessment of the preferred models for handling the available data and will serve as an introduction to Chapters 12 and 13.

Chapter 12: Probabilistic Fracture Mechanics

Work in probabilistic fracture mechanics is examined. Inputs will be used to characterize the significance of flaws as functions of size, orientation, and location. The aim is to define significance rather than to develop failure probability values in an absolute sense.

109

Chapter 13: Probability Models - Reliability of Flaw Detection - Statistical Data Confirming Detection Reliability

The appropriate probability models will be selected as a vehicle for reviewing available data regarding flaw detection and assisting in the development of the experimental program for gathering a statistically significant body of data on detection reliability and the factors affecting reliability.

Chapter 14: The ASME Codes, Testing Techniques, Analytic Procedures, and Suggested Modifications

Sections III, V, and XI are examined to see if there are changes in design, materials, or fabrication that could improve detection reliability in NDE procedures for pinpointing significant flaws with greater reliability or changes in operational histories of existing nuclear plants to optimize inservice inspection, burn-up, examination of significant areas, and assessment of the role of advance NDE techniques.

Chapter 15: Conclusions and Recommendations

Specific items are culled from all chapters to serve as guidance in future experimental and analytic programs.

TASK 4: FRACTURE MECHANICS

A review of a recently issued evaluation by D. O. Harris entitled, "The Influence of Crack Growth Kinetics and Inspection on the Integrity of Sensitized BWR Piping Welds," has been reviewed and analyzed. The results of this analysis are given below.

Harris seems to make two main points of interest. The first is that stress corrosion cracks will arrest in large pipes but not in small pipes. This trend is a direct consequence of qualitative differences in the assumed residual stresses in small versus large pipes. The second point is that in-service inspection is of little use for increasing the reliability of piping in stress corrosion cracking situations. Harris predicts the time to grow a crack from a detectable size to a critical size; this time is short compared to in-service inspection intervals.

110

The positive conclusion relative to large compared to small pipes may be questionable. The small pipe could be considered safe because the nonaxisymmetric residual stresses will ensure that the pipe will leak before breaking. On the other hand, the large pipe has an axisymmetric residual stress distribution. Therefore, if for some reason growing cracks do not arrest as predicted, a circumferential flaw could grow to critical size without leaking. Thus, one could consider the small pipe more safe than the large pipe.

Cracks may not always arrest in large pipes as claimed. Harris considered only one particular distribution of welding residual stress and considered no variation in this stress as occurs in practice. Also, no redistribution in these stresses were considered due to possible yielding under projected service loads. Harris did not consider subsequent growth of stress corrosion cracks by other mechanisms such as fatigue. A further limitation of the stress corrosion crack growth calculations is the severe lack at present of da/dt versus K_{max} data. Harris had only a few data points for a limited range of environments. While Harris considered the sensitivity of predictions to the exponent m, no other key parameters such as ap (8 in./year) or Kp (14 Mka - $m^{1/2}$) were varied in the sensitivity analyses.

In summary, the report by Harris gives some interesting results and may explain many aspects of piping performance. However, his conclusions on crack growth rates and possible arrest could be incorrect for the conditions and data other than those assumed in his analysis. In particular, there is probably far more variation in residual stress levels and distributions and crack growth rates and mechanisms than considered in the Harris report.

TASK 5: STATISTICAL PROGRAM DESIGN

The program review conducted on January 29, 1980, resulted in modification of the round robin test matrix. These modifications are significant but should not substantially increase the total inspection time and costs. However, the ad   ional information will provide a greatly improved basis for improved inspection requirements. The revised test matrix includes the following:

111

1. Four materials:

    - _ ·in. Schedule 80S, 304 stainless steel

    - 12-in. Schedule 100, 304 stainless steel

    - 27.5-in. ID, 2-3/8-in. wall centrifugally cast stainless steel

    - 33.5-in. OD, 2-3/8-in. wall A106 steel with stainless ID clad.

2. Three st procedures:

    - minimum code requirements based on amplitude

    - procedures as practiced in the field

    - improved test procedure based on results and recommendations of this program to date.

3. Two test conditions or environments:

    - laboratory

    - difficult field conditions (simulated).

4. Two access conditions:

    - near side (flaw on near side of weld)

    - far side.

The test matrix is a partial factorial design. Analysis of variance analysis will be performed. The objective of the design is to establish the probability of detection (POD) for each material using difficult environments, near-side access, and as-practiced field procedures. Sufficient measurements will be performed under the remaining test variables to determine the difference in POD resulting from these test variables.

TASK 6: SAMPLE PREPARATION

The thermal fatigue facility has been completed, and the basic procedures and test parameters are developed. An example of the cracks produced in 10-in. Schedule 80S stainless welded pipe are shown in Figure 1.
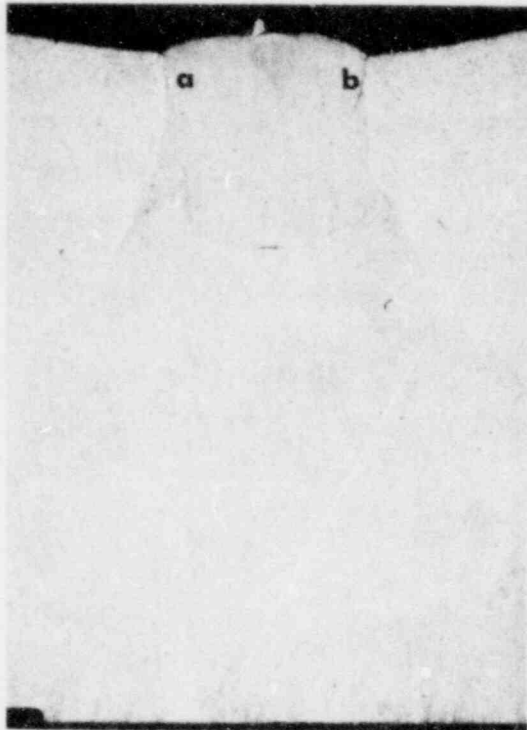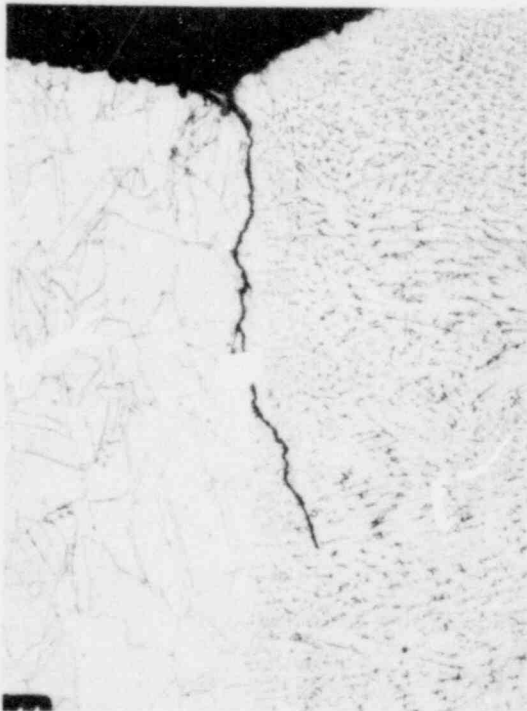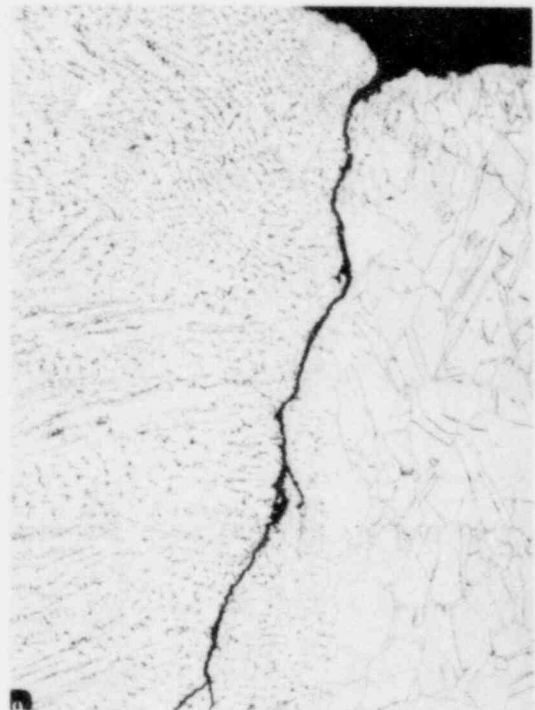
FIGURE 1. Example of Thermal Fatigue Cracks Produced
in Welded 10-in. Schedule 80 Pipe

113

The remaining task to be developed is the production of flaws greater than 50% of the wall thickness (greater than 1.0 in. deep) in thick-wall piping. Experiments are in progress to determine the parameters and maximum flaw depths that can be obtained in thick-wall material.

TASK 7: MEASUREMENT AND EVALUATION

Previous reports have described the influence of search unit selection, flaw orientation, and aspect ratio on test sensitivity and flaw detectability. These experiments were performed on 0.6-in. thick stainless plates with artificial notches of aspect ratio (length to depth) of 5 to 1. The influence of component thickness and reference reflectors are described below. In the next quarter, the study will be extended to other aspect ratios and pipe geometries.

Higher Wall Thickness

The influence of higher section thickness on flaw detectability can be extrapolated from full V and 3/2 V measurements on the 0.6-in. thick samples. For our flat 0.6-in. plates, a full V inspection of a flaw is identical to a 1/2 V inspection of the same flaw in 1.2-in. material. Likewise, 3/2 V inspection in 0.6-in. plate corresponds to 1/2 V inspection in 1.8-in. plate. ASME calibration notches with 0.120-in. and 0.180-in. depths are used to calibrate these inspections. The results are presented in Figures 2 through 4 with reflection amplitude plotted against flaw depth in percent of wall thickness for all three thicknesses with three transducer diameters. The influence of wall thickness on detectability is best illustrated by Figure 4 for the 1-in. transducer.

According to Table IWB-3514.3 of ASME Section XI Code, the maximum allowable flaw depth for this aspect ratio is about 11% through wall. Figure 4 shows clearly that for 11% crack depth, the reflection amplitude is powerfully influenced by wall thickness; small thickness results in small response. In fact, the maximum allowable flaw in 0.6 in. pipe is seen to be undetectable with a 50% DAC recording criterion.

114
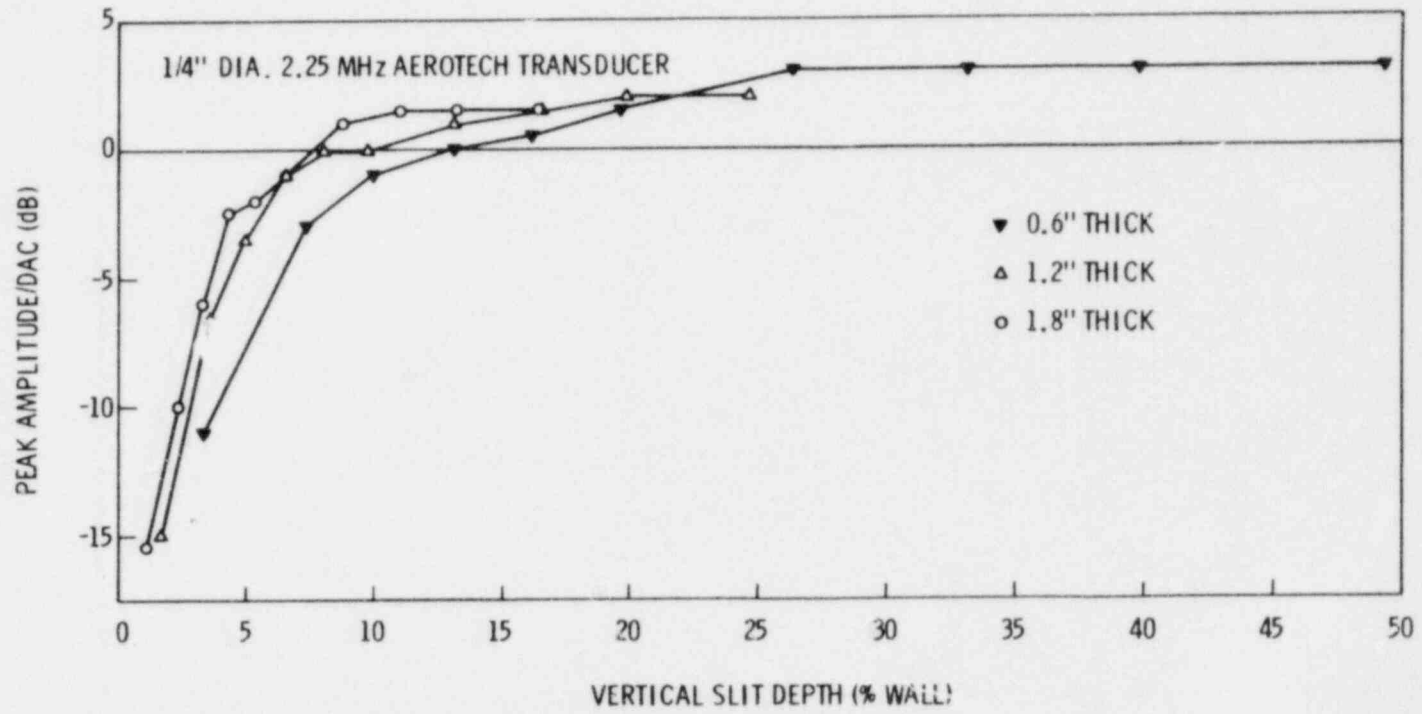
FIGURE 2. Simulated Inspection of Thicker Material with 1/4" Transducer
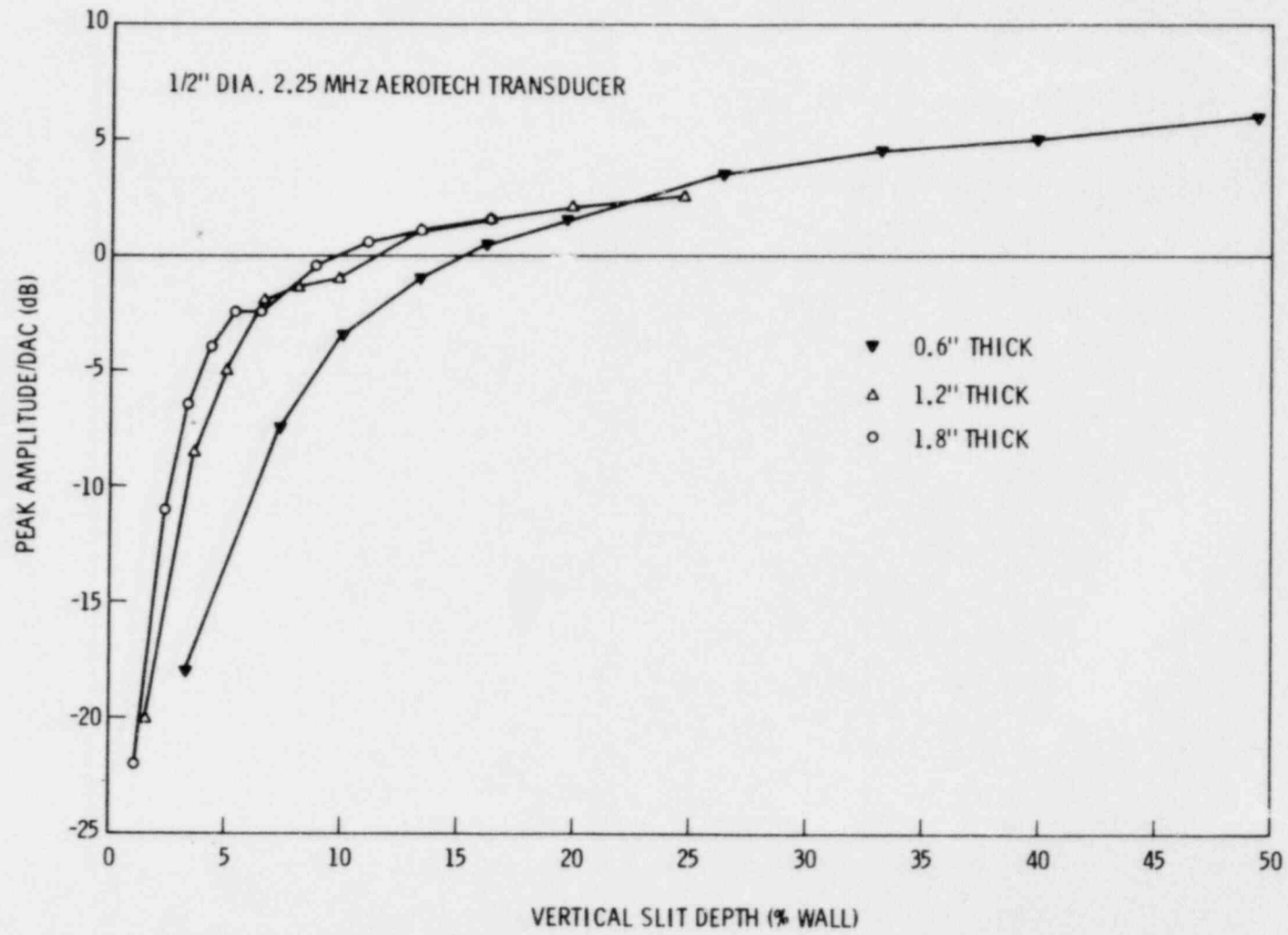
FIGURE 3. Simulated Inspection of Thicker Material with 1/2" Transducer

116
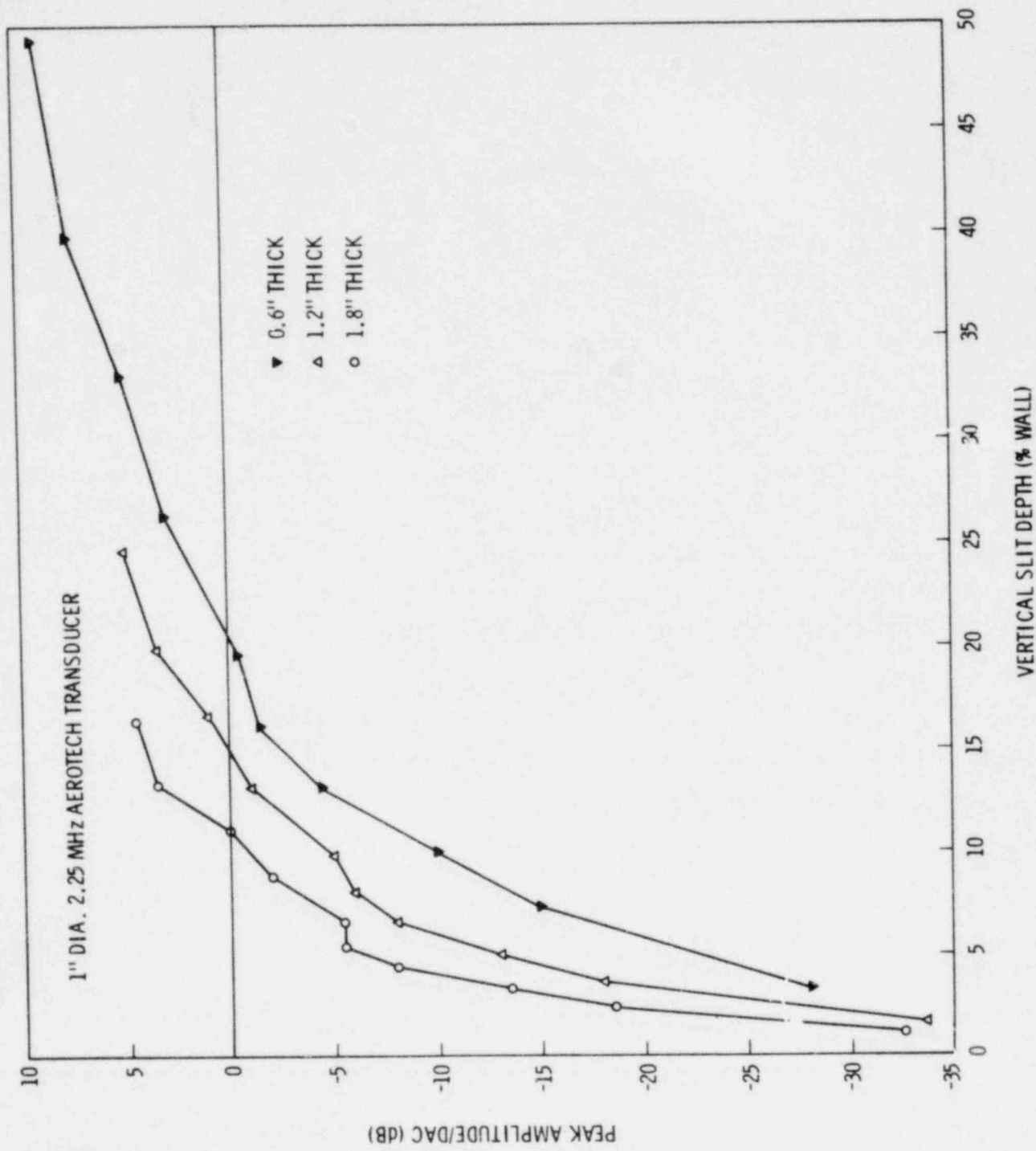
FIGURE 4. Simulated Inspection of Thicker Material with 1" Transducer

117

This effect is not as great for the 1/4 in. and 1/2 in. transducers (Figures 2 and 3) because the 11% flaws are large enough to be near the infinite-reflector response plateau and, therefore, have about the same response.

Calibration Reflector

The basic calibration reflector for these studies is the end-mill notch with depth equal to 10% of the pipe wall thickness. Another calibration reflector often used is the side-drilled hole, required by the 1974 version of Section XI. If the two calibrations differ significantly, they will not produce equal levels of detection reliability.

In order to compare the two, calibration was performed using the side-drilled hole and then the 10% notch was inspected. This was done for 45^0 beam (1/2 V, full V, 3/2 V) and 60^0 beam (1/2 V) and for several transducers. The results are shown in Table 3.

In 45^0 inspection, the 10% notch produced higher responses than the side-drilled hole for all beam paths and transducer diameters. Since a higher calibration response means reduced sensitivity, the 10% notch calibration results in a less sensitive inspection. The hole response is lower because the reflection area is smaller and geometrically dispersive.

In calibrating for 60^0 inspection, the larger area of the notch is negated by mode conversion, and the sensitivities of the two calibrations are about equal. No mode conversion occurs on reflection from the hole because all reflections from a side-drilled hole are at normal incidence.

Impact on Inspection Reliability

From test results to date, several factors that will influence in-service inspection (ISI) reliability are apparent. One is search unit selection. Even

TABLE 3. Decibel Response of 10% Notch, Compared to Side-Drilled Hole

Transducer	1/2 V 45^0	Full V 45^0	3/2 V 45^0	1/2 V 60^0
1/4", 2.25 MHz	+9	+11	+16	+2
1/2", 2.25 MHz	+9	+8	+8	0
1", 2.25 MHz	+3	+3	+2	-3

118

though calibration is performed strictly to code (Section XI, 10% notch), test results could be highly variable (6 dB or more) without requirements for search unit size and operating characteristics. Also, when choosing a search unit, a compromise must be reached between small flaw and off-angle flaw detectability on the one hand and large flaw detectability on the other.

Ultrasonic response for angled flaws and flaws on the counterbore varies widely with angle and flaw depth. In some cases, a small flaw can produce a higher response than a large flaw of the same orientation. It is entirely possible that as certain cracks grow, periodic inspections would show decreasing signal amplitude.

Inspection with a 60° beam appears to be less sensitive to flaw orientation and to provide better detectability than 45° inspection because the calibration reflector produces almost maximum mode conversion and, therefore, high sensitivity. Currently, only 45° inspection is mandatory. Also, off-angle detectability is improved by choosing transducers with high beam spread, that is, small diameter or low frequency. The same applies for instrument selection; given two inspection instruments operating at the same nominal frequency, the one with the lower actual frequency will provide better angled flaw and counterbore flaw detectability.

Choice of calibration reflector can be highly influential for 45° inspection; for transducers smaller than one inch, the use of side-drilled holes will lead to a much more sensitive inspection. For large transducers and for a 60° beam, there is not so much difference.

Finally, the detectability of the maximim allowable flaw with a given transducer varies with wall thickness. The variation is not large for small transducers but is large for the 1-in. transducer; detectability increased dramatically as thickness increased. Use of the 1-in. transducer would not provide a good inspection for this 10-in. Schedule 80 pipe.

TASK 8: INDUSTRIAL VERIFICATION OF INSPECTION RELIABILITY (ROUND ROBIN)

A major task activity of the past quarter has been the organization and planning for the round robin tests that will be initiated in June 1980. These activities include contacting ISI vendors, welded sample fabrication, data collection protocol, definition, and data analysis.

Six vendors of ISI services have recently been contacted. Three vendors had previously expressed an interest in participating in the round robin. None have yet declined to participate.

The purchase order for welding pipe samples has been issued with completion date of March 1, 1980. The A106, 33-1/2-OD pipe is being shipped from Ohio and may result in a short schedule slippage. We have presently a verbal understanding with Mel Lapids of the Electric Power Research Institute on the loan of the 12-in. Schedule 100 304 stainless steel pipe with intergranular stress corrosion cracks. Finalization of this agreement is expected by early March.

As a result of the recently completed program review, it was decided to include an improved test procedure based on program recommendations to date. Several factors concerning these recommendations require additional analysis before they are finalized. However, we believe that this can be accomplished before the June start date for the round robin.

Test protocol and data collection requirements are under development at this time but are expected to be finalized in March. A prime consideration of the data collection is that it can be easily entered into the computer for rapid analysis. Time limits will be imposed for the scanning and analysis of each sample; thirty minutes for each sample is considered adequate at this time.

FUTURE WORK PLANS

During the coming quarter, all efforts of the program will be directed toward finalization of preparation for the round robin. It is expected that the first inspection team will be tested in June. Efforts are also in progress

to extend flaw detectability experiments to larger pipe wall thicknesses and pipe geometries. The evaluation of material and weld metal attenuation effects on single side inspection reliability will be initiated.

REFERENCES

1. "Compilation and Comparative Examination of Existing Guidelines and Speci-fications for Design, Fabrication, Testing, and Inspection of Steel Pressure Vessels for Reactors - Final Report", GERRSR-21 (Vol. 2), originally EUR-5402d (Vol. 2), December 1974, 269 pp.

2. "Compilation and Comparative Examination of Existing Guidelines and Speci-fications for the Design, Fabrication, Testing, and Inspection of Steel Pressure Vessels for Reactors - Final Report" GERRSR-21 (Vol. 3) origi-nally EUR-5402d (Vol. 3), December 1974, 181 pp.

3. "Nuclear Power Plant Components", ASME Section III, Division 1, 1977 Edition.

4. "Nondestructive Examination", ASME Section III, Division 1, 1977 Edition.

5. "Rules for Inservice Inspection of Nuclear Power Plant Components", ASME Section XI, Division I, 1977 Edition.

6. Theiretzbacher, H., "Regulations for ISI of Reactor Pressure Vessels in Austria" in "Use of Non-destructive Testing Techniques for Inservice Inspection of Reactor Pressure Components", IWG-RRPC-78/3, Kobe, Japan, 25-27 April 1977.

7. Watkins, B., Swithenbank, T., Jackson, H., "Experiences in the Pre-Service and In-Service of Light Water Reactors", Periodic Inspection of Pressur-ized Components, Inst. Mech. Engrs. 1974, pp 118-128.

8. Prot, A. C. and Saglio, R., "Survey of the French Developments in the Field of ISI" in "Use of Non-destructive Testing Techniques for Inservice Inspection of Reactor Pressure Components", IWG-RRPC-78/3, Kobe, Japan, 25-27 April 1977.

9. Kothare, V. V., Nanjuneswaran, K., "In-Service Inspection of Tarapur Units No. 1 and No. 2 Reactor Pressure Vessels and Primary Coolant Pressure Boundary", Periodic Inspection of Pressurized Components, Inst. Mech. Engrs. 1976, pp 157-164.

10. Cioli, F. and Messore, G., "Italian Experience on NDT Techniques for ISI of Reactor Pressure Components" in "Use of Non-destructive Testing Techniques for Inservice Inspection of Reactor Pressure Components", IWG-RRPC-78/3, Kobe, Japan, 25-27 April 1977.

11. Takahashi, H., "Regulations on ISI in Japan" in "Use of Non-destructive Testing Techniques for Inservice Inspection of Reactor Pressure Components", IWG-RRPC-78/3, Kobe, Japan, 25-27 April 1977.

12. Lautzenheiser, C. E., "In-Service Inspection of Nuclear Power Plant Pressure Components", Nuclear Safety, 17, 1976, pp. 733-743.

13. Bashek, H., "ISI of Reactor Pressure Components in Switzerland" in "Use of Non-destructive Testing Techniques for Inservice Inspection of Reactor Pressure Components", IWG-RRPC-78/3, Kobe, Japan, 25-27 April 1977.

14. Chockie, L. J., "ASME Section XI" in "Use of Non-destructive Testing Techniques for Inservice Inspection of Reactor Pressure Components", IWG-RRPC-78/3, Kobe, Japan, 25-27 April 1977.

15. "IAEA Safety Guide on Inservice Inspection", Draft Copy, September 9, 1976.

16. Meyer, H. Jurgen, "Relation Between Ultrasonic Indications and Flaw Size in Pressure Vessel Welds", B&W-TUV Conference NDE, Washington, DC, November 18, 1976.

17. Meyer, H. Jurgen, "Probability of Detecting Planar Defects in Heavy Wall Welds by Ultrasonic Techniques According to Existing Codes", Report to Subcommittee V (Ultrasonics) of Commission V, International Institute of Welding (IIW) on Quantitative Evaluation of UT Indication, undated, probably 1977.

18. Trumpfheller, R., "The Sizes of the Largest Defects Which May Be Over-looked by Nondestructive Testing Methods", Rhineland Westphalia Technical Surveillance Agency LTD (TUV), April 11, 1972, Translated ABH, 11 pp.

19. Trumpfheller, R., "Requirements for Inservice Inspection of Water-Cooled Reactor Vessels by Nondestructive Testing Methods in Germany", Periodic Inspection of Pressurized Components, Inst. Mech. Engrs. 1974, pp 114-117.

20. Code of Federal Regulations Title 10 (Energy) Part 50.55(a) Codes and Standards of Part 50 - Licensing of Production and Utilization Facilities Effective May 24, 1978.

GRAPHITE NONDESTRUCTIVE TESTING[a]

W. C. Morgan, Project Manager

SUMMARY

All pre-oxidation measurements on the samples of PGX graphite have been completed and oxidation runs are in progress. Apparatus for obtaining eddy current measurements and for determining the velocity of ultrasonic surface waves on the oxidized samples are under construction. A topical report on the results of our correlation of through-transmission sonic velocity with compressive strength, using four other graphites, was distributed early in this quarter.

INTRODUCTION

This is a continuation of previous work that demonstrated the feasibility of monitoring changes in the compressive strength of oxidized graphite by measuring changes in the velocity of an ultrasonic wave propagated through the graphite. The FY-1979 scope of this project is to:

- continue the investigation of sonic velocity technique as applied to PGX and ATJ graphites

- investigate the potential for other sonic measurements, such as attenuation data, to provide useful information

- investigate the potential for other techniques, such as eddy current devices, to provide interpretable indications of graphite strength.

The objective of this investigation is to demonstrate feasibility of non-destructive testing techniques for determination of structural graphite strength.

(a) RSR Fin. Budget No.: B2101-9; RSR Contact: R. D. Schamberger

123

TECHNICAL PROGRESS

Compressive strength was measured on 12 cylinders (3 in. dia by 6 in. long), cut with their long axis parallel to the long axis of the parent PGX log. The average strength (plus or minus one standard deviation) for 11 of the 12 samples was 37.91 ± 1.16 MPa and the average density was 1.746 ± 0.005 mg/m^3; for the twelfth sample (BA-7) the respective strength and density were 29.10 MPa and 1.690 mg/m^3, (i.e., more than 7 and 11 standard deviations, respectively, from the averages of the other eleven samples). All individual measurements on the other samples were less than 3 standard deviations from the average values.

Examination of the fracture surfaces of sample BA-7 disclosed several nodules (approximately spherical particles or agglomerations of particles) up to about 6 mm in diameter, plus a larger nodule (about 1 cm in diameter) near the geometric center of the sample.

Research is being conducted simultaneously in three technical areas to develop non-destructive tests for graphite oxidation. These areas are through-transmission ultrasonic velocity, ultrasonic surface-wave velocity, and eddy current testing. A project plan we have developed for internal guidance and progress assessment is shown in Figure 1 and provides some detail on these tasks.

EDDY CURRENT TESTING

As previously reported, eddy current methods demonstrate a strong correlation between graphite oxidation and electrical conductivity. Our current effort is centered on profiling oxidation versus depth. Eddy current measurements at different depths can be obtained by controlling the test frequency and/or the coil size. Our desired result is a hardware-implementable algorithm to predict oxidation profile based on measurements at various frequencies and coil sizes.
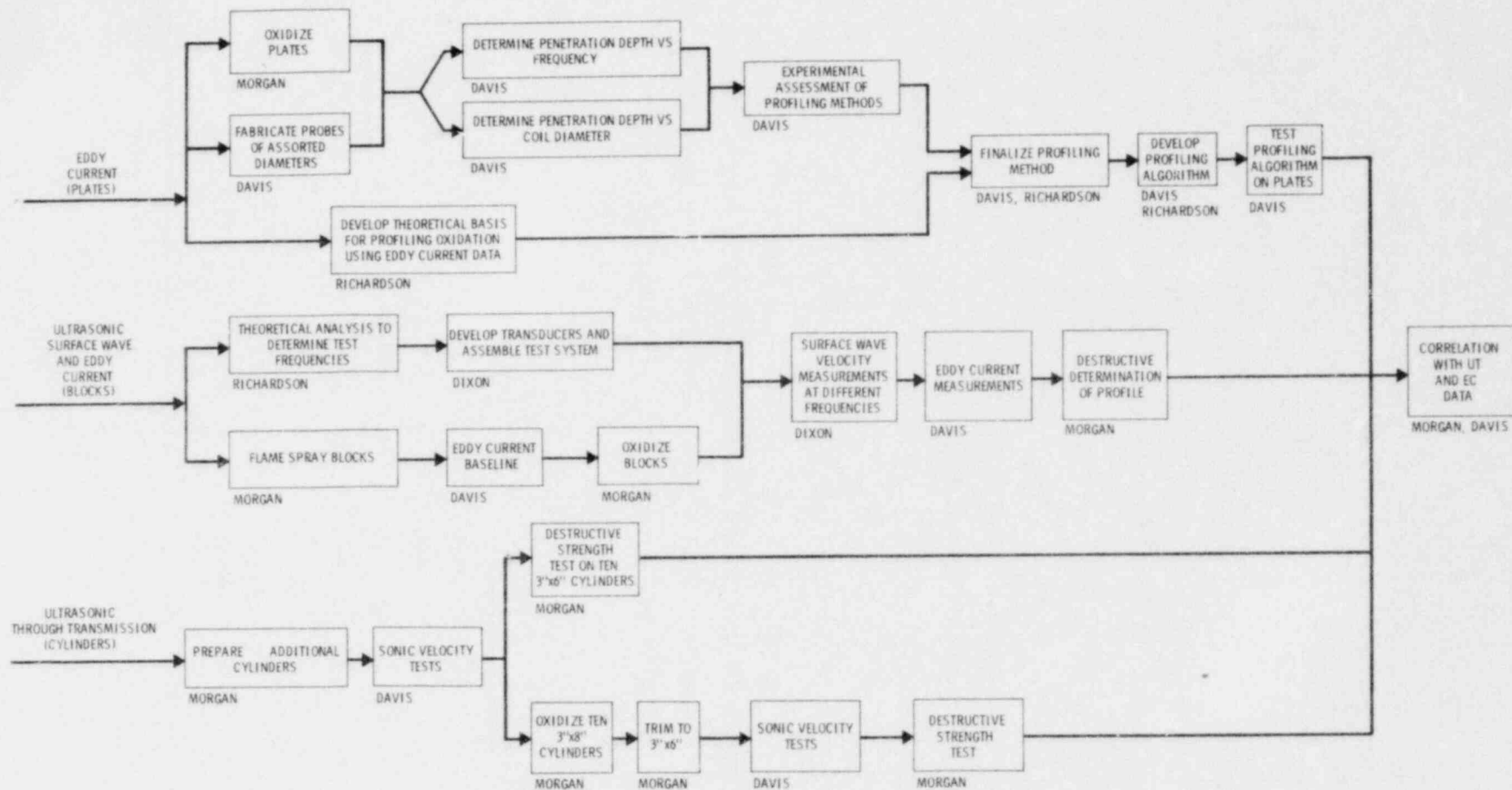
FIGURE 1. Project Plan - Graphite Oxidation Test Development

As a data base for developing this algorithm, we have fabricated a large number of PGX graphite plates, 3.0-in. square and 0.050-in. thick. Thirty-four of these plates have been oxidized to form a series with weight losses up to about 20%. The plates can be stacked to simulate stepwise-continuous profiles of any desired contour. A series of eddy current coils has been fabricated ranging in diameter from 1/8 in. to 1 in. A single frequency precision eddy current instrument is being prepared for measurements of plate stacks using several test frequencies and coil diameters. The instrument is being equipped with digital readouts to facilitate making a large number of measurements.

A theoretical analysis of methods for predicting oxidation profile from eddy current data is in progress. This effort is directed at supporting our empirical work in development of a profiling algorithm. The analysis includes an assessment of finite element methods, which are being widely developed by other researchers for predicting eddy current response to material parameters.

THROUGH-TRANSMISSION ULTRASONIC VELOCITY TESTS

Baseline ultrasonic velocity measurements have been completed on 23 PGX cylinders (3-in. dia and 6- or 8-in. long). The measurements included both longitudinal and shear velocities in three directions. Compressive strength and density measurements on 12 of the 3-in. dia by 6-in. long samples are reported above; the 13th sample, cut with its long axis transverse to the long axis of the parent log, had a density of 1.747 mg/m^3 and a compressive strength of 34.14 MPa.

Ten samples (3-in. dia by 8-in. long) are being oxidized to obtain a series out to 20% reduction in density. Oxidation conditions ($875^{o}C$ in a mix-ture of 90% CO_2 and 10% CO) were chosen to give a fairly homogeneous decrease in density throughout the samples.[a] This will establish a baseline for

---

[a] PGX graphite has been reported to oxidize in H_2O plus H_2 mixtures at rates that are two or more orders of magnitude higher than reactor-grade graphites; however, in our mixture of CO_2 plus CO the oxidation rate is quite similar to the graphites we studied previously.[1]

the loss-of-strength versus density and sonic velocity correlations and will allow comparison with our prior results on four other graphites.[1]

UILTRASONIC SURFACE-WAVE VELOCITY

Test apparatus and graphite samples are being prepared for determining the ability to profile oxidation with ultrasonic surface waves. Various test frequencies will be used to control penetration of the energy, and surface-wave velocity will be measured at each frequency.

The test apparatus consists of a transmitter and two receivers that are coupled to the graphite with silicone rubber membranes. The incident angle of the transmitter is adjusted to the critical angle for surface wave generation, and the propagation time of surface waves between the two receivers is measured to determine velocity. This technique has been successfully used at Battelle to measure surface-wave velocity in carbon-carbon composites. Its distinguishing features are that couplant variations at the transmitter are eliminated from the velocity measurement by the double receiver technique and that a wide frequency range can be accommodated by a given set of transducers.

Six blocks (6.5 in. x 7.5 in. x 4.5 in.) were cut from the PGX log with the 4.5-in. direction parallel to the long axis of the log. One of the blocks was retained as a standard; the others were plasma sprayed with ZrO_2 on five faces, leaving the remaining (6.5 in. x 7.5 in.) face uncoated. Prior testing indicated that plasma sprayed ZrO_2 provided an adherent and impermeable coating on PGX graphite; thus, oxidation of these blocks will proceed only from the uncoated face. Therefore, we should be able to obtain an oxidation gradient with depth into block that is quite uniform over the entire 6.5-in. $\times$ 7.5-in. surface.

Eddy current measurements indicated that one of these blocks has a distinct area of lower electrical conductivity. Optical examination confirms that there is a fairly sharp line of demarcation between this area and the remainder of the block; this distinct area is more porous than the remainder. This block has been excluded from our current tests but will be archived for future reference.

One block is currently being oxidized, nominally to 10% final weight loss, at 875°C. The rate of weight loss, relative to the rates observed for the 3-in. diameter samples, indicates that the oxidation is fairly homogeneous throughout the block.

The three remaining blocks will be oxidized at higher temperatures to develop different oxidation-depth profiles. Physical measurements of the density profiles will be made by removing a section from each block; the remainder of the block will then be available for eddy current measurements, in addition to the surface-wave measurements.

FUTURE PLANS

Remaining work in the three areas of investigation is as follows:

Eddy Current Testing

- inspect PGX plate stacks with varying frequencies and coil diameters
- complete theoretical analysis for profiling oxidation with multi-parameter eddy current data
- develop and test profiling algorithm.

Through-Transmission Ultrasonic Velocity

- complete oxidation of cylinders
- complete post-oxidation velocity tests
- perform destructive strength tests
- correlate data.

Ultrasonic Surface-Wave Velocity

- complete oxidation of blocks
- complete ultrasonic test apparatus
- perform surface-wave velocity tests at selected frequencies
- perform eddy current measurements
- perform destructive determination of oxidation profile
- correlate data.

REFERENCES

1. Morgan, W. C., and F. L. Becker. 1979. <u>Feasibility of Monitoring the Strength of HTGR Core Support Graphite--Part II</u>. NUREG/CR-0995 (PNL-3126, Pacific Northwest Laboratory, Richland, Washington).

LOCA SIMULATION IN NRU[a]

C. L. Mohr, Project Manager

SUMMARY

The proposed test train and loop modification designs have been completed. Fabrication of the first test train is underway and will be available for testing October 4, 1980. The required loop modification of the U-2 loop in the NRU reactor has been initiated. The data acquisition system has been assembled and is being prepared for shipment to the NRU reactor.

INTRODUCTION

The objective of the LOCA Simulation in NRU Program is to provide information on the heat up, reflood, and quench phases of a loss-of-coolant accident (LOCA). The tests are designed to give information on the quench front velocities within a fuel bundle, the liquid entrainment, and the heat transfer coefficients for full length pressurized water reactor designed fuel as a function of reflood rate and delay time before reflood starts. A total of 6 test trains will be prepared for the program, with the first test train devoted to thermal hydraulic behavior. A total of 18 tests are planned for the first test train. The remaining 5 test trains will be used for only one test each. These test trains will have pressurized cladding and, as a result, will deform and rupture during the test. These tests, called "materials tests," will evaluate the effects of ballooning and rupture on the quench-front velocities and associated heat transfer coefficients.

The NRU reactor, located at Chalk River, Canada, has a test loop that will accommodate a 12-ft long, 32-pin bundle on a 6 x 6 array with the corner pins removed. The bundle design uses commercial enrichments, cladding dimension, and grid spacers.

TECHNICAL PROGRESS

The complete design package for the test train has been completed. The majority of the components have either been ordered or are being fabricated. The fuel will be fabricated at Pacific Northwest Laboratory from powder provided by the Department of Energy. The current fuel design uses thermocouples to measure the inside cladding temperature and fuel centerline temperatures, as well as outside temperatures. Several rods in each test train will have three thermocouples placed circumferentially around the cladding. This will provide azimuthal temperature variation information needed to predict ballooning and rupture strains.

The test assembly is designed to be dismantled in the fuel examination pool and to allow the center 12-rod cluster to be removed and replaced for the next test. The design uses the outer 20 fuel pins as guard rods and the center 12 locations as test pins. The outer guard rods are unpressurized and should withstand several tests.

The design of the loop modification to the U-2 loop in the NRU reactor at Chalk River, Canada, have been completed. These modifications include a high volume steam supply system and a reflood/quench piping loop that can accurately control the flow of quench water back into the loop. These features will allow the loop to simulate the major boundary conditions that are anticipated during a LOCA.

Both the loop instrumentation and the test train instrumentation are connected to a process computer to monitor the operation of the loop and to record the data for later analysis. The computer system has been received, and the software is currently being developed.

The safety analysis review process of the test program has been partially completed. Several drafts of the safety analysis report (SAR) have been completed. This report details the neutronics, thermal hydraulics, and fuel performance behavior of the test train for normal operation as well as postulated limiting faults.

FUTURE PLANS

The planned activities include completing the modifications to the U-2 loop in the NRU reactor and beginning assembly of the first test train. The SAR will be presented to the Canadian reactor safety review board.

RESIDENT ENGINEER AT CADARACHE, FRANCE[a]

D. S. Trent, Project Manager
C. L. Wheeler, Resident Engineer

SUMMARY

The acceptance testing program was essentially finished with the comple-
tion of two blowdown tests using nuclear heating. Also, all major loop modifi-
cations were completed by the addition of the two instrumentation spool pieces
in the hot and cold legs.

INTRODUCTION

The objective of this program is to facilitate the exchange of informa-
tion between the U.S. and France. To this end, a resident engineer is being
supported at the PHEBUS program in France. The PHEBUS experimental program
for in-pile studies is operated by the Service D'Essais de Surete (Safety
Tests Service) of the French Atomic Energy Commission. The facility, located
at Cadarache, consists of a closed test loop driven by a pool-type reactor
that develops about 60 mW for a 20-minute test period. The test loop, which
passes through the center of the core, contains an 80-cm test section and is
capable of operating at pressurized water reactor (PWR) conditions. Current
plans call for blowdown and reflood type testing on rod bundles containing
either single-rod or 25-rod assemblies having geometries typical of those found
in large PWRs.

CURRENT STATUS

The acceptance testing or start-up phase of the PHEBUS program was essen-
tially finished with the successful completion of the two depressurizations,
which utilized nuclear-heated prototypic fuel assemblies.

The first test used a single-rod assembly under the following conditions:

- core power, 5 mW
- maximum linear heat rate on the test rod, 285 W/cm
- test assembly initial pressure, 155 bars
- test inlet temperature, $275^{o}C$
- assembly flowrate, 1.58 t/hr.

The second experiment used a 25-rod assembly. The initial conditions established for this test were:

- core power, $\sim$20 mW
- maximum linear heat rate, $\sim$285 W/cm
- test assembly initial pressure, 155 bars
- test inlet temperature, $320^{o}C$
- assembly flowrate, 35 t/hr.

In general, both tests were accomplished in the expected manner. However, these tests did point out some problems that need further investigation before the actual fuels test program could begin. After the completion of these tests, the reactor system was turned over to the maintenance and modification personnel for trouble shooting of the problems discovered during the acceptance testing program and for the insertion of the two instrumental spool pieces for measuring flowrate, pressure, and density in the simulated hot and cold legs. These modifications have been completed and, at this time, it appears that most of the problems discovered earlier have been corrected.

FUTURE PLANS

There are four blowdown tests planned for the next quarter. These will be performed in the following sequence:

1. 25-rod non-nuclear cold leg break,
2. 25-rod nuclear (27 kW/m) cold leg break,
3. 25-rod non-nuclear hot leg break, and
4. 25-rod nuclear (27 kW/m) hot leg break.

Tests 1 and 2 are planned to be run from identical, initial conditions and trip points: the parameter under study is the effect of nuclear heating. The first and third tests are planned to be identical except for the location of the break, and the only difference between the third and fourth test will be nuclear heating.

After the completion of these tests, an accurate weighing device for measuring the amount of fluid in the reflood accumulator, along with a flowmeter in the injection line, will be added to the system.

STEAM GENERATOR TUBE INTEGRITY[a]

R. A. Clark, Project Manager
V. F. FitzPatrick, Deputy Project Manager
J. M. Alzheimer
R. L. Burr
P. G. Doctor
G. H. Lyon
C. J. Morris
K. R. Wheeler

INTRODUCTION

The Steam Generator Tube Integrity Program is a multiphase, multitask laboratory program. The program's principle objective is to provide the Nuclear Regulatory Commission (NRC) with validated information on the remaining integrity of pressurized water reactor (PWR) steam generator tubes where service induced degradation has been indicated. An additional objective is to evaluate nondestructive instrumentation and techniques for examining defects in piping or tubing that serve as the reactor primary system pressure boundary.

Initial program tasks included producing a matrix of steam generator tube specimens with mechanically or chemically induced flaws simulating defects found in nuclear steam generator service. These flawed specimens were fully nondestructively characterized by means of positive replication and various nondestructive testing (NDT) techniques, mainly eddy current testing. The tube specimens were then tested to failure at PWR steam generator operating temperatures. The failure strength, actual flaw dimensions, and NDT-indicated flaw dimensions are used to derive mathematical relationships. These relationships are plotted to provide, within a statistical certainty band, the remaining mechanical integrity of a steam generator tube as a function of its flaw type and size as indicated by eddy current testing.

Early work showed that conventional, single-frequency eddy current evaluation of steam generator tubes, used for in-service inspections, could be improved. Thus, program efforts were expanded to include new eddy current

measurement techniques, the effects of different calibration standards, and a more complex statistical analysis of NDT data.

The first two phases of the program involved the study of mechanically (Phase I) and chemically (Phase II) defected tubing. Phase III of the program includes correlating the mathematical models developed in Phases I and II with actual service-flawed tubing. Lack of suitable specimens led to the redirection of Phase III into the Surry Generator Program, a subprogram of the Steam Generator Tube Integrity Program. The Surry Generator Program is responsible for relocating a nuclear steam generator removed from service at Surry, Virginia, to Hanford, Washington. Once at Hanford, the steam generator will be housed in a specially designed facility to allow nondestructive as well as destructive examination of the unit. Research will be conducted in the areas of NDT technique verification and instrument development, defect matrix identification, profiling of defect types, determination of the extent and location of defects, identification of deposits and sources or corrosion, and health physics. The generator will also become a source of specimens with service-induced flaws for various NRC programs. Potential research phases include simulated operation of a portion of the generator to assess the long-term effects on generator serviceability of chemical cleaning or decontamination procedures that may be proposed to NRC for licensing. Study of the recovery and reuse of materials in decommissioned reactor components is also a potential research task.

One further area of research involves primary system integrity in boiling water reactor (BWR) piping. The 304 stainless steel alloy used in existing BWRs has exhibited stress corrosion cracking (SCC) in the heat-affected zone around welds. A principle concern is monitoring susceptible regions for crack initiation and growth, allowing repair at scheduled shutdowns. We are examining for NRC a monitoring device using the principle of internal friction measurements. The device is attached to a specimen incorporated into a high-flow water loop operated under BWR conditions. The specimen is cyclically loaded to failure while measurements are taken in an environment representative of field operating conditions.

TECHNICAL PROGRESS

The following paragraphs detail progress in program tasks active this past quarter.

STRESS CORROSION CRACKING OF INCONEL 600

Programmatic specimen requirements were completed last quarter. This quarter, additional SCC tubing specimens were fabricated, at the request of NRC, for other uses. Specimens were made for shipment to an NRC NDT program at Oak Ridge National Laboratory (ORNL). In addition, specimens requested from NRC by investigators in Germany were supplied. A total of 139 SCC specimens have been fabricated.

All SCC testing had pre.iously been performed on tubing acquired through Westinghouse. Babcock and Wilcox (B&W) fabricates their tubing with different heat treatments, and they supplied several lengths of their tubing for comparative SCC tests. Results of tests this past quarter indicate that B&W tubing develops stress corrosion cracks in our apparatus in much the same way and the same time as Westinghouse tubing. There may be some difference in behavior based on the level of applied stress to time of failure; B&W tubes were subjected to slightly higher stresses than Westinghouse tubes. Further information on the relative yield strengths of the tubing will be required for better interpretation of results.

All stress corrosion cracks produced to date have been along the tube axis (longitudinal). Efforts for the next quarter will concentrate on producing circumferentially oriented cracks. This will require design and fabrication of a loading device in the SCC autoclave. To achieve circumferential cracking, the axial stress component will have to be made larger than the hoop stress. Under present pressure, only loading the hoop stress produces twice the axial stress.

A technical note was prepared on our SCC process, and with NRC approval we have submitted this for publication. It should be noted that the Inconel 600

141

tubing used in steam generators is extremely resistant to SCC. To produce SCC specimens under laboratory conditions in reasonable time requires a severe caustic environment.

STRESS CORROSION CRACKING OF 4-INCH DIAMETER BWR PIPING

A single experiment was conducted this past quarter, concluding the first series of tests. Background and details of these tests were presented in the previous quarterly reports. This experiment studied the effects of static (noncyclic) loading at several levels, prior to initiation of cyclic loading. The specimen was held at $550^{O}F$ and loaded for one day each at 100%, 110%, 120%, 130%, and 140% of the $550^{O}F$ yield strength. The experiment was designed to assess background signal level on the internal friction instrumentation being used to detect crack initiation and growth. Baseline signal data as a function of stress was also acquired. After one day at 140% of yield, the standard cyclic load sequence was initiated, with 140% as the load maximum. Employees of the instrumentation contractor were to call a crack initiation, at which time the test was to be terminated and the pipe destructively examined for a crack. After 11 cycles, the test was terminated, and subsequent examination showed a couple of large cracks (>50% of wall). Results of the test series were presented by Daedalean Associates, Inc., at the Seventh Water Reactor Safety Research Information Meeting (November 5-9, National Bureau of Standards, Gaithersburg, MD) in a paper titled "The Application of the Internal Friction Damping Nondestructive Evaluation Technique for Detecting IGSCC Crack Initiation in BWR Piping Systems."

NONDESTRUCTIVE TESTING

A round robin nondestructive examination (NDE) of ten SCC tubing specimens was initiated last quarter. Last quarter's effort consisted of specimen fabrication and Pacific Northwest Laboratory (PNL) NDE evaluation. This quarter, the specimens have been to Adaptronics for measurement. Arrangements were completed for shipping these specimens to Dr. Deuster of the University of Saarlandes, Federal Republic of Germany. When returned, they will be sent to ORNL.

142

Another approach for characterizing stress corrosion cracked tubing was use of an electrical resistivity gauge (ERG). The ERG uses a constant square wave current that is applied to the part under test via two electrodes placed on either side of the crack(s). A four point probe is used for testing, as shown in Figure 1. Current flow is from the outer two terminals A and D. If there is a change in the resistance of the specimen under test due to changes in flaw depth (i.e., current path length changes), this change is reflected in a voltage potential drop across terminal B and C. The instrument is calibrated to read crack depth in percent of wall thickness. In order to determine ERG accuracy, a series of electro-discharge machined (EDM) slots of known depth were measured (Tables 1 and 2). Tables 1 and 2 show that measurement accuracy for EDM slots was poor. According to the device manufacturer, there has been little experience using the device on tubular products. The manufacturer has agreed to attempt in-house testing of their device, and we have supplied them with an EDM-slotted specimen to aid their efforts.
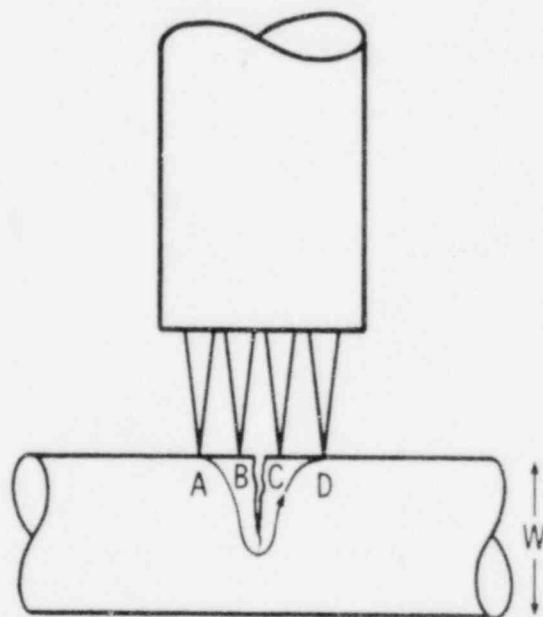

FIGURE 1.   Four Point Probe Used for Electrical
Resistivity Gauge

143

TAbLE 1. Steam Generator Tube Integrity Phase II-Electrical Resistivity Gauge Measurements[a] on EDM Tube PNL-1[b]

PNL-2 EDM Slot No.	Actual Depth (% wall)	Slot Width (in.)	Slot Length (in.)	Slot Aspect Ratio (Q)[c]	Measured Depth (% wall)		Measurement Error (% wall)[f]	
					Tester 1[d]	Tester 2[e]	Tester 1	Tester 2
F-2	28	0.005	0.205	14.64	16	19	-12	-9
F-1	28	0.004	0.195	13.93	14	15	-14	-13
E-2	24	0.004	0.200	16.67	10	12	-14	-12
E-1	25	0.004	0.195	15.60	10	13	-15	-12
D-3	20	0.0035	0.195	19.50	7	6	-13	-14
D-2	20	0.004	0.200	20.00	10	9	-10	-11
D-1	20	0.004	0.200	20.00	6	4	-14	-16
C-3	16	0.004	0.200	25.00	8	7	-8	-9
C-2	15	0.003	0.200	26.67	6	5	-9	-10
C-1	16	0.004	0.200	25.00	10	10	-1	-6
B-2	12	0.003	0.200	33.33	12	14	0	+2
B-1	12	0.003	0.200	33.33	4	6	-8	-6
A-2	5	0.003	0.200	80.00	4	5	-1	0
A-1	5	0.003	0.195	78.00	2	4	-3	-1
M-2[g]	92	0.016	0.200	4.35	92	92	Cal.	Cal.

(a) Instrument: ERG CC400 No. 002722.
(b) PNL-1 Heat B tubing 0.875 x 0.050 in. nominal
(c) Q = Slot Length/Slot Depth
(d) C. Morris
(e) G. Lyon
(f) Measurement Error (% wall) = measured depth - actual depth
(g) Calibration reference slot: M-2.

144

TABLE 2. Steam Generator Tube Integrity Phase II-Electrical Resistivity Gauge Measurements[a] on EDM Tube PNL-2[b]

PNL-2 EDM Slot No.	Actual Depth (% wall)	Slot Width (in.)	Slot Length (in.)	Slot Aspect Ratio (Q)[d]	Measured Depth (% wall) Tester 1[e]	Measured Depth (% wall) Tester 2[f]	Measurement Error (% wall)[g] Tester 1	Measurement Error (% wall)[g] Tester 2
M-2[c]	92	0.016	0.200	4.35	92	91	Cal.	Cal.
M-1	92	0.016	0.210	4.57	100+	100+	+8	+8
L-2	84	0.011	0.200	4.76	92	90	+8	+6
L-1	82	0.007	0.190	4.63	100	100+	+18	+18
K-2	78	0.006	0.210	5.38	70	72	-8	-6
K-1	82	0.006	0.200	4.88	55	52	-27	-30
J-2	74	0.008	0.180	4.86	54	53	-20	-21
J-1	80	0.007	0.180	4.50	92	94	+12	+14
I-2	70	0.006	0.190	5.43	45	47	-25	-23
I-1	71	0.0055	0.190	5.35	52	51	-19	-20
H-2	63	0.010	0.190	6.03	50	48	-13	-15
H-1	63	0.011	0.190	6.03	44	46	-19	-17
G-2	36	0.0035	0.185	10.23	14	13	-22	-23
G-1	31	0.004	0.185	11.94	11	10	-20	-21

(a) Instrument: ERG CC400 No. 002722.
(b) PNL-2 Heat B tubing 0.875 x 0.050 in. nominal.
(c) Calibration reference slot: M-2.
(d) Q = Slot Length/Slot Depth
(e) G. Morris
(f) G. Lyon
(g) Measurement Error (% wall) = measured depth - actual depth.

The use of radiographic tomography in characterizing SCC tubing shows good promise. The equipment at Los Alamos has been upgraded, allowing more rapid determinations. We currently have two specimens with singl stress corrosion cracks at Los Alamos for characterization.

Ultrasonic testing (UT) is being considered as another possible technique for evaluating SCC in tubing. UT is already used to inspect tubular products, including reactor fuel pin cladding, for defects. Contacts have been initiated with Westinghouse Hanford regarding capabilities for accurate flaw determination in SCC tubing. This testing aspect will be pursued further in coming months.

Another area of research pursued this past quarter was the evaluation of alternate eddy current standards. The American Society of Mechanical Engineers (ASME) Boiler and Pressure Vessel Code specifies a calibration standard consisting of a tube containing a series of flat-bottom drill holes (FBH) of varying diameters and depths. The calibration standard is used to calibrate the eddy-current system and used to generate a flaw depth interpretation curve to relate the phase angle of the eddy-current signal pattern to the FBH depth. The flaw depth interpretation curve is used to determine the depth of service-induced tube flaws of unknown geometry during inservice inspection of the steam generator.

Extensive laboratory data from Phase I of the Steam Generator Tube Integrity Program showed results for machine flawed tubes indicating that flaw geometry is a dominant factor in determining single frequency eddy-current measurement accuracy. Using flaw depth interpretation curves generated from ASME Code FBH calibration standards, the depth of several hundred machine-flawed tube specimens was determined. The flawed-tube specimen matrix consisted of small volume EDM slots and medium volume (elliptical) and large volume (uniform thinning) wastage flaws. The eddy-current results from Phase I suggested that the EDM slots, elliptical wastage, and uniform thinning wastage flaws could be more accurately sized for depth using flaw depth interpretation curves generated from calibration standards other than the ASME FBH standards. Therefore, alternate flaw tube standards were developed for EDM slot, elliptical wastage, and uniform thinning wastage flaws in steam generator tubes. A depth series

of each type flaw was machined in 0.875 in. OD x 0.050 in. wall Inconel 600 tubing. Each standard was inspected in the laboratory at a frequency of 400 kHz using a differential wound (2 coil) eddy current bobbin-probe and an EM3300 eddy current excitation generator.

Figure 2 shows plots of interpretation curves for EDM slot, elliptical wastage, uniform thinning, and ASME FBH standards. These curves show the relationship between the eddy-current pattern phase angle and true flaw depth, as determined by optical and mechanical gauging techniques. It is also apparent that the EDM slot and uniform thinning wastage curves exhibit a different relationship between pattern phase angle and flaw depth compared to the ASME FBH curve; the elliptical wastage curve closely approximates the ASME FBH curve.
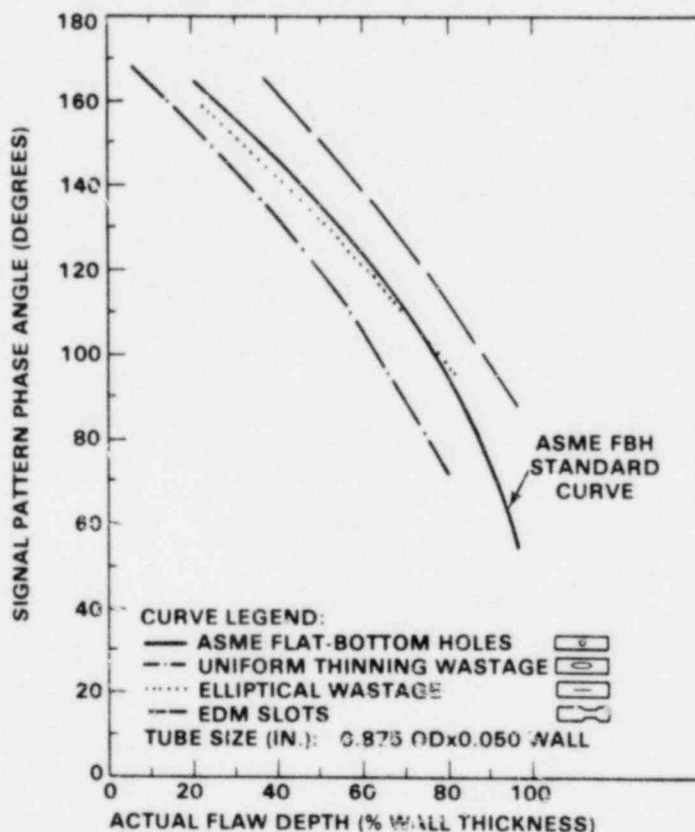

FIGURE 2. Single Frequency Eddy-Current Interpretation Curves Generated From ASME Flat-Bottom Hole, Electro-Discharge Machined Slot, Elliptical Wastage, and Uniform Thinning Wastage Standards

147

The eddy-current data from Phase I was re-evaluated using the new interpretation curves of Figure 2. Figures 3 through 5 show the eddy-current indicated depths plotted against actual flaw depths. The indicated depths are based on both the FBH standard and the appropriate alternate standard for the known defect being examined. The solid line on each figure represents the linear relationship that would result if there were no eddy-current measurement error. Points above the line represent overestimates of flaw depth; this would be a "conservative" measurement error. The three figures show that the data exhibits different trends for each flaw type at a given flaw depth.

The objective of this study was to determine the degree of improvement that may result with the use of alternate standards to assess flaw depth. The analysis approach taken in the study was first to determine the eddy-current
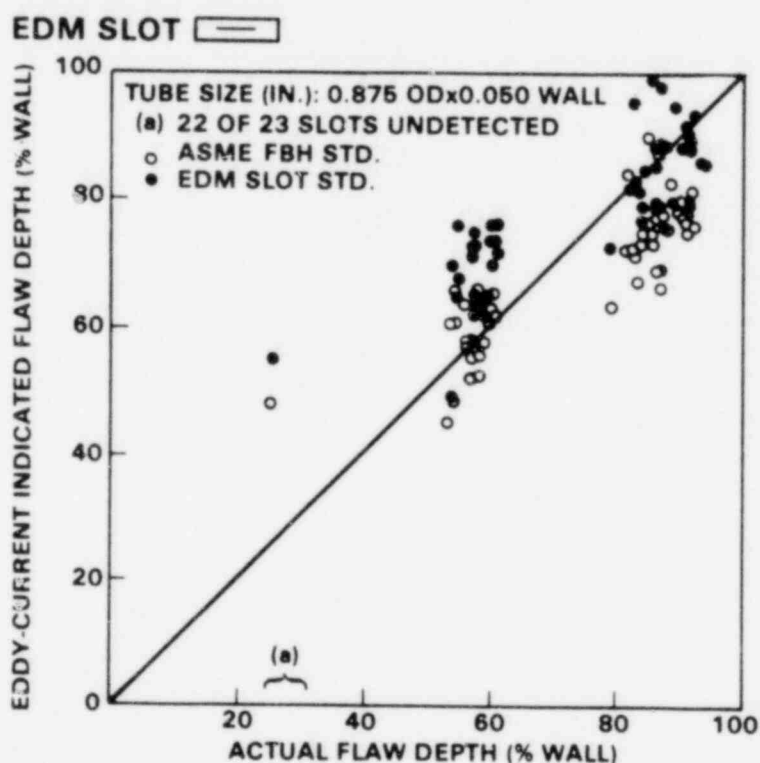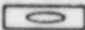
FIGURE 3. Electro-Discharge Machined Slot Specimen Eddy-Current Depth Sizing Results Achieved Using ASME Flat-Bottom Hole and Electro-Discharge Machined Slot Standards

ELLIPTICAL WASTAGE ⬭

FIGURE 4. Elliptical Wastage Specimen Eddy-Current Depth Sizing Results Achieved Using ASME Flat-Bottom Hole and Elliptical Wastage Standards

UNIFORM THINNING ⬲

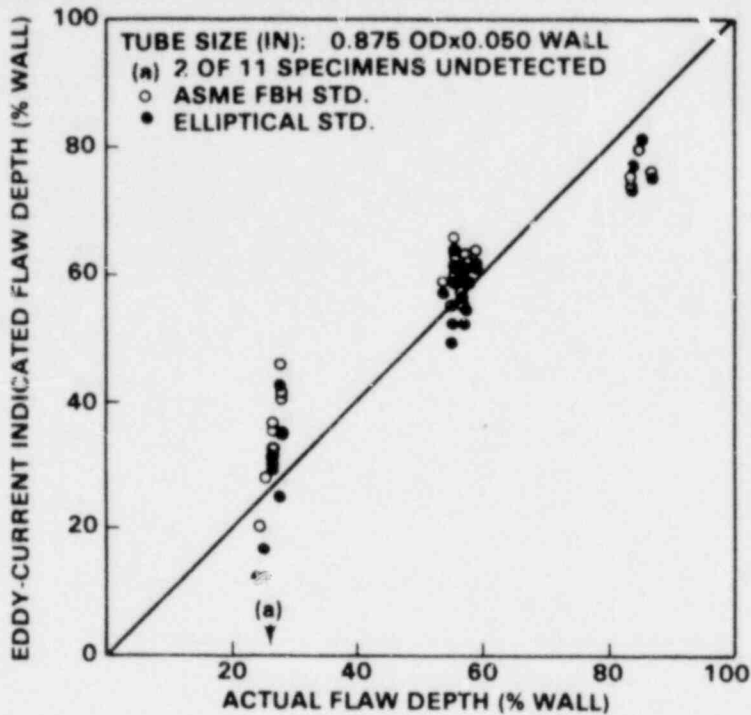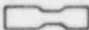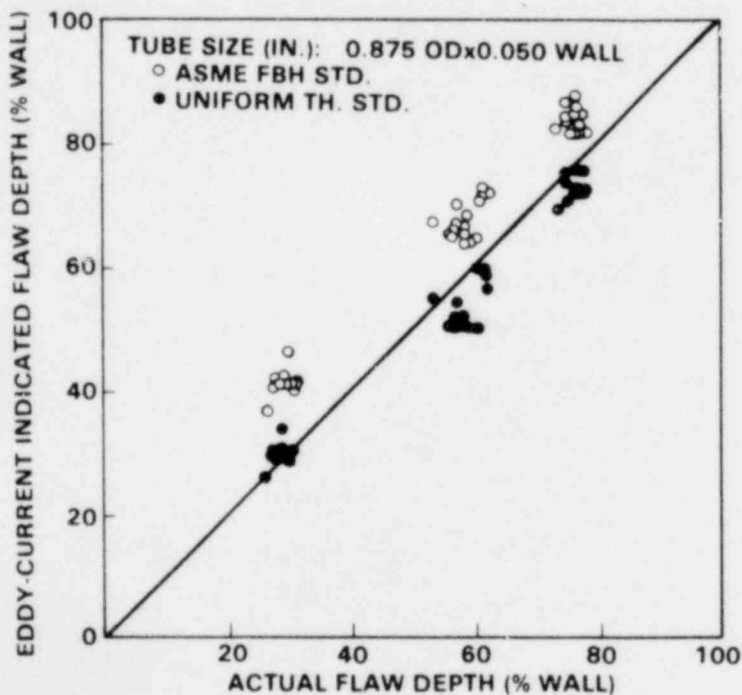FIGURE 5. Uniform Thinning Wastage Specimen Eddy-Current Depth Sizing Results Achieved Using ASME Flat-Bottom Hole and Uniform Thinning Wastage Standards

149

flaw depth measurement error which is defined as

Flaw Depth Measurement Error (% wall thickness) = [Eddy-current
indicated flaw depth (% wall)] - [Actual flaw depth (% wall)]   (1)

for each depth measurement. Statistical calculations of eddy-current flaw
depth measurement accuracy and precision, which are measured by the mean (X)
and standard deviation (S), were then calculated using Equations 2 and 3,
respectively. The mean of the flaw depth measurement error values (mean error)
was calculated as follows:

$$\overline{X} = \frac{1}{N} \sum_{i-1}^{N} X_i \tag{2}$$

where: X = the mean error in precent of tube wall thickness,

X_i = the error for the ith eddy-current measurement, and

N = the number of data points in the set.

The standard deviation of the measurements (a measure of the dispersion
around the mean) was calculated as follows:

$$S = \sqrt{\sum_{i-1}^{N} (X_i - \overline{X})^2/(N - 1)} \tag{3}$$

where: S = the standard deviation of the eddy-current measurements,

$\overline{X}$ = the mean error in percent of tube wall thickness,

X_i = the error for the ith measurement, and

N = the number of data points in the set.

Table 3 shows the flaw type, flaw depth range, number of specimens in the data
set (N), mean error (X), 2 standard deviations of the mean (2S), and interpre-
tation curve used to determine flaw depth.

150

TABLE 3. Statistical Data for Electro-Discharge Machined Slot, Elliptical Wastage, Uniform Thinning Wastage and Flat-Bottom Hole Standards[a]

Flaw Type	Flaw Depth (% wall)	No. Specimens (N)	Mean Error (% wall)	2 Standard Deviation (% wall)	Interpretation Curve[b]
EDM Slot					
	25 - 30	23	(c)	--	--
	50 - 60	25	2.36	10.41	ASME
	50 - 60	25	11.60	12.01	EDM
	78 - 90	33	-10.95	11.23	ASME
	78 - 90	33	-0.63	13.82	EDM
Elliptical Wastage					
	25 - 28	9	6.18	16.58	ASME
	25 - 28	9	-1.03	20.58	ELLIPTICAL
	53 - 57	18	4.69	7.23	ASME
	53 - 57	18	2.8	8.41	ELLIPTICAL
	82 - 86	4	-6.75	3.98	ASME
	82 - 86	4	-5.73	6.03	ELLIPTICAL
Uniform Thinning Wastage					
	25 - 28	14	13.66	4.27	ASME
	25 - 28	14	1.77	4.35	UNIFORM
	51 - 60	18	9.75	5.14	ASME
	51 - 60	18	-4.02	6.00	UNIFORM
	72 - 76	16	7.88	4.35	ASME
	72 - 76	16	-1.97	3.53	UNIFORM

(a) Tube size (inc.): 0.875 OD x 0.050 wall thickness.
(b) Re: Figure 2.
(c) 22 of 23 EDM slots undetected.

151

Table 3 shows that EDM slots 25% to 30% of wall thickness in depth were difficult to detect. Of 23 slots, 22 were not detected. Slots 50% to 60% of wall depth produced overestimated results using the EDM slot curve with a mean error of 11.60% of wall thickness, whereas the ASME FBH curve gave an over-estimated result of only 2.35% of wall thickness. Slots 78% to 90% of wall depth produced slightly under-estimated results using the EDM slot curve with a mean error of -0.63% of wall thickness, whereas the ASME FBH curve gave an under-estimated result of -10.95% of wall thickness.

The EDM slot results show improved accuracy in depth sizing for slots 78% to 90% of wall depth. However, slots 50% to 60% of wall thickness were better sized for depth using the ASME FBH curve. EDM slots less than 40% of wall depth are difficult to detect. Only one slot 25% of wall depth was detected; both the ASME FBH curve and EDM slot curve greatly overestimated the depth of this slot.

Data in Table 3 show that the standard deviation of the measurements remained essentially constant for each standard. Elliptical wastage flaws with depths ranging from 25% to 28%, 53% to 57%, and 82% to 86% of wall thickness produced over- and under-estimated mean error results of -1.03%, 2.80%, and -5.73% of wall thickness, respectively, using an elliptical wastage standard. Correspondingly, the mean errors were 6.18%, 4.69%, and -6.75% of wall, respectively, for the ASME FBH curve. The elliptical wastage results showed improved accuracy in flaw depth sizing with the use of the elliptical wastage standard.

Uniform thinning wastage with depth ranging from 25% to 28%, 51% to 60%, and 72% to 76% of wall thickness produced slightly over- and under-estimated mean error results of 1.77%, -4.02% and -1.97% of wall thickness, respectively, using a uniform thinning standard. Correspondingly, the ASME FBH curve produced overestimated mean error results of 13.66%, 9.75%, and 7.88% of wall thickness. The uniform thinning wastage results show that there is a dramatic improvement in measurement accuracy for the depth sizing of uniform thinning wastage specimens with the use of uniform thinning wastage standards.

Our study has shown that alternate tube standards with machine induced elliptical wastage and uniform thinning wastage flaws resulted in a more

152

accurate determination of depth for elliptical wastage and uniform thinning wastage specimens compared to the ASME FBH standards. However, the improved accuracy in measuring flaw depth has not decreased the standard deviation (increased the precision). The EDM slot standard produced results that were more accurate in determining the depth of EDM slots 78% to 90% of wall thickness. However, EDM slots 50% to 60% of the wall thickness were better sized in depth using the ASME FBH standard. Axial EDM slots of depth less than 40% of the wall thickness were difficult to detect, and a statistically valid sample of data points was not obtained.

The above results were based on curves generated from a one-of-a-kind standard. The interpretation curves were drawn giving a best-fit curve to the data points generated from each standard. This approach is not unique and is the same method used to construct interpretation curves using ASME FBH standards. An important point to recognize is that the use and application of alternate standards requires the ability to correctly classify and accurately interpret (pattern phase angle) each eddy-current indication. If the type of flaws are incorrectly classified, the wrong interpretation curve would be chosen to determine flaw depth. The interpretation curves of Figure 2 show that if an EDM slot flaw (known depth at 80% of wall thickness) with a pattern phase angle of 120° is incorrectly classified as a uniform thinning wastage flaw, the slot depth would be assessed using the uniform thinning curve, at 55% of the wall thickness. However, the EDM slot curve would have sized the slot to be 75% of the wall thickness. The incorrect classification of the flaw has inadvertantly resulted in a substantial flaw depth measurement error of 25% of the wall thickness.

A detailed report of this work, "Alternate Standards for the Interpretation of Eddy-Current Data for Steam Generator Tubing", was presented at the Seventh Water Reactor Safety Research Information Meeting, Gaithersburg, Maryland, November 5-9, 1979.

SURRY GENERATOR PROJECT

This project, a subprogram of the Steam Generator Tube Integrity Program, entails retreiving a nuclear steam generator removed from service at the

153

Surry II plant at Surry, Virginia, and transporting the generator to Hanford, Washington. Once at Hanford, the generator will be located in a specially designed temporary facility to allow nondestructive and destructive examination.

Research on a removed-from-service steam generator originated out of Phase III of the Steam Generator Tube Integrity Program, obtaining and testing service defected tubing to confirm models of remaining tube strength developed in Phases I and II on mechanically and chemically simulated tube defects. An inability to obtain representative service defected tubing was a prime motivation for proposing research on a removed-from-service generator.

Tasks on the Surry Steam Generator Program this past quarter involved establishing procedures and contracts for preparing and licensing the generator for shipment. Design was initiated on the Steam Generator Examination Facility (SGEF), a temporary structure to house the generator during the research program. Since the SGEF will not be ready at the time the generator arrives at Hanford, engineering was commenced for appropriate storage at an assigned temporary storage location.

Temporary Storage

Figure 6 is an artist's rendition of the Interim Storage Facility (ISF) for the steam generator. The generator will sit on two concrete supports located beneath the transport cradles. Also shown on the figure is a structure enclosing the waterbox end of the generator. Although we do not currently anticipate any research activity on the generator until it is housed in the SGEF, it may be desirable to conduct limited NDT while at the ISF. This would require access through the manways in the waterbox under the tube sheet. The structure pictured around the waterbox end of the generator represents a rigid greenhouse that would be used for any early NDT. Detailed design of this greenhouse will be completed in the first quarter of CY 1980.

Steam Generator Examination Facility

The final "Conceptual Design Report, Steam Generator Examination Facility," was issued in November 1979 by Vitro Engineering Corporation and PNL. Copies of this report were forwarded to NRC program management. The
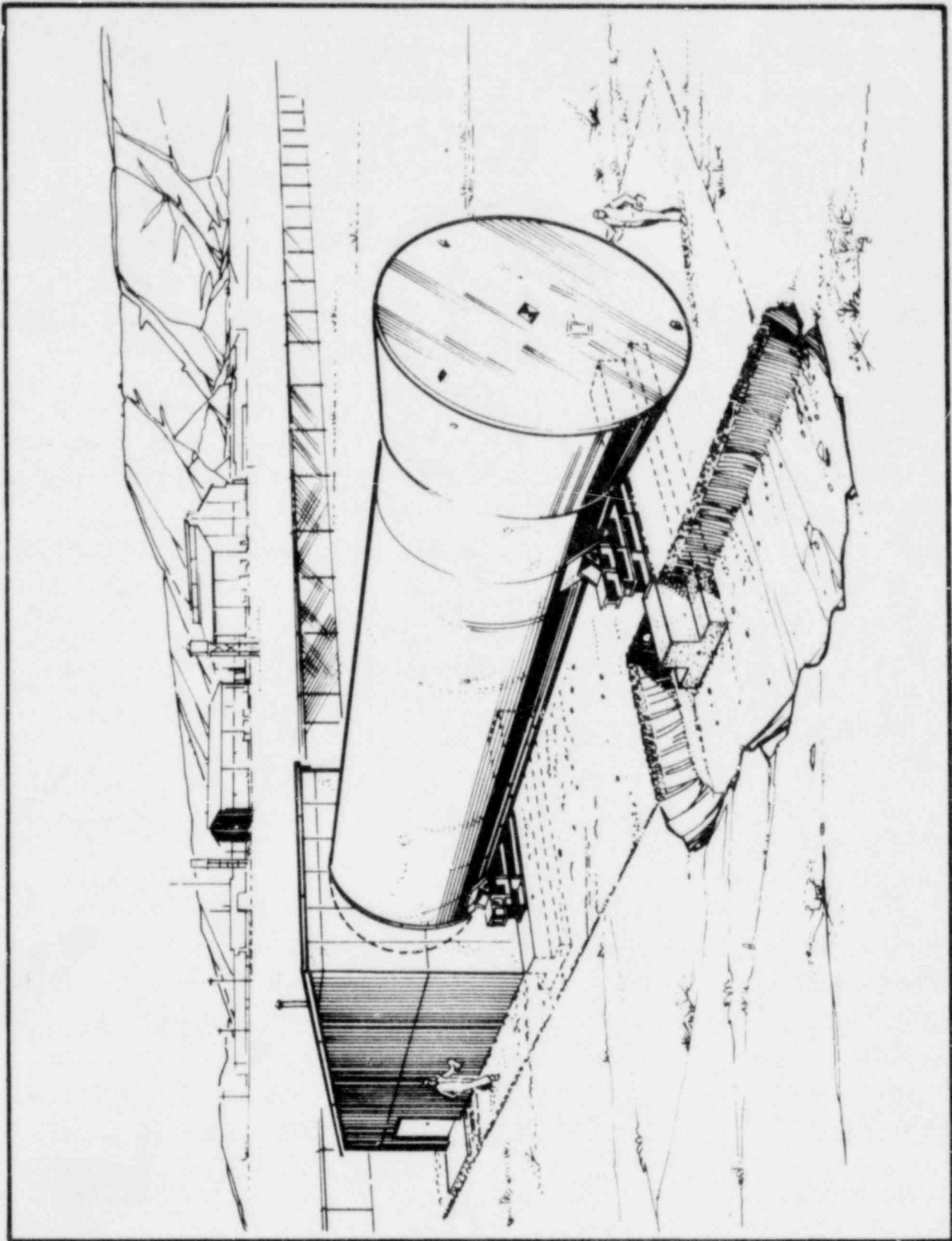
154

FIGURE 6. Interim Storage Facility for Steam Generator

final conceptual design comprises a 700 ft^2, four story high tower to house the steam generator and a support wing with two stories comprising 1750 ft^2 of floor space. Figure 7 is an artist's rendition of this structure. The Conceptual Design Report covers in detail project cost estimates, performance requirements of the facility, construction schedules, and quality assurance requirements. In addition, appendicies in the document include an approved Functional Design Criteria for the facility, an Environmental Impact Assessment (EIA) for locating the facility in the 300 area of the Hanford Reservation, and other documentation pertaining to energy conservation, accommodations for the physically handicapped, etc.

The costs estimate for the SGEF at the conceptual design level is $1,740,000. This is divided between $176,000 for engineering (including $45,000 for escalation and contingency) and $1,564,000 for construction (including $148,200 for escalation and $336,300 for contingency). The $1,740,000 figure compares well with the cost range of $1,493,700 to $1,906,600 established in our original feasibility study.

Based on the Conceptual Design Report, and a Statement of Work for Architect Engineering Services, Steam Generator Examination Facility (issued by PNL to the Department of Energy Richland Operations Office), a request for proposal was issued for an Architect-Engineering firm for Title I, II, and III design; Facilities Systems Engineering Corporation submitted the winning bid. Title I design was initiated in December 1979 with scheduled completion in March 1980.

Transportaion Licensing of a Surry Generator

Transportation of the generator currently hinges on a licensing decision by the Department of Transportation (DOT). We have submitted a request to allow the steam generator to be shipped as a Low Specific Activity (LSA) package. This requires an exemption from the limit of 0.001 mCi/cm^2 for an LSA shipment. Our exemption request is based on consideration of the 3 in. thick carbon steel steam generator shell as the package; typically, an LSA package can consist of a cardboard container. The generator has about 0.003 mCi/cm^2 activity, essentially uniformly distributed in the tenacious oxide coating on
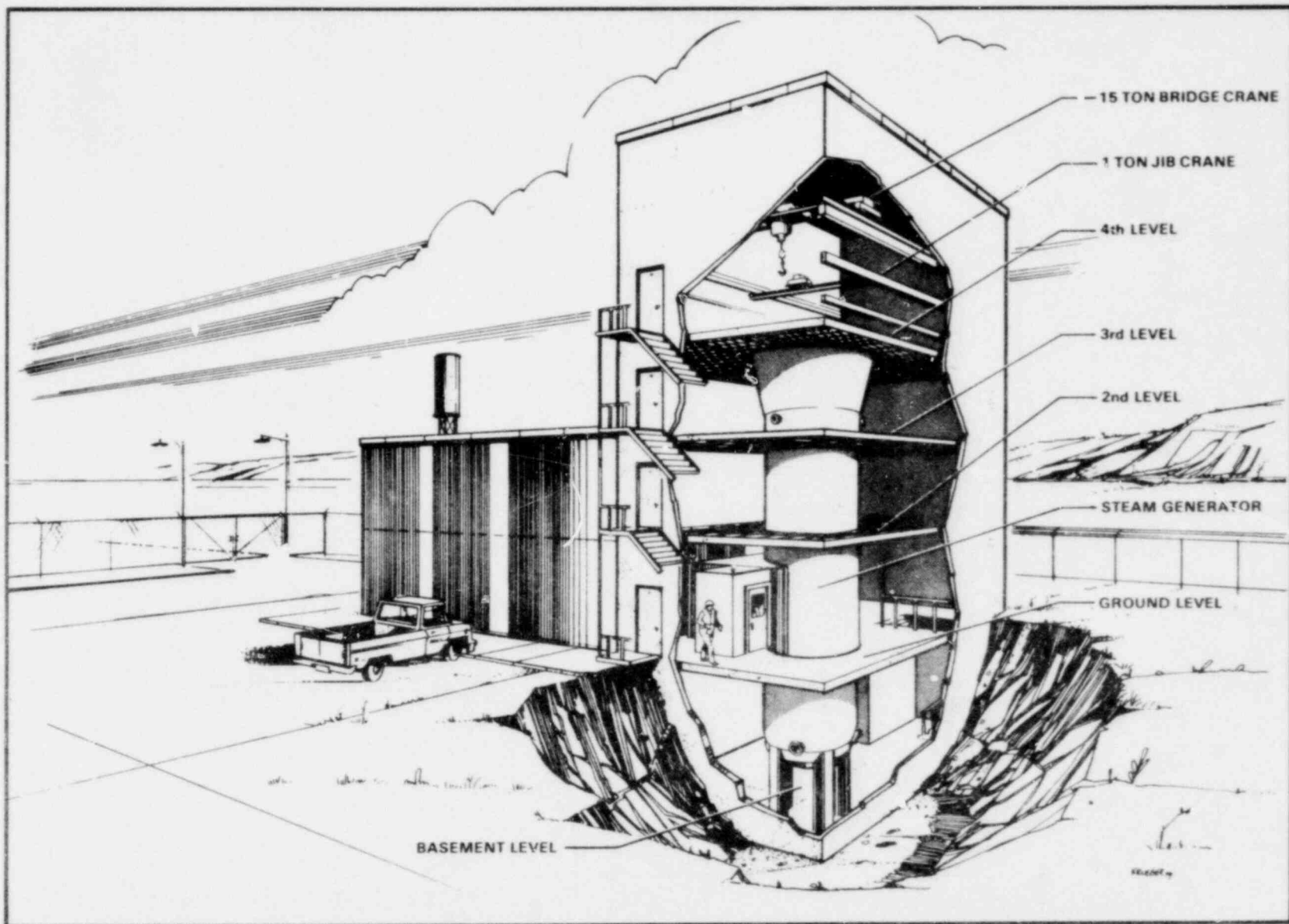
156

FIGURE 7. Steam Generator Examination Facility

Labels in figure:
- 15 TON BRIDGE CRANE
- 1 TON JIB CRANE
- 4th LEVEL
- 3rd LEVEL
- 2nd LEVEL
- STEAM GENERATOR
- GROUND LEVEL
- BASEMENT LEVEL

the inside of the steam generator tubes. We contend that the 3-in. thick pressure vessel is more than three times as protective as a cardboard container. Therefore, the exemption from the 0.001 mCi/cm^2 limit is justified.

DOT requested a detailed Operational Plan and this plan was submitted in December 1979. After a suitable public comment period with the Operational Plan in the public files, DOT will rule on our licensing request. We expect this ruling in the coming quarter. Our current intended shipping date is March 31, 1980.

Transportation Preparation of the Surry Generator

Some open issues remain in this area. The most crucial issue is obtaining a working arrangement with Virginia Electric and Power Company (VEPCO) to permit PNL to operate on VEPCO's Surry reactor site for preparation of the generator for shipment. PNL is seeking to establish a Cooperative-Permit with VEPCO to allow Surry site activities. Issues still being discussed at the end of this quarter include details of generator ownership transfer and liability under Price-Anderson Act nuclear indemnity insurance. VEPCO is not willing to incur any insurance risk, and to protect VEPCO from any such risk we are attempting to establish that primary insurance liability is with the Department of Energy (DOE) under their Price-Anderson Act coverage. This requires PNL, as a DOE prime contractor, to provide flow through DOE's insurance to VEPCO.

Other activities on generator transport preparation have been delayed while awaiting DOT licensing action and establishment of a PNL-VEPCO cooperative permit. A contract for shielding fabrication and Surry site handling has been established with Williams Crane and Rigging of Richmond, Virginia. The only portion of this contract activated has been establishment of designs and operating plans necessary for the DOT Operational Plan submittal. Likewise, Foss Tug and Barge has been established as the carrier, and shipping contract negotiations are underway. Foss has, under letter contract, developed the detailed shipping plan necessary for the DOT submittal.

Prior to shipping the generator, it is necessary to establish that it is in transportable condition. Concern has also been expressed that there may have been degradation due to storage conditions. To assure the generator is a

viable research vehicle, we plan to conduct a secondary side inspection prior to initiating shipping preparations. Contract negotiations with Combustion Engineering have been initiated for this inspection.

ENVIRONMENTAL IMPACT ASSESSMENT

DOE is deeply involved in this project. Work will be conducted at DOE's Hanford site; DOE will take ownership of the generator and provide insurance during the shipment. DOE requested that PNL provide an EIA for the program. This included transport of the generator, research activities at Hanford, and decontamination/decommissioning of Hanford facilities after program completion. A draft EIA was submitted for DOE comment at the end of December. After all comments are received and addressed, a final EIA will be issued. At that time, DOE will decide, based on the EIA, if an Environmental Impact Statement (EIS) is required.

MILESTONES

- first 4 in. pipe test series completed

- alternate eddy-current standards evaluated

- Conceptual Design Report, Steam Generator Examination Facility issued

- Statement of Work for Architect-Engineering Services issued

- Functional Design Criteria for Steam Generator Examination Facility issued

- Hanford Environmental Impact Assessment for Steam Generator Examination Facility issued

- Architect-Engineer Contract let for design of Steam Generator Examination Facility, Title I design initiated

- Operational Plan for preparation and transport of a Surry Generator submitted to DOT

159

- Williams Crane and Rigging contract established

- Draft Environmental Impact Assessment issued to DOE for comment.

PROBLEMS

Three major issues require resolution before transport of a Surry generator is possible:

- establishment of a PNL-Vepco cooperative permit

- acceptance by DOE of our EIA with a negative declaration of need for an EIS

- DOT Low Specific Activity shipping exemption.

DISTRIBUTION

No. of
Copies

No. of
Copies

OFFSITE

A. A. Churm
DOE Patent Division
9300 S. Cass Avenue
Argonne, IL 60439

788 U.S. Nuclear Regulatory
Commission
Division of Technical Information
and Document Control
7920 Norfolk Avenue
Bethesda, MD 20014

2 DOE Technical Information Center

R. F. Abbey, Jr.
Reactor Safety Research Division
Nuclear Regulatory Commission
Washington, DC 20555

S. Fabic
Reactor Safety Research Division
Nuclear Regulatory Commission
Washington, DC 20555

D. A. Hoatson
Reactor Safety Research Division
Nuclear Regulatory Commission
Washington, DC 20555

W. V. Johnston
Reactor Safety Research Division
Nuclear Regulatory Commission
Washington, DC 20555

10 J. Muscara
Reactor Safety Research Division
Nuclear Regulatory Commission
Washington, DC 20555

R. D. Schamberger
Reactor Safety Research Division
Nuclear Regulatory Commission
Washington, DC 20555

H. H. Scott
Reactor Safety Research Division
Nuclear Regulatory Commission
Washington, DC 20555

R. Van Houton
Reactor Safety Research Division
Nuclear Regulatory Commission
Washington, DC 20555

M. A. Wolf
Department of Atmospheric
Sciences
Oregon State University
Corvallis, OR 97330

L. Agee
Electric Power Research
Institute
3212 Hillview Avenue
P.O. Box 10412
Palo Alto, CA 94304

B. R. Sehgal
Electric Power Research
Institute
3212 Hillview Avenue
P.O. Box 10412
Palo Alto, CA 94304

F. Shakir
Department of Metallurgy
Association of American
Railroads
3140 S. Federal
Chicago, IL 60616

SM-ALC/MMET
Attn: Capt. John Rodgers
McClellan AFB, CA 95652

Dr. Sotirios, J. Vahaviolos
Western Electric, ERC
P.O. Box 900
Princeton, NJ 08540

Mr. Jerry Whittaker
Union Carbide Company
Oak Ridge National Laboratories
Y-12
Oak Ridge, TN 37830

Mr. L. J. Anderson, B2402
Dow Chemical Company
Texas Division
P.O. Drawer K
Freeport, TX 77541

Mr. M. C. Jon
Western Electric, ERC
P.O. Box 900
Princeton, NJ 08540

P. Caussin
Vincotte
1640 Rhode-Saint-Genese
Belgium

W. G. Cunliffe
Building 396
British Nuclear Fuels Ltd.
Springfields Works
Salwick, Preston
Lances. PR4OXJ
U.K.

ACE Sinclair
Research Division
Berkeley Nuclear Laboratories
Berkeley
Gloucestershire, GL 13 9 PB
U.K.

Don Birchon
Admiralty Materials Laboratory
Holton Health Poole
Dorser, England
020-122-2711

W. L. Pearl
Nuclear Water & Waste Technology
P.O. Box 6406
San Jose, CA 95150

ONSITE

50 Pacific Northwest Laboratory

J. M. Alzheimer
M. C. Bampton
F. L. Becker
T. D. Chikalla
R. A. Clark
E. L. Courtright
J. M. Cuta
J. F. Dawson
R. L. Dillon
C. W. Dotson
C. E. Elderkin
J. E. Garnier
R. K. Hadlock
C. R. Hann (3)
A. J. Haverfield
T. W. Horst
P. H. Hutton (3)
J. M. Kelly
R. J. Kurtz
P. T. Landsiedel
D. D. Lanning
R. P. Marshall
C. L. Mohr
W. C. Morgan
C. J. Morris
R. D. Nelson
P. W. Nickola
L. T. Pedersen
G. J. Posakony
E. B. Schwenk (2)
J. R. Skorpik
A. M. Sutey
M. J. Thurgood
G. L. Tingey
D. S. Trent (3)
C. L. Wheeler
Technical Information (5)
Publishing Coordination Fe(2)

1. REPORT NUMBER (Assigned by DDC)
NUREG/CR-1349
PNL-3040-4

TITLE AND SUBTITLE (Add Volume No., if appropriate)	2. (Leave blank)
Reactor Safety Research Programs Quarterly Report October - December 1979	3. RECIPIENT'S ACCESSION NO.

7. AUTHOR(S)	5. DATE REPORT COMPLETED	
Compiled and edited by C.W. Dotson	MONTH June	YEAR 1980

9. PERFORMING ORGANIZATION NAME AND MAILING ADDRESS (Include Zip Code)	DATE REPORT ISSUED	
Pacific Northwest Laboratory Richland, WA 99352	MONTH August	YEAR 1980
	6. (Leave blank)	
	8. (Leave blank)	

12. SPONSORING ORGANIZATION NAME AND MAILING ADDRESS (Include Zip Code)	10. PROJECT/TASK/WORK UNIT NO.
Division of Reactor Safety Research Office of Nuclear Regulatory Research U.S. Nuclear Regulatory Commission Washington, DC 20555	11. CONTRACT NO. FIN No. B2041

13. TYPE OF REPORT	PERIOD COVERED (Inclusive dates)

15. SUPPLEMENTARY NOTES	14. (Leave blank)

16. ABSTRACT (200 words or less)

This document summarizes the work performed by Pacific Northwest Laboratory from October 1 through December 31, 1979, for the Division of Reactor Safety Research within the Nuclear Regulatory Commission. Evaluation of nondestructive examination (NDE) techniques and instrumentation are reported; areas of investigation include demonstrating the feasibility of determining structural graphite strength, evaluating the feasibility of detecting and analyzing flaw growth in reactor pressure boundary systems, examining NDE reliability and probabilistic fracture mechanics, and assessing the remaining integrity of pressurized water reactor steam generator tubes where service-induced degradation has been indicated. Test assemblies and analytical support are being provided for experimental programs at other facilities. These programs include the loss-of-coolant accident simulation tests at the NRU reactor, Chalk River, Canada; the fuel rod deformation and post-accident coolability tests for the ESSOR Test Reactor Program, Ispra, Italy; the blowdown and reflood tests in the test facility at Cadarache, France; the instrumented fuel assembly irradiation program at Halden, Norway; and the experimental programs at the Power Burst Facility, Idaho National Engineering Laboratory. These programs will provide data for computer modeling of reactor system and fuel performance during various abnormal operating conditions.

17. KEY WORDS AND DOCUMENT ANALYSIS	17a. DESCRIPTORS

17b. IDENTIFIERS/OPEN-ENDED TERMS

18. AVAILABILITY STATEMENT	19. SECURITY CLASS (This report) Unclassified	21. NO. OF PAGES
Unlimited	20. SECURITY CLASS (This page) Unclassified	22. PRICE S